# FU JEN STUDIES

## NATURAL SCIENCES

NO. 10 1976

## CONTENTS



**FU JEN UNIVERSITY**

**TAIPEI, TAIWAN, REPUBLIC OF CHINA**

# THE SCIENCE COLLEGE AT FU JEN UNIVERSITY

HEINRICH HESSELFELD, SVD, Dean

Fu Jen University was founded in Peiping fifty years ago, and was reopened on Taiwan in October, 1963. On its modern campus of 31 hectares, it has developed into one of the most modern universities on the island. Thirty three concrete buildings cover 87.578 square meters of architectural area. By far the largest area is occupied by the College of Sciences.

Fu Jen University presently consists of 10,721 students, including 4,156 students of the evening session, and has an academic staff of 950 teachers and employees. The day-school students are distributed among the five Colleges, namely Liberal Arts (1818 students), Foreign Languages (891), Natural Sciences (1486), Law (1009), and Business Administration (1361). All students are Chinese. Table 1 shows the number of students in the College of Sciences during the last 13 years.

*Table 1.* Number of students in the College of Sciences in the first and second semester of each school-year.

| School-year | Students | | School-year | Students | |
|---|---|---|---|---|---|
| | First semester | Second semester | | First semester | Second semester |
| 1963 | 80 | 78 | 1970 | 1063 | 1038 |
| 1964 | 305 | 294 | 1971 | 1148 | 1114 |
| 1965 | 576 | 563 | 1972 | 1209 | 1176 |
| 1966 | 843 | 835 | 1973 | 1361 | 1304 |
| 1967 | 997 | 978 | 1974 | 1409 | 1364 |
| 1968 | 1027 | 1015 | 1975 | 1447 | 1385 |
| 1969 | 1022 | 989 | 1976 | 1486 | |

The seven departments of the College of Natural Sciences will be introduced here with a short description of their characteristics.

1. **Department of Mathematics.** Head: *Dr. Hildegard Pohanka, SSpS*

The Department of Mathematics offers courses for students who major in the two sections of *Pure Mathematics* and *Applied Mathematics.* A graduate school in mathematics was established in 1974. In addition, the Department of Mathematics offers service courses to all colleges of the university.

The curriculum of the section of *Pure Mathematics* puts emphasis on the theoretical aspect, mainly algebra, and the curriculum of *Applied Mathematics* offers courses in Computer Science, Operational Research, and Statistics. Students are free to select courses of either section. In the Graduate School of Mathematics, research is done especially in the three areas of Theory of Numbers (Quadratic Forms), Partial Differential Equations (propagation of vibrations, electromagnetic waves, heat pulses), and Functional Analysis (harmonic analysis). The department has 281 undergraduate and 7 graduate students. With respect to the number of students, it is the biggest department of the College of Sciences.

2. **Department of Physics.** Head: *Dr. Heinrich Hesselfeld, SVD*

The Department of Physics has 196 undergraduate students and 8 graduate students. Significant research is done by faculty members and graduate students in the areas of optics, biophysics, solid state physics, and theoretical nuclear physics.

The department provides 10 large rooms for undergraduate experiments, and 3 well-equipped research laboratories. A digital computer, installed at Fu Jen University in 1971, has improved the department's capacity to train physicists and scientists. Interest in laboratory work is stressed throughout the four years of undergraduate studies by young and dedicated full-time faculty members. The department tends more towards areas of *Applied Physics* (like Electricity, Electronics and Laboratory Techniques) in order to assure employment for graduating students in Taiwan.

Graduate work in physics leads to a Master of Science degree. A thesis is required, based upon not less than four semesters of graduate studies. Each candidate for the M. S. degree is required

to take an examination, written and oral, covering his graduate work, including his thesis.

3. **Department of Chemistry.** Head: *Dr. S. L. Lin*

The Department of Chemistry now totals 192 students, distributed among four years of undergraduate classes. Since the beginning of the department, a considerable effort has been made in planning and preparing the facilities for both teaching and research. At present, most of the basic tool instruments are available, such as ultraviolet spectrophotometer, infrared spectrometer, atomic absorption spectrophotometer, gas chromatography, thin layer chromatography, refractometer, liquid scintillation counter, high-speed refrigerated centrifuge, etc.

All full-time faculty members and about one-half of the senior undergraduate students are involved in research work. During the past academic year, the research included five topics in organic chemistry, two topics in inorganic chemistry, and one program in physical chemistry. This research work provides the opportunity for senior students to learn the use of periodicals, to design new experimental procedures, to learn basic methods in research, and most important, to deepen the knowledge obtained from classes and textbooks.

A Graduate School of Chemistry is in preparation.

4. **Department of Biology.** Head: *Dr. Franz Huber, SVD*

The Biology Department presently consists of 159 undergraduate students. The aim of the department is to teach these students a thorough knowledge in the area of biology and give them a good training in laboratory techniques. After graduation the students ought to be qualified to do research as well as teach. The faculty of the department consists of 10 professors, 5 associate professors, and 6 lecturers. The teaching staff is mostly on part-time assignment, and all of them are nation-wide leading specialists in their respective areas.

In its research activities, the Department of Biology selects projects which can benefit the needs of the people in Taiwan. Work

is done mainly on bihalves and fish infected with harmful parasites. For this work most modern equipment is available. If a parasite is detected, a dissecting microscope dissects and takes pictures at the same time. Then a scanning electron microscope studies the surface of the parasite in the finest details. A microtome is used to study the parasite on the cellular level. An ultra-microtome makes sections with a thickness of only 600 angstroms. These extremely thin sections are then examined under the transmission electron microscope on the subcellular level. In addition, a micro-spectrophotometer studies the histo- or cytochemical aspect of the parasite. All these various procedures used at Fu Jen University give complete knowledge of the morphology of the parasite.

The Biology Department is also well equipped for studies in Histology, Biochemistry, and Animal Physiology. Undergraduate students have an opportunity to use the laboratories and the equipment to their greatest advantage. The laboratories are open daily from 6 a. m. until 10:30 p. m. all year round.

A graduate program is planned. The center of research will be focused on Cytology and Mistochemistry, with special attention given to bacteria, fungi, parasites, insects, and higher plants.

### 5. Department of Nutrition and Food Science.

Head: *Prof. J. M. Tsiang*

This department includes the nutrition section with 125 students and the food science section with 166 students. The *Nutrition Section* trains students for hospital dietetics, for nutrition research, and for community nutrition extension work. Students trained for hospital dietetics undergo a training period of more than five weeks in different hospitals which have been cooperating with the department for several years. Under the direction of a nutritional biochemist nutrition research in the department is carried out on the hormonal response in rats with various nutritional conditions. The *Food Science Section* prepares students for food industry operation and management and for food science research. Students can sign up for summer practice in food factories, food research laboratories, or

food inspection institutes. Senior students are presently working on different subjects concerning Chinese fruit juices, Chinese sausages, the packing of Chinese salted vegetables, and storage tests on Chinese food products. Plans for building a pilot plant for laboratory courses in food processing, packaging, and factory sanitation have been made. This important department tries to meet the need of the food industry in Taiwan, and tries to play a special role in the developing program of the "Industrialization of Chinese Food".

6. **Department of Home Economics.**

Head: *Prof. Sr. Urbania Tueshaus, SSPS*

The Department of Home Economics was opened under the College of Natural Sciences from the start of Fu Jen University in 1963. It has presently 182 students. Of the 714 alumnae who graduated from this department, 480 now work in Taiwan: 102 are engaged in research and teaching, 60 in various governmental and private community services, 220 in business. More than 200 alumnae went abroad for advanced study. Of these, 120 have obtained their Master's degree and 14 their Doctorate in various areas related to home economics.

The department concentrates its teaching curriculum in three areas of home economics: 1. *Food Service Administration.* This option is for students interested in administrative positions in food service systems such as in hotels, restaurants, and similar institutions. 2. *Child Development and Family Studies.* This option is intended for future nursery school diretors, teachers in day care centers, teachers for handicapped children, family consultants, etc. 3. *Housing, Equipment, and Home Management.* This option is for those interested in house planning and furnishing, in positions with business firms, especially utility companies, etc. The Home Economics Department operates in its own 3-story building which includes well-equipped and functioning laboratories in the areas of food service administration, clothing management, and family housing. A 2-story laboratory for observation, research, and teaching of Child Development is under construction, it will include a practice

house for experience in all phases of home-making. Emphasis is placed on a balanced integration of theory and practical application. The students of the Home Economics Department enrich their experience in self-government and team cooperation through editing the departmental magazine *My Home, My Love.*

**7. Department of Textiles and Clothing.**

Head: *Sr. Maryta Laumann, SSpS*

The Department of Textiles and Clothing, established in 1970, is the youngest of the seven departments belonging to the College of Sciences at Fu Jen University. Besides offering basic courses of natural sciences, the department extends its curriculum from technology courses to the social sciences, from art and design courses to business related courses. The original purpose of the department was to provide women with the opportunity to enter the professional area of textiles in Taiwan, to supply qualified personnel to the local textile and apparal industry, and to enable Chinese women to pursue advanced studies abroad in the area of textiles and clothing.

In keeping with the development of the textile industry in Taiwan, the department, beginning with this present school-year, offers a more specialized program of study, which allows the students to choose one of the following three options after completing their second year of undergraduate studies: 1. *Textile Designing.* 2. *Apparel Design.* 3. *Textile and Apparel Marketing.* The Ministry of Education has welcomed this new plan of study, especially since this department is still the only one of its kind in Taiwan.

The department has a present enrollment of 212 students. A recent survey indicates that of the 111 graduates of this department, 4 are working in research institutes, 67 in private organizations (factories, trade companies, sales departments), 4 in education; 27 are studying abroad for advanced degrees in textile areas.

Though it is an undergraduate and young department, a limited amount of research is carried out. Some good results, however, are already obtained from studies on the effectiveness of local detergents and their damaging impact on textile substrates. Research like this will contribute to raising the quality, improving the labeling and packaging of local products. It also will advance consumer information and education.

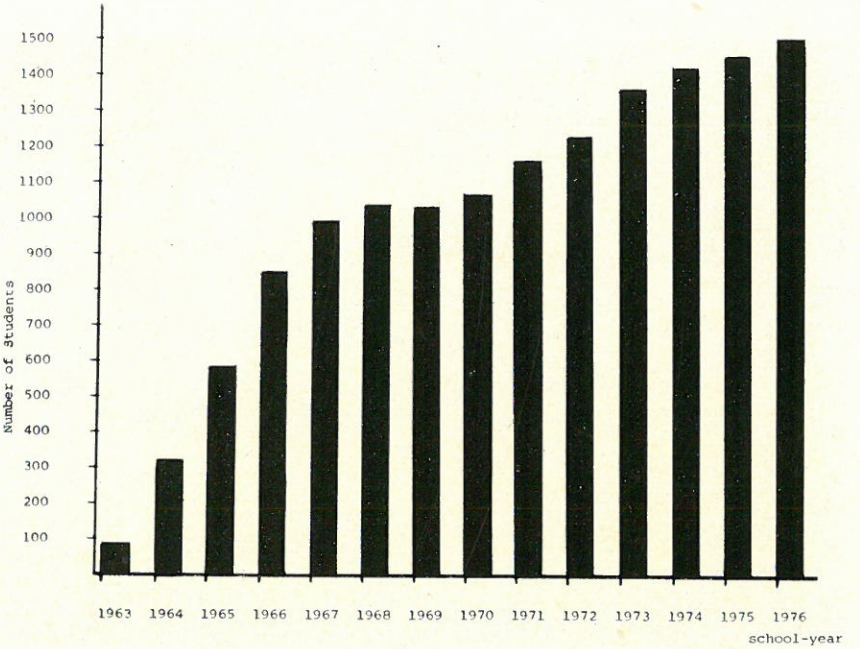


Fig. 1. Total number of Science students at Fu Jen University up to the present school-year (see Table 1).

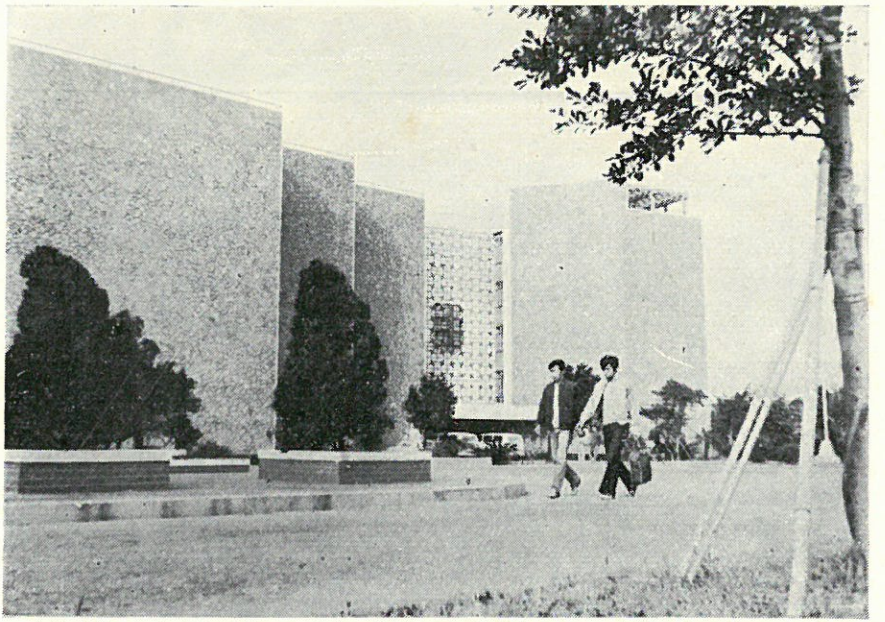

Administration Building of the Colleges of Sciences and Foreign Languages.

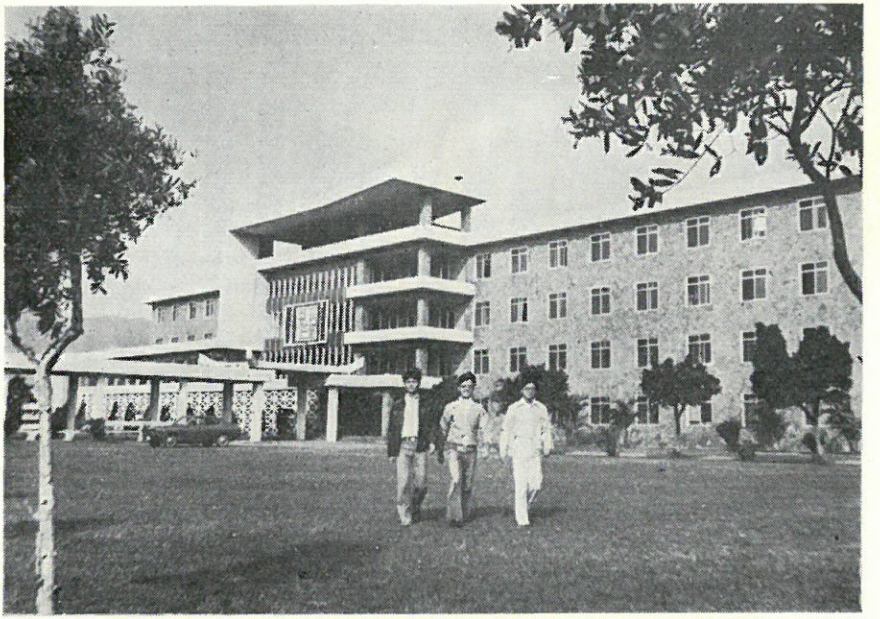

One of the Men's Residences of the College of Sciences.

The Women's Residence at Fu Jen University.

The Library of the Colleges of Sciences and Foreign Languages.

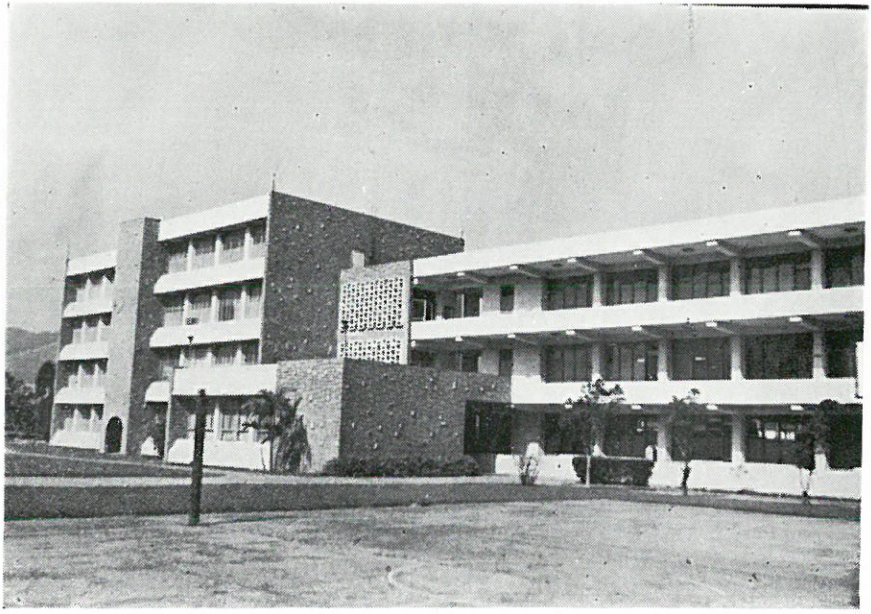

The Departments of Home-Economics, Nutrition & Food Science, and Textiles & Clothing.

The Optics Research Laboratory in Physics (Light Scattering).

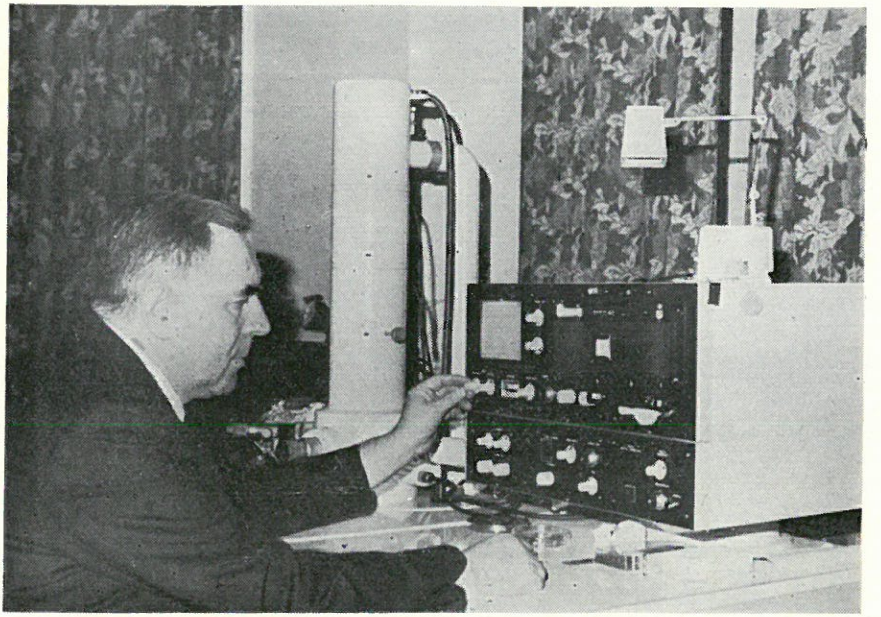

The Scanning Electron Microscope (JEOL 15), with Dr. Huber SVD, Chairman of Biology.

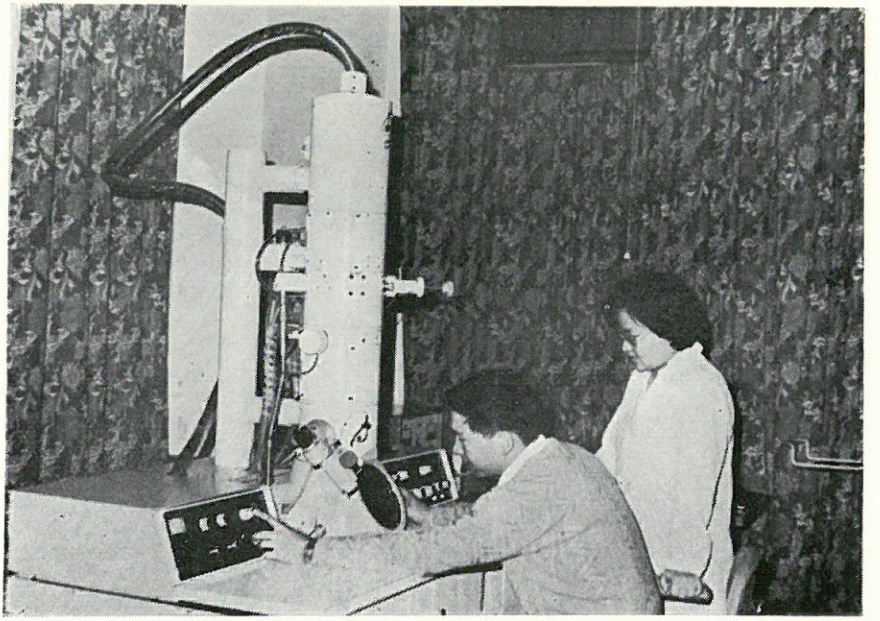

The Transmission Electron Microscope (JEOL 100S).

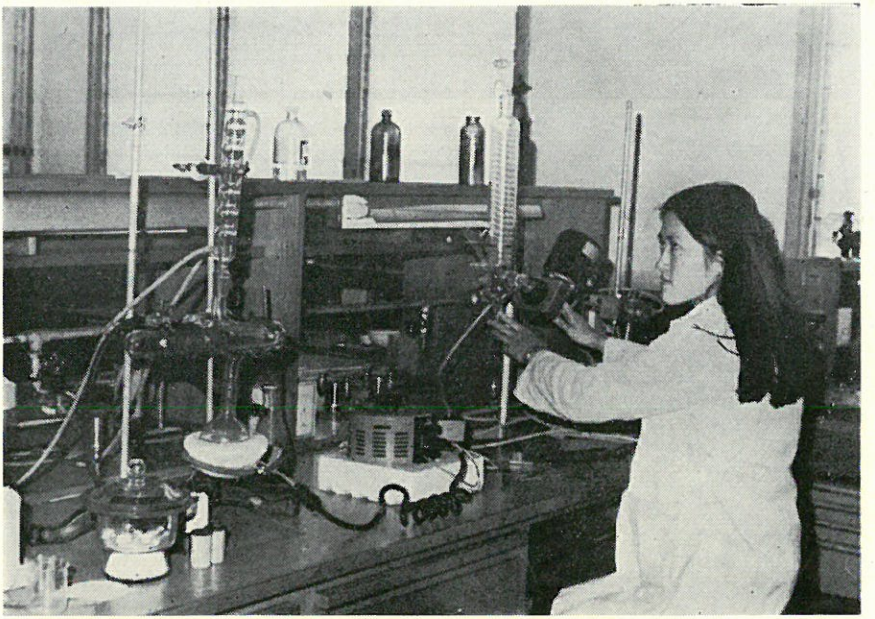

Experiment on Organic Synthesis in Chemistry.

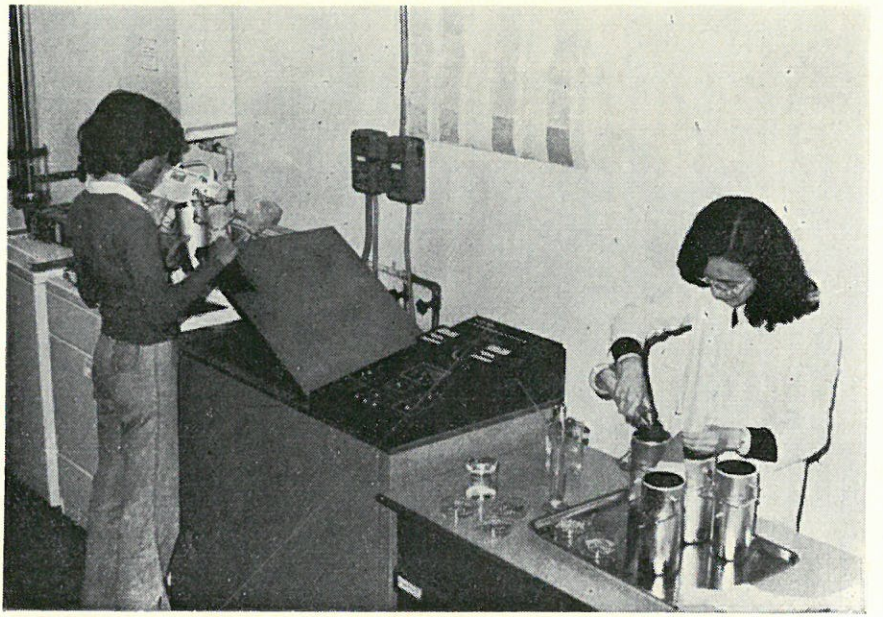

The Analytical Laboratory of the Department of Textiles & Clothing.

# A REFORMATION OF PICARD APPROXIMATION*

YI-CHING YEN

## INTRODUCTION

For a system of first order DEs of the forms

$$\left.\begin{aligned} \frac{dy_1}{dx} &= f_1(x, y_1, \ldots, y_n) \\ &\cdots\cdots\cdots\cdots\cdots\cdots \\ \frac{dy_n}{dx} &= f_n(x, y_1, \ldots, y_n) \end{aligned}\right\} \tag{1}$$

or written in vector notation such as

$$\frac{d\vec{y}}{dx} = \vec{y}'(x) = \vec{F}(x, \vec{y}), \tag{2}$$

where $\vec{y} = (y_1, \ldots, y_n)$, $F = (f_1, \ldots, f_n)$, we define the length of a vector $\vec{y}(x) = (y_1(x), \ldots, y_n(x))$ as $|\vec{y}| = \sum_{i=1}^{n} \mathrm{Max}\,|y_i|$, for every $x$ belonging to the domain of $\vec{y}(x)$. It is known from the Existence and Uniqueness Theorem[1] that if F is continuous and satisfies the Lipschitz condition for some Lipschitz constant L on a compact convex domain

$$D : \begin{cases} |x - x_0| \le a \\ |y_i - y_i^0| \le b_i, \qquad i = 1, 2, \ldots, n \end{cases} \tag{3}$$

of $xy$-space, i.e.,

$$|\vec{F}(x, \vec{y}) - \vec{F}(x, \vec{z})| \le L|\vec{y} - \vec{z}|,$$
$$\forall\,(x, \vec{y}), \qquad (x, \vec{z}) \in D, \tag{4}$$

then we have a unique solution $\vec{y}(x)$ of (2), $x \in [x_0 - h, x_0 + h]$, where

$$h = \min\left(a, \frac{b_1}{M}, \ldots, \frac{b_n}{M}\right),$$
$$M \ge \mathrm{Max}\,|f_i(x, y)|, \qquad i = 1, 2, \ldots, n, \tag{5}$$

and $\vec{y}(x)$ satisfies the initial condition $\vec{y}(x_0) = \vec{y}^0$, $\vec{y}^0 = (y_1^0, \ldots, y_n^0)$.

* This paper was supported by the National Science Council, Republic of China.

Picard had the idea of iterating an integral operator $A: D' \to D'$,

$$D': |y_i - y_i^0| \leq b_i, \quad i = 1, 2, \ldots, n, \quad \text{s.t.}$$

$$A(\vec{y}(x)) = \vec{y}^0 + \int_{x_0}^{x} \vec{F}(u, \vec{y}(u))\, du, \quad \vec{y}^1 = A(\vec{y}^0),$$

$$\vec{y}^r = A(\vec{y}^{r-1}) = A^r(\vec{y}^0), \quad r = 2, 3, \ldots,$$

and showed that the sequence of functions $\{\vec{y}^r(x)\}$ converges to a function $\vec{y}(x)$ uniformly on $|x - x_0| \leq h$ satisfying the DE (2) and the condition $\vec{y}(x_0) = \vec{y}^0$. The Picard approximation is formed by the sequence $\{\vec{y}^r\}$,[1].

Now we will show that by reforming the sequence $\{\vec{y}^r\}$ we can obtain a better approximation than that Picard gave.

## THE MAIN RESULT

Given an explicit form of $n$-th order DE.

$$y^{(n)} = f(x, y, y', \ldots, y^{(n-1)}), \tag{6}$$

which can be written as a system of first order DEs

$$\left.\begin{aligned} &\frac{dy}{dx} = y_1, \\ &\frac{dy_1}{dx} = y'' = y_2, \\ &\cdots\cdots\cdots\cdots\cdots\cdots \\ &\frac{dy_{n-2}}{dx} = y^{(n-1)} = y_{n-1}, \\ &\frac{dy_{n-1}}{dx} = y^{(n)} = f(x, y, y_1, \ldots, y_{n-1}), \end{aligned}\right\} \tag{7}$$

or

$$\frac{d\vec{y}(x)}{dx} = \vec{F}(x, \vec{y}(x))$$

with

$$\vec{y} = (y, y_1, \ldots, y_{n-1}),$$
$$\vec{F}(x, \vec{y}) = (y_1, y_2, \ldots, y_{n-1}, f(x, \vec{y})), \tag{8}$$

a special form of (1) and (2). It can be shown that if $f$ is continuous and $\partial f/\partial y_i$, $i = 0, 1, \ldots, n-1$, exist and are bounded in the domain

$$D : \begin{cases} |x - x_0| \le a \\ |y_i - y_i^0| \le b_i, \end{cases} \quad i = 0, 1, \ldots, n-1, \quad y_0^0 = y_0, \tag{9}$$

then the DEs (7) satisfy the Lipschitz condition (4) for some Lipschitz constant L and have a unique set of solution $\vec{y}(x) = (y_0(x), y_1(x), \ldots, y_{n-1}(x))$ which satisfies the initial condition $\vec{y}(x_0) = \vec{y}^0 = (y_0^0, y_1^0, \ldots, y_{n-1}^0)$, $x \in [x_0 - h, x_0 + h]$, where

$$h = \min\left(a, \frac{b_0}{M}, \ldots, \frac{b_{n-1}}{M}, \frac{1}{2L} \text{ e.t.c.}\right),$$

$$M = \text{Max}\,(|y_1(x)|, \ldots, |y_{n-1}(x)|, |f(x, \vec{y}(x))|), \quad |x - x_0| \le a. \tag{10}$$

Let a subdomain D′ of D be

$$D' : |y_i - y_i^0| \le b_i, \quad i = 0, 1, 2, \ldots, n-1. \tag{11}$$

Consider the integrals

$$y_i^1(x) = y_i^0 + \int_{x_0}^{x} y_{i+1}^0 \, dt, \quad i = 0, 1, \ldots, n-2,$$

$$y_{n-1}^1(x) = y_{n-1}^0 + \int_{x_0}^{x} f(t, y_0^1(t), \ldots, y_{n-2}^1(t), y_{n-1}^0) \, dt;$$

$$y_i^r(x) = y_i^0 + \int_{x_0}^{x} y_{i+1}^{r-1}(t) \, dt, \quad r = 2, 3, \ldots, \quad i = 0, 1, \ldots, n-2,$$

$$y_{n-1}^r(x) = y_{n-1}^0 + \int_{x_0}^{x} f(t, y_0^r(t), \ldots, y_{n-2}^r(t), y_{n-1}^{r-1}(t)) \, dt, \quad x \in [x_0 - h, x_0 + h]. \tag{12}$$

Then

$$\vec{y}^{r-1}(x) = (y_0^{r-1}(x), y_1^{r-1}(x), \ldots, y_{n-1}^{r-1}(x)) \in D'$$

implies that $\vec{y}^r(x) \in D'$, since

$$|y_i^r(x) - y_i^0| = \left| \int_{x_0}^{x} y_{i+1}^{r-1}(t) \, dt \right| \le \left| \int_{x_0}^{x} |y_{i+1}^{r-1}(t)| \, dt \right| \le Mh \le b_i, \quad i = 0, 1, 2, \ldots, n-2,$$

and

$$\begin{aligned} |y_{n-1}^r(x) - y_{n-1}^0| &= \left| \int_{x_0}^{x} f(t, y_0^r(t), \ldots, y_{n-2}^r(t), y_{n-1}^{r-1}(t)) \, dt \right| \\ &\le \left| \int_{x_0}^{x} |f(t, y_0^r(t), \ldots, y_{n-2}^r(t), y_{n-1}^{r-1}(t))| \, dt \right| \\ &\le Mh \le b_{n-1}, \qquad r = 1, 2, \ldots. \end{aligned}$$

For two mappings A, B of D′, such that

$$A\vec{y}^r(x) = \vec{y}^{r+1}(x),$$

$$B\vec{y}^r(x) = (y_0^{r+1}(x), \ldots, y_{n-2}^{r+1}(x), y_{n-1}^r(x)), \qquad r = 0, 1, 2, \ldots.$$

A, B are mappings of D′ into D′.

A, B also bring two points closer together, since

$$\begin{aligned}
&|B\vec{y}^r(x) - B\vec{y}^s(x)| \\
&\quad = |y_0^{r+1}(x) - y_0^{s+1}(x), \ldots, \\
&\qquad\qquad , y_{n-2}^{r+1}(x) - y_{n-2}^{s+1}(x), y_{n-1}^r(x) - y_{n-1}^s(x)| \\
&\quad = \sum_{i=1}^{n-1} \mathrm{Max} \left| \int_{x_0}^{x} (y_i^r(t) - y_i^s(t))\, dt \right| + \mathrm{Max}\, |y_{n-1}^r(x) - y_{n-1}^s(x)| \\
&\quad \leq \sum_{i=1}^{n-1} Lh\, \mathrm{Max}\, |y_i^r(x) - y_i^s(x)| + \mathrm{Max}\, |y_{n-1}^r(x) - y_{n-1}^s(x)| \\
&\quad < \sum_{i=0}^{n-1} \mathrm{Max}\, |y_i^r(x) - y_i^s(x)| = |\vec{y}^r - \vec{y}^s(x)|, \\
&\qquad\qquad |x - x_0| \leq h \qquad (13)
\end{aligned}$$

for small $h$ satisfying

$$\begin{aligned}
&Lh(\mathrm{Max}\, |y_{n-1}^r(x) - y_{n-1}^s(x)|) \\
&\quad < \mathrm{Max}\, |y_0^r(x) - y_0^s(x)|, \qquad 2Lh < 1. \qquad (14)
\end{aligned}$$

$$\begin{aligned}
&|A\vec{y}^r(x) - A\vec{y}^s(x)| \\
&\quad = |(y_0^{r+1}(x) - y_0^{s+1}(x), \ldots, y_{n-1}^{r+1}(x) - y_{n-1}^{s+1}(x))| \\
&\quad = \sum_{i=1}^{n-1} \mathrm{Max} \left| \int_{x_0}^{x} (y_i^r(t) - y_i^s(t))\, dt \right| \\
&\qquad\qquad + \mathrm{Max} \left| \int_{x_0}^{x} [f(t, B\vec{y}^r(t)) - f(t, B\vec{y}^s(t))]\, dt \right| \\
&\quad \leq Lh \left( \sum_{i=1}^{n-1} \mathrm{Max}\, |y_i^r(x) - y_i^s(x)| + |B\vec{y}^r(x) - B\vec{y}^s(x)| \right) \\
&\text{by (13)}, \quad < Lh \left( \sum_{i=1}^{n-1} \mathrm{Max}\, |y_i^r(x) - y_i^s(x)| + |\vec{y}^r(x) - \vec{y}^s(x)| \right) \\
&\text{by (10)}, \quad < |\vec{y}^r(x) - \vec{y}^s(x)|, \qquad |x - x_0| \leq h. \qquad (15)
\end{aligned}$$

Thus A, B are two compressed mappings of D′ into D′. Hence $\{A\vec{y}^r(x)\}$, $\{B\vec{y}^r(x)\}$ converge uniformly on $[x_0 - h, x_0 + h]$ to $\vec{y}(x)$, $\vec{z}(x)$ respectively, which are stationary[2], i.e. $A\vec{y}(x) = \vec{y}(x)$, $B\vec{z}(x) = \vec{z}(x)$. But $A\vec{y}^r(x) = (y_0^{r+1}(x), \ldots, y_{n-1}^{r+1}(x))$, $B\vec{y}^r(x) = (y_0^{r+1}(x), \ldots, y_{n-2}^{r+1}(x), y_{n-1}^r(x))$, with $\lim_{r\to\infty} y_{n-1}^r(x) = \lim_{r\to\infty} y_{n-1}^{r+1}(x)$

imply that $\vec{y}(x) = \vec{z}(x)$. The stationary condition with $\vec{y}(x) = \vec{z}(x)$ gives $\vec{y}(x) = \vec{y}^0 + \int_{x_0}^{x} \vec{F}(t, \vec{y}(t))\, dt$. This means that $\vec{y}(x) = (y(x), y_1(x), \ldots, y_{n-1}(x))$, which is unique, satisfies the DE. (8) and the initial condition $\vec{y}(x_0) = \vec{y}^0$. In other words, there exists a unique solution $y(x)$ of (6) satisfying $y^{(i)}(x_0) = y_i^0$, $i = 0, 1, \ldots, n-1$.

The sequence $\{\vec{y}^r(x)\}$ is our reformed Picard approximation. It is more accurate than the Picard method, since for the $(r+1)$-th step approximation of ours,

$$\vec{y}^{r+1}(x) = \vec{y}^0 + \int_{x_0}^{x} \vec{F}(t, B\vec{y}^r(t))\, dt,$$

while the Picard approximation is

$$\vec{y}^{r+1}(x) = \vec{y}^0 + \int_{x_0}^{x} F(t, \vec{y}^r(t))\, dt.$$

We will show that the length $|B\vec{y}^r(x) - \vec{y}(x)|$ is shorter than $|\vec{y}^r(x) - \vec{y}(x)|$, so that $F(x, B\vec{y}^r(x))$ is a better function of $F(x, \vec{y}(x))$ than $F(x, \vec{y}^r(x))$. Since the domain of $\vec{y}(x)$ does not exceed D′,

$$\begin{aligned}
&|B\vec{y}^r(x) - \vec{y}(x)| \\
&\quad = |(y_0^{r+1}(x) - y_0(x), \ldots, \\
&\qquad\qquad , y_{n-2}^{r+1}(x) - y_{n-2}(x),\ y_{n-1}^r(x) - y_{n-1}(x))| \\
&\quad = \sum_{i=1}^{n-1} \mathrm{Max} \left| \int_{x_0}^{x} (y_i^r(t) - y_i(t))\, dt \right| + \mathrm{Max}\, |y_{n-1}^r(x) - y_{n-1}(x)| \\
&\quad = \sum_{i=1}^{n-1} Lh\, \mathrm{Max}\, |y_i^r(x) - y_i(x)| + \mathrm{Max}\, |y_{n-1}^r(x) - y_{n-1}(x)| \\
&\quad < \sum_{i=0}^{n-1} \mathrm{Max}\, |y_i^r(x) - y_i(x)| = |\vec{y}^r(x) - \vec{y}(x)|
\end{aligned}$$

whenever $h$ is so small that

$$Lh\, (\mathrm{Max}\, |y_{n-1}^r(x) - y_{n-1}(x)|) < |y_0^r(x) - y_0(x)|, \tag{16}$$

$h$ in (10) must satisfy (14) and (16).

We conclude the above result as follows:

**Theorem.** Let the explicit form of the $n$-th order DE

$$y^{(n)} = f(x, y, y', \ldots, y^{(n-1)})$$

be such that $f$ is continuous and $\partial f/\partial y^{(i)}$ exist and are bounded in the domain D defined by (9). Rewrite (6) as (7). Define $y_i^r(x)$ as in (12), let $\vec{y}^r(x) = (y_0^r(x), y_1^r(x), \ldots, y_{n-1}^r(x))$, then $y_0^r(x)$ converges uniformly to a continuous function $y(x)$ which satisfies the initial conditions $y^{(i)}(x_0) = y_i^0$, $i = 0, 1, \ldots, n-1$, $x \in [x_0 - h, x_0 + h]$, $h$ is defined as in (10), (14) and (16). The sequence $\{\vec{y}^r(x)\}$ is a better approximation of the solution function $\vec{y}(x)$ than $\{\vec{y}^r(x)\}$ obtained by the Picard method.

## EXAMPLES

In the following examples we give the approximate solutions of the DEs by our reformed Picard method, Picard method and the Maclaurin series of the solutions of the DEs in order to compare the accuracy of the former two to the latter. In this paragraph, we do not need so many indices as were used in the previous chapter.

**Example 1.** $y''' - (1+x)y' - y = 0$, $y(0) = 1 = y'(0)$, $y''(0) = -1$

Sol. Let $y' = z$, $y_0 = 1$,
$z' = u$, $z_0 = 1$,
then $u' = (1+x)z + y$, $u_0 = -1$

By our reformed approximation,

$$y_1(x) = 1 + \int_0^x dt = 1 + x,$$

$$z_1(x) = 1 + \int_0^x -dt = 1 - x,$$

$$u_1(x) = -1 + \int_0^x [(1+t)(1-t) + (1+t)]\,dt$$
$$= -1 + 2x + \frac{x^2}{2} - \frac{x^3}{3};$$

$$y_2(x) = 1 + \int_0^x (1-t)\,dt = 1 + x - \frac{x^2}{2},$$

$$z_2(x) = 1 + \int_0^x \left(-1 + 2t + \frac{t^2}{2} - \frac{t^3}{3}\right) dt = 1 - x + x^2 + \frac{x^3}{6} - \frac{x^4}{12},$$

$$u_2(x) = -1 + \int_0^x \left[(1+t)\left(1 - t + t^2 + \frac{t^3}{6} - \frac{t^4}{12}\right) + \left(1 + t - \frac{t^2}{2}\right)\right] dt$$
$$= -1 + 2x + \frac{x^2}{2} - \frac{x^3}{6} + \frac{7x^4}{24} + \frac{x^5}{60} - \frac{x^6}{72};$$

$$y_3(x) = 1 + \int_0^x z_2(t)\,dt = 1 + x - \frac{x^2}{2} + \frac{x^3}{3} + \frac{x^4}{24} - \frac{x^5}{60},$$

$$z_3(x) = 1 + \int_0^x \left(-1 + 2t + \frac{t^2}{2} - \frac{t^3}{6} + \frac{7t^4}{24} + \frac{t^5}{60} - \frac{t^6}{72}\right) dt$$

$$= 1 - x + x^2 + \frac{x^3}{6} - \frac{x^4}{24} + \frac{7x^5}{120} + \frac{x^6}{360} - \frac{x^7}{504},$$

$$u_3(x) = \ldots,$$

$$y_4(x) = 1 + \int_0^x z_3(t)\,dt$$

$$= 1 + x - \frac{x^2}{2} + \frac{x^3}{3} + \frac{x^4}{24} - \frac{x^5}{120} + \frac{7x^6}{720} + \frac{x^7}{2520} - \frac{x^8}{4032}.$$

By Picard method,

$$\bar{y}_1(x) = 1 + \int_0^x dt = 1 + x,$$

$$\bar{z}_1(x) = 1 + \int_0^x -dt = 1 - x,$$

$$\bar{u}_1(x) = -1 + \int_0^x [(1+t)\cdot 1 + 1]\,dt = -1 + 2x + \frac{x^2}{2};$$

$$\bar{y}_2(x) = 1 + \int_0^x (1-t)\,dt = 1 + x - \frac{x^2}{2},$$

$$\bar{z}_2(x) = 1 + \int_0^x \left(-1 + 2t + \frac{t^2}{2}\right) dt = 1 - x + x^2 + \frac{x^3}{6},$$

$$\bar{u}_2(x) = -1 + \int_0^x [(1+t)(1-t) + 1 + t]\,dt$$

$$= -1 + 2x + \frac{x^2}{2} - \frac{x^3}{3};$$

$$\bar{y}_3(x) = 1 + \int_0^x \bar{z}_2(t)\,dt = 1 + x - \frac{x^2}{2} + \frac{x^3}{3} + \frac{x^4}{24},$$

$$\bar{z}_3(x) = 1 + \int_0^x \bar{u}_2(t)\,dt = 1 - x + x^2 + \frac{x^3}{6} - \frac{x^4}{12},$$

$$\bar{u}_3(x) = \ldots;$$

$$\bar{y}_4(x) = 1 + \int_0^x \bar{z}_3(t)\,dt = 1 + x - \frac{x^2}{2} + \frac{x^3}{3} + \frac{x^4}{24} - \frac{x^5}{60},$$

while

$$y(x) = 1 + x - \frac{x^2}{2} + \frac{x^3}{3} + \frac{x^4}{24} - \frac{x^5}{120} + \frac{x^6}{80} + \frac{x^7}{1260} + \frac{x^8}{13440} + \ldots$$

in Maclaurin expansion.

**Example 2.** $y'' = -2x\,y' + y^2$, $y(0) = 0$, $y'(0) = -1$

Sol. Let $y' = z$, $y_0 = 0$
then $z' = -2xz + y^2$, $z_0 = -1$

By our reformed approximation,

$$y_1(x) = \int_0^x -\,dt = -x,$$

$$z_1(x) = -1 + \int_0^x (2t + t^2)\,dt = -1 + x^2 + \frac{x^3}{3};$$

$$y_2(x) = \int_0^x \left(-1 + t^2 + \frac{t^3}{3}\right) dt = -x + \frac{x^3}{3} + \frac{x^4}{12},$$

$$z_2(x) = -1 + \int_0^x \left[-2t\left(-1 + t^2 + \frac{t^3}{3}\right) + \left(-t + \frac{t^3}{3} + \frac{t^4}{12}\right)^2\right] dt$$

$$= -1 + x^2 + \frac{x^3}{3} - \frac{x^4}{2} - \frac{4x^5}{15} - \frac{x^6}{36} + \frac{x^7}{63} + \frac{x^8}{144} + \frac{x^9}{1296};$$

$$y_3(x) = \int_0^x z_2(t)\,dt$$

$$= -x + \frac{x^3}{3} + \frac{x^4}{12} - \frac{x^5}{10} - \frac{2x^6}{45} - \frac{x^7}{252} + \frac{x^8}{504} + \frac{x^9}{1296} + \frac{x^{10}}{12960}.$$

By Picard Method,

$$\bar{y}_1(x) = \int_0^x -\,dt = -x,$$

$$\bar{z}_1(x) = -1 + \int_0^x 2t\,dt + -1 + x^2;$$

$$\bar{y}_2(x) = \int_0^x \bar{z}_1(t)\,dt = -x + \frac{x^3}{3},$$

$$\bar{z}_2(x) = -1 + \int_0^x [-2t(-1 + t^2) + t^2]\,dt = -1 + x^2 + \frac{x^3}{3} - \frac{x^4}{2};$$

$$\bar{y}_3(x) = \int_0^x \bar{z}_2(t)\,dt = -x + \frac{x^3}{3} + \frac{x^4}{12} - \frac{x^5}{10},$$

while the Maclaurin series gives

$$y(x) = -x + \frac{x^3}{3} + \frac{x^4}{12} - \frac{x^5}{10} - \frac{2x^6}{45}$$
$$+ \frac{5x^7}{252} + \frac{19x^8}{1260} - \frac{x^9}{540} + \frac{1717x^{10}}{453600} + \cdots.$$

**Example 3.** $y'' + xy' - y = 0, \quad y(0) = 1, \quad y'(0) = 2$

Sol. Let $y' = z, \quad y_0 = 1$
then $z' = y - xz, \quad z_0 = 2$

The reformed approximation is

$$y_1(x) = 1 + \int_0^x 2dt = 1 + 2x,$$

$$z_1(x) = 2 + \int_0^x (1 + 2t - 2t)\, dt = 2 + x;$$

$$y_2(x) = 1 + \int_0^x z_1(t)\, dt = 1 + 2x + \frac{x^2}{2},$$

$$z_2(x) = 2 + \int_0^x \left[\left(1 + 2t + \frac{t^2}{2}\right) - t(2 + t)\right] dt = 2 + x - \frac{x^3}{6};$$

$$y_3(x) = 1 + \int_0^x z_2(t)\, dt = 1 + 2x + \frac{x^2}{2} - \frac{x^4}{24},$$

$$z_3(x) = 2 + \int_0^x \left[\left(1 + 2t + \frac{t^2}{2} - \frac{t^4}{24}\right) - t\left(2 + t - \frac{t^3}{6}\right)\right] dt$$

$$= 2 + x - \frac{x^3}{6} + \frac{x^5}{40};$$

$$y_4(x) = 1 + \int_0^x z_3(t)\, dt = 1 + 2x + \frac{x^2}{2} - \frac{x^4}{24} + \frac{x^6}{240},$$

$$z_4(x) = 2 + \int_0^x \left[\left(1 + 2t + \frac{t^2}{2} - \frac{t^4}{24} + \frac{t^6}{240}\right) - t\left(2 + t - \frac{t^3}{6} + \frac{t^5}{40}\right)\right] dt$$

$$= 2 + x - \frac{x^3}{6} + \frac{x^5}{40} - \frac{x^7}{336};$$

$$y_5(x) = 1 + \int_0^x z_4(t)\, dt = 1 + 2x + \frac{x^2}{2} - \frac{x^4}{24} + \frac{x^6}{240} - \frac{x^8}{2688}.$$

The Picard method gives

$$\bar{y}_1(x) = 1 + \int_0^x 2dt = 1 + 2x,$$

$$\bar{z}_1(x) = 2 + \int_0^x (1 - 2t)\, dt = 2 + x - x^2;$$

$$\bar{y}_2(x) = 1 + \int_0^x \bar{z}_1(t)\, dt = 1 + 2x + \frac{x^2}{2} - \frac{x^3}{3},$$

$$\bar{z}_2(x) = 2 + \int_0^x [1 + 2t - t(2 + t - t^2)]\, dt = 2 + x - \frac{x^3}{3} + \frac{x^4}{4};$$

$$\bar{y}_3(x) = 1 + \int_0^x \bar{z}_2(t)\, dt = 1 + 2x + \frac{x^2}{2} - \frac{x^4}{12} + \frac{x^5}{20},$$

$$\bar{z}_3(x) = 2 + \int_0^x \left[1 + 2t + \frac{t^2}{2} - \frac{t^3}{3} - t\left(2 + t - \frac{t^3}{3} + \frac{t^4}{4}\right)\right] dt$$

$$= 2 + x - \frac{x^3}{6} - \frac{x^4}{12} + \frac{x^5}{15} - \frac{x^6}{24};$$

$$\bar{y}_4(x) = 1 + \int_0^x \bar{z}_3(t)\, dt = 1 + 2x + \frac{x^2}{2} - \frac{x^4}{24} - \frac{x^5}{60} + \frac{x^6}{90} - \frac{x^7}{168},$$

$$\bar{z}_4(x) = 2 + \int_0^x \left[\left(1 + 2t + \frac{t^2}{2} - \frac{t^4}{12} + \frac{t^5}{20}\right)\right.$$

$$\left. - t\left(2 + t - \frac{t^3}{6} - \frac{t^4}{12} + \frac{t^5}{15} - \frac{t^6}{24}\right)\right] dt$$

$$= 2 + x - \frac{x^3}{6} + \frac{x^5}{60} + \frac{x^6}{45} - \frac{x^7}{105} + \frac{x^8}{192};$$

$$\bar{y}_5(x) = 1 + \int_0^x \bar{z}_4(t)\, dt$$

$$= 1 + 2x + \frac{x^2}{2} - \frac{x^4}{24} + \frac{x^6}{360} + \frac{x^7}{315} - \frac{x^8}{840} + \frac{x^9}{1728}.$$

The Maclaurin expansion of the solution is

$$y(x) = 1 + 2x + \frac{x^2}{2} - \frac{x^4}{24} + \frac{x^6}{240} - \frac{x^8}{2688} + \cdots.$$

**Example 4.** $y'' - x^3 y = 0, \quad y(0) = 1, \quad y'(0) = 0$

Sol. Let $y' = z, \quad y_0 = 1$
then $z' = x^3 y, \quad z_0 = 0$ }

Our approximation gives

$$y_1(x) = 1 + \int_0^x 0 dt = 1,$$

$$z_1(x) = \int_0^x t^3\, dt = \frac{x^4}{4};$$

$$y_2(x) = 1 + \int_0^x z_1(t)\, dt = 1 + \frac{x^5}{20},$$

$$z_2(x) = \int_0^x t^3 \left(1 + \frac{t^5}{20}\right) dt = -\frac{x^4}{4} + \frac{x^9}{180},$$

$$y_3(x) = 1 + \int_0^x z_2(t)\, dt = 1 + \frac{x^5}{20} + \frac{x^{10}}{1800},$$

$$z_3(x) = \int_0^x t^3 \left(1 + \frac{t^5}{20} + \frac{t^{10}}{1800}\right) dt = \frac{x^4}{4} + \frac{x^9}{180} + \frac{x^{14}}{25200},$$

$$y_4(x) = 1 + \int_0^x z_3(t)\, dt = 1 + \frac{x^5}{20} + \frac{x^{10}}{1800} + \frac{x^{15}}{37800}.$$

The Picard method has the results

$$\bar{y}_1(x) = 1 + \int_0^x 0\,dt = 1,$$

$$\bar{z}_1(x) = \int_0^x t^3\,dt = \frac{x^4}{4};$$

$$\bar{y}_2(x) = 1 + \int_0^x \frac{t^4}{4}\,dt = 1 + \frac{x^5}{20},$$

$$\bar{z}_2(x) = \int_0^x t^3\,dt \quad \frac{x^4}{4};$$

$$\bar{y}_3(x) = 1 + \int_0^x \frac{t^4}{4}\,dt = 1 + \frac{x^5}{20},$$

$$\bar{z}_3(x) = \int_0^x t^3\left(1 + \frac{t^5}{20}\right)dt = \frac{x^4}{4} + \frac{x^9}{180};$$

$$\bar{y}_4(x) = 1 + \int_0^x \left(\frac{t^4}{4} + \frac{t^9}{180}\right)dt = 1 + \frac{x^5}{20} + \frac{x^{10}}{1800}.$$

The Maclaurin expansion of the solution function is

$$y(x) = 1 + \frac{x^5}{4 \cdot 5} + \frac{x^{10}}{4 \cdot 5 \cdot 9 \cdot 10} + \frac{x^{15}}{4 \cdot 5 \cdot 9 \cdot 10 \cdot 14 \cdot 15} + \cdots$$

$$= 1 + \frac{x^5}{20} + \frac{x^{10}}{1800} + \frac{x^{15}}{37800} + \cdots.$$

In this example, if we continue the approximation process, we can get every term as exactly as we have in Maclaurin series.

From the above examples we see that the reformation of Picard method gives a more accurate and quick approximation of the solution of the DEs.

## REFERENCES

(1) Birkhoff & Rota, *Ordinary Differential Equations*, 2nd Edition, Blaisdell Publishing Co. 1969.

(2) L. E. El'sgoltz, *Differential Equations*, 1961.

"The fruits of science did much to make our civilization worthwhile; now only political leadership combined with yet more science can save that civilization."

Philip Handler in *Biology and the Future of Man.*

# HIGH ENERGY MULTIPARTICLE REACTIONS AND STATISTICAL MODEL

JEN-I CHEN


## ABSTRACT

A simple statistical model for high energy multiparticle reactions is proposed. The total cross section, single particle inclusive spectrum, multiplicity, and angular distribution of partial cross section are analyzed and compared with experiments. The theoretical results are found in good consistancy with experiments.


## I. INTRODUCTION

There are several reasons for the pursuit of the very high energy behavior of hadron physics. First, most physicists believe that in the high energy limit, the strong interaction of hadrons is much more simple and exhibits the highest symmetry of nature. Many theories have been proposed and results were predicted in this limit. This is simply an approximation due to the power series method in mathematics. Any physical quantities of high energy collisions may be expanded in a power series of the collision energy $s$, with coefficients which are functions of other variables, including rest masses and characteristic quantum numbers of particles involved. In the limit of $s \to 0$ or $s \to \infty$, the lowest or the highest term respectively will dominate. The limit of $s = 0$ can not be reached due to the finite masses of stable particles. Approximate analysis in the unphysical region (i.e. $s = 0$), such as the soft pion calculations, have produced fruitful results. In the high energy limit, a large number of particles is produced in the final state and each has an energy much bigger than its rest mass, thus rest masses and other characteristic quantum numbers of individual particles are immaterial, and so the coefficient of the dominant term looks even more simple. Secondly, since the study of low and medium energy behavior had been almost done and did not produce a good theory of strong

interaction, people are looking for additional information from higher energy region. Besides, a consistent theory should prevail at any energy. Thirdly, some countries are rich enough to finance giant accelerators, and experimentalists are happy about it. But where is the high energy limit, above which nature shows its simplicity and highest symmetry? This limit depends on various models. If some model is found to be consistent with experiments, the author may claim that the limit is reached.

As the energy of collision increases, the number of particles produced is so large that it causes complication in data analysis and partial collection of data in experiments. However, there are several important empirical rules concerning the nature of high energy collisions, which are well accepted as basic criteria of any theory. They are

(a) The total cross sections approach constant values in the high energy limit.

(b) For multiparticle reactions, transverse momenta are usually small. The average value[1-2] of the transverse momentum $p_\perp$ is about 0.3 to 0.4 Gev/c, and almost independent of the incident energy, and does not depend strongly on the type or the number of particles produced. However, recent experiments[3-7] discovered some, although not serious, large transverse momentum phenomena in wide angle scattering.

(c) Low multiplicity of particles produced: The average number of particles produced grows slowly with energy—much more slowly than the energy available. Experimental fit[8] shows that the multiplicity of charged particles goes like

$$\langle n_{\text{ch.}} \rangle = A \ln s + B \qquad (1)$$

where A, B are constants and $s$ is the collision energy in the CM system. Considering the smallness of $p_\perp$, it means that most of the energy available is carried away by particles in the form of large longitudinal momentum.

In high energy multiparticle reactions, the number of particles produced and the number of channels available to the final state are

so large that a precise analysis is either impossible or impractical due to imcomplete data collection or mathematical difficulty. It is quite natural to resort to the statistical method. The first statistical model of high energy collisions was proposed by Fermi.[9-10] It was refined and developed by Hagedorn and collaborators[11-13], which is too complicated and has left many areas untouched. The essence of statistical model lies in the assumption of "equal probability" of all channels available, neglecting all interferences of different states. For low energy collisions, selection rules corresponding to conservation laws of quantum numbers play an important role. In high energy collisions, the number of particles and the energy acquired by each particle are so large that the effects of these selection rules and the characteristics of an individual particle become negligible. So that it is quite natural to assume equal probablity for all states permitted, unless experiments show any perference.

In this paper, a simple statistical model of high energy collision is proposed to explain and examine the total cross-section, single particle inclusive spectrum, multiplicity, and angular distribution of partial cross-section.

## II. GENERAL IDEAS AND BASIC ASSUMPTIONS

Our model is based on the following assumptions in a simple picture.

(a) A particle is a sphere (or region of interaction) of finite radius at its rest system. Experiments have shown that particles do have certain sizes, although their inner structures are still not clear. The final solution to the strong interaction theory will inevitably be related to these inner structures.

(b) The collision of two particles is considered as the following process,

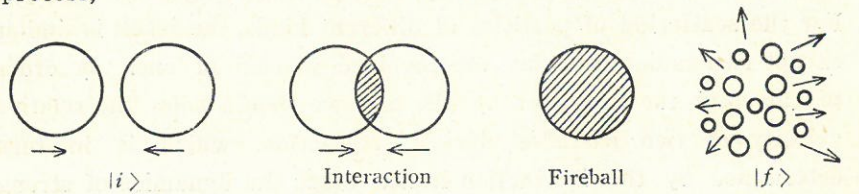

First, two particles interact with each other during overlapping and thus form an excited state called "Fireball"—a thermodynamical equilibrium state of hadronic matter. Then the fireball decays into various final states accessible according to the statistical distribution of thermodynamics. Accordingly, we assume that the probability for this process is equal to

$$\text{Probability of } \langle i|f\rangle = I_i \cdot F_f \qquad (2)$$

where $I_i$ is an interaction factor, $F_f$ is the statistical distribution function of the decay of the fireball.

(c) The interaction occurs only during overlapping. In other words, we assume that

$$I_i = \int H\, dx\, dy\, dz\, dt \qquad (3)$$

integrating over the volume and time of overlapping, H is some interaction function. The simplest choice is H=constant. In general, $I_i$ depends on the radii of interacting particles and the incident energy.

(d) $F_f$ is a normalized distribution function of the fireball decays, which is assumed to be equally probable for all final states available. Here we use a semi-empirical mass density spectrum[11] to take into account the mass degeneracy of all hadron states,

$$\rho(m) = c\, m^a\, e^{bm}, \qquad a = -\frac{5}{2}. \qquad (4)$$

## III. INTERACTION FACTOR AND TOTAL CROSS SECTION

Let us proceed to investigate the interaction factor through the assumption (3), and for simplicity, take $pp$ scattering as an example. For the scattering of particles of different kinds, the result is similar except two radius constants are involved instead of one. In order to calculate the $I_i$ factor by (3), first we should know the relative velocity of two particles during interaction, which is in turn determined by the interaction itself. Since the dynamics of strong

interaction is still unknown, further assumption about the relative velocity or its overall average effect is necessary. For this purpose, Feynman[14] introduced a distribution function of partons, while Hagedorn[12] used a distribution function of local velocity of fireballs to account for the average effects of the relative velocity change during interaction and different impact parameters. Here we simply assume that the particle moves as a whole with constant velocity, even during interaction. This may be over simplified, but the result is expected to be correct qualitatively and pretty close quantitatively.

Let $m$ be the rest mass, and $r_0$ the radius of the proton, $v = p/E$ and $\gamma = (1 - v^2)^{-1/2}$. In the case of H = constant, which is similar to the square-well potential assumption, the interaction factor is found to be

$$\begin{aligned} I_i &= \text{const.} \int dx\, dy\, dz\, dt = \text{const.} \int V(t)\, dt \\ &= \text{const.} \frac{4\pi}{\gamma} \int_0^{2r_0/\gamma v} \left[ \frac{5}{24} r_0^3 + \frac{3}{8} r_0^2 \gamma v t \right. \\ &\qquad \left. + \frac{r_0}{8} (\gamma v t)^2 - \frac{1}{24} (\gamma v t)^3 \right] dt \\ &= \text{const.} \frac{16\pi r_0^4}{3\gamma^2 v} \qquad (5) \\ &\propto \frac{1}{E^2} \to 0 \qquad \text{as} \quad E \to \infty \end{aligned}$$

This result is obvious if we calculate the invariant integral in the rest system of one of the particles instead of the CM system. Then as $E \to \infty$, the other particle will contract into a thin disk without volume, and so $V(t) = 0$ and $I_i = 0$. Since $F_f$ is a normalized final state distribution function, from (2) and (5), the total cross section is proportional to $I_i$, which would approach zero as $1/E^2$ as $E \to \infty$. This prediction is not favored by present experimental data, if not completely excluded.

Alternatively we assume that $H \propto \varepsilon_1 \cdot \varepsilon_2$, and $\varepsilon_1$, $\varepsilon_2$ are energy densities of two particles respectively. Energy conservation requires that $\varepsilon_1 = \varepsilon_0 \gamma_1$, where $\varepsilon_0$ is the rest energy density and $\gamma_1 = (1 - v_1^2)^{-1/2}$, and so on. In $p\bar{p}$ collision in the CM system, $\varepsilon_1 = \varepsilon_2 = \varepsilon_0 \gamma$, so that

$$I_i = \int \varepsilon_1 \varepsilon_2 \, dx\, dy\, dz\, dt \qquad (6)$$

$$= (\varepsilon_0 r)^2 \int dx\, dy\, dz\, dt$$

$$= \frac{3m^2}{\pi r_0^2 v} \xrightarrow[E\to\infty]{} \text{const.} \qquad (7)$$

This leads to the result that the total cross section decreases as the incident energy increases, and approaches a constant as $E \to \infty$, in good agreement with experiments. Hereafter, we will base our analysis and discussions on the second assumption, i. e., $H \propto \varepsilon_1 \varepsilon_2$.

## IV. MULTIPLICITY AND PARTIAL CROSS SECTIONS— PHASE SPACE CALCULATION

Now we proceed to calculate the $F_f$ factor by microcanonical ensemble, that is, all final states available are equally probable. Usually, various selection rules determine which states are available. However, as reaction energy is large enough, the multiplicity of products is so large and each particle produced will have such high energy that its individual quantum numbers are irrelevant and the effects of selection rules are negligible. Thus the probability for a $n$-particle final state $F_n$ is proportional to the corresponding phase space volume.

(A) *Without mass spectrum consideration:* If we assume that in the CM system (take $\hbar = c = 1$)

$$F_n = N \left(\frac{V}{(2\pi)^3}\right)^n \frac{1}{n!} \int \prod_{i=1}^{n} d^3 p_i \, \delta \left(\sum_{i=1}^{n} E_i - E\right) \delta^3 \left(\sum_i \boldsymbol{p}_i = 0\right) \qquad (8)$$

where $n!$ is a factor for correct counting and N is a proportionality constant fixed by the normalization condition, $\sum_n F_n = 1$. Note this is justified only for high multiplicity states, for low multiplicity states, selection rules should be considered. The overestimate due to counting two or more fermions in the same state is only slight.[15] We will evaluate the integral (8) by dropping the restriction of momentum conservation $\sum_i \boldsymbol{p}_i = 0$, which is usually fulfilled in the CM system for a system of many particles, and neglecting rest

masses of produced particles since each acquires energy much larger than its rest mass. Integrating over all angular variables, we get

$$F_n \simeq N \left(\frac{V}{2\pi^2}\right)^n \int_0^E p_1^2\, dp_1 \int_0^{E-p_1} p_2^2\, dp_2 \cdots \int_0^\infty p_n^2\, dp_n\, \delta\left(E - \sum_n p_n\right) \qquad (9)$$

The integration can be done through the iteration of a typical integral

$$\int_0^y p_i^2\, dp_i (y - p_i)^r = \frac{2y^{r+3} r!}{(r+3)!} \qquad (10)$$

and the result is

$$F_n \simeq \frac{N}{E} \left(\frac{E^3 V}{\pi^2}\right)^n \frac{1}{n!(3n-1)!} \qquad (11)$$

The partial cross section $\sigma_n$ of the $n$-particle final state is proportional to $F_n$, i.e.

$$\frac{\sigma_n}{\sigma_{tot.}} = F_n \simeq \frac{N}{E} \left(\frac{E^3 V}{\pi^2}\right)^n \frac{1}{n!(3n-1)!}$$

The most probable multiplicity at fixed energy $\bar{n}$ is determined by $(\partial/\partial n) F_n = 0$, i.e. where $F_n$ becomes maximum. The value of $\bar{n}$ is found to be,

$$\bar{n} = \left(\frac{VE^3}{27\pi^2}\right)^{1/4} \propto E^{3/4} \qquad (12)$$

which agrees with Fermi.[10] The growth of multiplicity with energy is too fast to be consistent with experiments (1).

(B) *With Mass Spectrum Consideration:* In order to overcome the difficulty of (A), we must introduce a mass spectrum function to take into account the degeneracy in mass observable due to different states of spin, charge, strangeness, baryon number etc. The mass spectrum $\rho(m)$ is defined by the property that $\rho(m)\, dm$ is equal to the number of different hadronic states with mass in $(m, m + dm)$. Hagedorn[11] and Frautschi[15] have obtained the result

$$\rho(m) = c\, m^a\, e^{bm} \tag{13}$$

with $a = -5/2$, and $b \simeq (160\,\mathrm{Mev})^{-1}$, through the statistical bootstrap model. Dual Models and Veneziano models[20] produce a similar form. The low energy portion of (13) has been fitted to experiments[16] in such form

$$\rho(m) = c(m_0^2 + m^2)^{-5/4}\,\mathrm{Exp.}\,(m/\mathrm{T}_0) \tag{14}$$

with $c = 2.63 \times 10^4\,\mathrm{Mev}^{3/2}$, $m_0 = 500\,\mathrm{Mev}$ and $\mathrm{T}_0 = 160\,\mathrm{Mev}$.

Taking the mass spectrum (13) into account, the statistical factor for the $n$ particle final state is

$$\begin{aligned} \mathrm{F}_n &= \mathrm{N}\left(\frac{\mathrm{V}}{(2\pi)^3}\right)^n \frac{1}{n!} \prod_{i=1}^{n} \int dm_i\, \rho(m_i) \\ &\qquad \cdot \int d^3 p_j\, \delta(\mathrm{E} - \textstyle\sum \mathrm{E}_i)\, \delta^3(\sum \boldsymbol{p}_i) \\ &= \mathrm{N}\,\frac{(c\mathrm{V})^n}{(2\pi)^{3n}}\,\frac{1}{n!} \prod_{i=1}^{n} \int dm_i\, m_i^a\, e^{bm_i} \\ &\qquad \cdot \int d^3 p_i\, \delta(\mathrm{E} - \textstyle\sum \mathrm{E}_i)\, \delta^3(\sum \boldsymbol{p}_i) \end{aligned} \tag{15}$$

where N is a normalization constant. The lower limit of the $m_i$ integration can not be zero, otherwise the integral diverges. Setting $\mathrm{E}_i = m_i + \mathrm{Q}_i$, in terms of kinetic energy $\mathrm{Q}_i$, the exponential factor becomes

$$\prod_{i=1}^{n} e^{bm_i} = e^{b\sum m_i} = e^{b(\sum \mathrm{E}_i - \sum \mathrm{Q}_i)} = e^{b\mathrm{E}} \prod_{i=1}^{n} e^{-b\mathrm{Q}_i} \tag{16}$$

and

$$\begin{aligned} \mathrm{F}_n &= \mathrm{N}\,\frac{(c\mathrm{V})^n}{(2\pi)^{3n}}\,\frac{e^{b\mathrm{E}}}{n!} \prod_{i=1}^{n} \int dm_i\, m_i^a \\ &\qquad \cdot \int d^3 p_i\, e^{-b\mathrm{Q}_i}\, \delta(\mathrm{E} - \textstyle\sum \mathrm{E}_i)\, \delta^3(\sum \boldsymbol{p}_i) \end{aligned} \tag{17}$$

The integral (17) can be evaluated only approximately. Consider the relation between momentum and kinetic energy

$$p_i^2 = \mathrm{E}_i^2 - m_i^2 = 2m_i\,\mathrm{Q}_i + \mathrm{Q}_i^2 \tag{18}$$

Since the momentum integration is effectively cut off at $\mathrm{Q}_i \simeq b^{-1}$ due to the factor $e^{-b\mathrm{Q}_i}$, the integral favors large $m_i$. For large $m_i$,

we can approximate $p_i \simeq (2m_i Q_i)^{1/2}$ and thus the integral for the $i$th particle has the approximate value

$$\begin{aligned} I_i &\equiv \int dm_i\, m_i^a \int d^3 p_i\, e^{-bQ_i} \\ &\simeq \int_{m_0}^{A_i} dm_i\, m_i^{a+3/2} \int_0^\infty 4\pi\sqrt{2}\, Q_i^{-1/2} e^{-bQ_i}\, dQ_i \\ &\simeq \left(\frac{2\pi}{b}\right)^{3/2} \ln \frac{A_i}{m_0} \end{aligned} \tag{19}$$

where the upper limit $A_i$ is fixed by energy conservation. So that

$$F_n \simeq N \frac{(cV)^n}{(2\pi)^{3n}} \frac{e^{bE} A_n^{-5/2}}{n!} \left(\frac{2\pi}{b}\right)^{3(n-1)/2} \prod_{i=1}^{n-1} \ln\left(\frac{A_i}{m_0}\right) \tag{20}$$

$$\sum_{i=1}^{n} A_i = E$$

where $A_n^{-(5/2)}$ is the integration of the $n$th particle considering momentum and energy conservation. $F_n$ is maximal when $A_i \simeq E/n$, and so is of order

$$F_n \simeq N \frac{cV}{(2\pi)^3} \left(\frac{E}{n}\right)^{-5/2} \frac{1}{n!} \left(\frac{cV}{(2\pi b)^{3/2}} \ln \frac{E}{nm_0}\right)^{n-1} \tag{21}$$

For high multiplicity reactions, the most probable multiplicity $\bar{n}$ can be obtained by the condition $(\partial/\partial n) \ln F_n = 0$. With the aid of Stirling's formula and neglecting the terms of order $\ln n/n$, we get

$$\begin{aligned} \bar{n} &\simeq \frac{cV}{(2\pi b)^{3/2}} \ln \frac{E}{\bar{n} m_0} \simeq \frac{cV}{(2\pi b)^{3/2}} \ln \frac{E}{m_0} \\ &\simeq A \ln s + B \end{aligned} \tag{22}$$

with $s = E^2$, $A = cV/2(2\pi b)^{3/2}$ and $B = -2A \ln m_0$. Equation (22) is consistent with experiments (1).

In terms of $\bar{n}$,

$$F_n \simeq N \frac{cV}{(2\pi)^3} \left(\frac{E}{n}\right)^{-5/2} \frac{\bar{n}^{n-1}}{n!} \tag{23}$$

The normalization constant N can further be fixed through the approximation of the saddle point method,

$$\begin{aligned}\sum F_n &= 1 \\ &\simeq \int^{\infty} F_n \, dn \\ &\simeq \left[\frac{2\pi}{(\ln F_{\bar{n}})''}\right]^{1/2} F_{\bar{n}} \\ &\simeq N e^{b\mathrm{E}} e^{\bar{n}} \left(\ln \frac{\mathrm{E}}{\bar{n} m_0}\right)^{-1} \left(\frac{\mathrm{E}}{\bar{n}}\right)^{-5/2} \end{aligned} \tag{24}$$

Eliminating N from (23) and (24), we obtain the result

$$\frac{\sigma_n}{\sigma_{\mathrm{tot.}}} = F_n \simeq \left(\frac{n}{\bar{n}}\right)^{5/2} \frac{\bar{n}^n e^{-\bar{n}}}{n!} \simeq \frac{\bar{n}^n e^{-\bar{n}}}{n!} \tag{25}$$

which is almost the Poisson distribution except for the factor $(n/\bar{n})^{5/2}$ which should be dropped for consistency of the approximation made in (24), otherwise the right hand side of (25) would not be exactly normalized to unity. This is surprisingly in good consistency with experiments[17] in view of rough approximations we have made in calculation.

## V. MULTIPLICITY—GRAND CANONICAL ENSEMBLE CALCULATION

For numerical comparison with experiments, we will calculate the average multiplicity again through the grand canonical ensemble and under better approximation. Considering only central collision, the total angular momentum is zero. According to quantum statistical mechanics, the average number of particles in a state of energy $\varepsilon$ produced in the volume V of the fireball during decay should be proportional to

$$\frac{1}{e^{\beta\varepsilon} - 1} \tag{26}$$

with constant $\beta$ fixed by the condition that the total energy of particles produced is equal to the energy E of the fireball. Here we use the formula for bose particles. It will be shown in the following calculation that the type of statistics of the particles does not matter much in high energy collisions. The average number of particles of mass $m$ and momentum $p$ and energy $\varepsilon$ is given by

$$d\bar{n} = \frac{V}{(2\pi)^3} \frac{\rho(m)\, dm\, d^3p}{e^{\beta\varepsilon} - 1}, \qquad \varepsilon^2 = p^2 + m^2 \tag{27}$$

For avoiding the complication at the lower limit of $m$-integration, taking $\rho(m)$ as given in (13), the average total number of particles produced becomes

$$\begin{aligned} \bar{n} &= \frac{V}{(2\pi)^3} \int_{m_0}^{\infty} dm\, \rho(m) \int_0^{\infty} \frac{4\pi p^2\, dp}{e^{\beta\varepsilon} - 1} \\ &= \frac{cV}{2\pi^2} \int_{m_0}^{\infty} dm\, m^{-5/2} e^{bm} \sum_{l=1}^{\infty} \int_0^{\infty} dp\, p^2 e^{-l\beta\varepsilon} \end{aligned} \tag{28}$$

For fermions, the series in (28) is alternative instead. The appearence of fermions in the final state would at most correct the second term in the expansion, which will be shown to be negligible in comparison with the dominant first term in the high energy limit. For the same reason, we will take only the first two terms for estimation. Change variables,

$$\varepsilon = mu, \qquad p = m\sqrt{u^2 - 1} \tag{29}$$

then

$$\bar{n} = \frac{cV}{2\pi^2} \int_{m_0}^{\infty} dm\, m^{1/2} e^{bm} \sum_{l=1}^{\infty} I_l \tag{30}$$

with

$$I_l = \int_1^{\infty} du\, u\sqrt{u^2 - 1}\, e^{-l\beta m u} \tag{31}$$

$$= \int_0^{\infty} du(u+1)\sqrt{u+2}\,\sqrt{u}\, e^{-l\beta m(u+1)} \tag{32}$$

The maximum of the integrand of (32) occurs at $u < 2$ if $\beta m_0 \geq 1$, the factor $\sqrt{u+2}$ can then be approximated as

$$\sqrt{2+u} \simeq \sqrt{2}\left(1 + \frac{u}{4} - \frac{u^2}{32} + \ldots\right)$$

Thus

$$\begin{aligned} I_l &\simeq e^{-l\beta m} \int_0^{\infty} du(u+r)\, u^{1/2} \sqrt{2}\left(1 + \frac{u}{4} - \frac{u^2}{32}\right) e^{-l\beta m u} \\ &\simeq \sqrt{2}\, e^{-l\beta m} \frac{\Gamma(3/2)}{(l\beta m)^{3/2}} \left(1 + \frac{15}{8l\beta m} + \frac{105}{128} \cdot \frac{1}{(l\beta m)^2}\right) \end{aligned} \tag{33}$$

If we substitute (33) into (30) and keep only the first two terms, we obtain the average number of particles

$$\bar{n} \simeq \frac{cV}{(2\pi\beta)^{3/2}} \left[ \mathrm{E}_i(x) + e^{-x} \left( \frac{15}{8\beta m_0} + \frac{105}{256(\beta m_0)^2} - \frac{105x}{256(\beta m)^2} \right) - \left( \frac{15}{8\beta m_0} - \frac{105x}{256(\beta m_0)^2} \right) x \, \mathrm{E}_i(x) \right] + (\beta \to 2\beta) \tag{34}$$

where $x = (\beta - b)\, m_0$ and $\mathrm{E}_i(x)$ is the exponential integral defined as

$$\mathrm{E}_i(x) = \int_x^\infty \frac{e^{-t}}{t}\, dt \tag{35}$$

It should be mentioned that $\beta$ can not be smaller than $b$, otherwise the integral (30) diverges. Actually the value of $\beta$, as determined from the energy relation will be derived later, is larger than and about the value of $b$, and approaches to $b$ as $\mathrm{E} \to \infty$. Given $b = 1/160$ Mev, the factor $\beta m_0 \gtrsim 1$ if we take $m_0$ either as the rest mass of pion or 500 Mev as (14). As $\mathrm{E} \to \infty$, $x \to 0$ and

$$\begin{aligned} \bar{n} &\simeq \frac{cV}{(2\pi\beta)^{3/2}} \left[ -\ln x - \gamma + x + e^{-x} \left( \frac{15}{8\beta m_0} + \frac{105}{256(\beta m_0)^2} \right) - \frac{15}{8\beta m_0} x \, \mathrm{E}_i(x) \right] + (\beta \to 2\beta) \\ &\simeq \frac{cV}{(2\pi\beta)^{3/2}} \left\{ -\ln x - \gamma + x + e^{-x} \left( \frac{15}{8\beta m_0} + \frac{105}{256(\beta m_0)^2} \right) - \frac{15}{8\beta m_0} x \, \mathrm{E}_i(x) + \frac{1}{2\sqrt{2}} \left[ \frac{13}{80} \mathrm{E}_i(\beta m_0 + x) + e^{-\beta m_0 - x} \left( \frac{15}{16\beta m_0} - \frac{1}{10\beta m_0} \right) \right] \right\} \end{aligned} \tag{36}$$

where $\gamma$ is the Euler number 0.577. The second term is quite small. For $x = 0.1$, it contributes less than 5%.

The total energy of particles produced is given by

$$\mathrm{E} = \frac{cV}{(2\pi)^3} \int \frac{\rho(m)\, \varepsilon}{e^{\beta\varepsilon} - 1}\, dm\, d^3p \tag{37}$$

$$= \frac{cV}{2\pi^2} \int_{m_0}^\infty dm\, m^{-5/2} e^{bm} \sum_{l=1}^\infty \int_0^\infty dp\, p^2 \varepsilon\, e^{-l\beta\varepsilon} \tag{38}$$

by changing variables as (29). We follow a similar process and approximation, and reach the result,

$$E \simeq \frac{cV}{(2\pi\beta)^{3/2}} m_0 \left[ \frac{e^{-x}}{x} + \frac{27}{8\beta m_0} E_i(x) + \frac{45}{8(\beta m_0)^2} (e^{-x} - x E_i(x)) \right] + (\beta \to 2\beta) \quad (39)$$

As $x \to 0$, $E \to \infty$ and

$$E \simeq \frac{cVm_0}{(2\pi\beta)^{3/2}} \left[ \frac{e^{-x}}{x} + \frac{27}{8\beta m_0} E_i(x) + \frac{45}{8(\beta m_0)^2} (e^{-x} - x E_i(x)) \right] \quad (40)$$

and

$$\ln E \simeq \ln \frac{cV}{(2\pi\beta)^{3/2}} m_0 - \ln x - x + x e^x \left[ \frac{27}{8\beta m_0} E_i(x) + \frac{45}{8(\beta m_0)^2} (e^{-x} - x E_i(x)) \right] \quad (41)$$

From equations (36) and (40), as $x \to 0$, the average multiplicity becomes

$$\bar{n} \simeq A \ln s + B \quad (43)$$

with

$$A = \frac{cV}{2(2\pi\beta)^{3/2}} \quad (44)$$

$$B = 2A \left\{ - \ln 2Am_0 - \gamma + 2x + e^{-x} \left( \frac{15}{8\beta m_0} + \frac{105}{256(\beta m_0)^2} \right) - \frac{15}{8\beta m_0} x E_i(x) + \frac{1}{2\sqrt{2}} \left[ \frac{13}{80} E_i(\beta m_0 + x) + e^{-\beta m_0 - x} \left( \frac{15}{16\beta m_0} - \frac{1}{10\beta m_0} \left( 1 - \frac{1}{\beta m_0} \right) \right) \right] - x e^x \left[ \frac{27}{8\beta m_0} E_i(x) + \frac{45}{8(\beta m_0)^2} (e^{-x} - x E_i(x)) \right] \right\} \quad (45)$$

$$\simeq 2A \left[ - \ln 2Am_0 - \gamma + \left( \frac{15}{8\beta m_0} + \frac{105}{256(\beta m_0)^2} \right) \right] \quad (46)$$

The result of (43)-(46) is the same as that obtained from direct phase space calculation (22), except (46) gives a more accurate value of B. Another important point is that among the two constants A and B in (43), only one is independent. And (46) provides

the relation between A and B. The multiplicity distribution of the grand canonical ensemble is a Gaussian distribution around $\bar{n}$, in contrast to the Poisson distribution of (25). This is no contradiction. As E increases, $n$ would be so large that the Poisson distribution will approach a Gaussian distribution in mathematics. Physically the grand canonical ensemble is equivalent to the microcanonical ensemble only in the same limit where terms of order $\ln n/n$ are negligible.

The average multiplicity (43) is in good consistency with the form of experimental average multiplicity of charged particles (1). It is interesting to see how the two constants A and B fit, and how accurate the relation (46) is. The results are given in Table 1.

*Table 1.* The Average Multiplicity $\langle n \rangle = A \ln s + B$

| | | | A | B |
|---|---|---|---|---|
| Experimental[17] $\langle n_{\text{ch.}} \rangle$ | | | 0.97±0.33 | 0.28±2.00 |
| | | (L) | 0.91±0.05 | 0.79±0.20 |
| Theoretical $\bar{n}$ | $x = 0$ E → ∞ | $m_0$ = 140 Mev | 2.58 | 6.74 ( 1.56) |
| | | 300 | | 1.95 (−0.14) |
| | | 500 | | 0.13 |
| | $x = 0.1$ | $m_0$ = 140 Mev E = 6.3 Gev | 2.11 | 3.20 |
| | | $m_0$ = 300 Mev E = 9.3 Gev | 2.34 | 0.96 |
| | | $m_0$ = 500 Mev E = 13 Gev | 2.55 | −0.34 |

The numerical results of Table 1 are obtained under the following conditions: (a) Experimentally, only charged particles are observed. The entry (L) indicates that low energy data are included. (b) In theoretical calculation, we take the volume of the fireball $V = (4\pi/3) R^3$ and $R \simeq 1/m_\pi$, $b^{-1} = 160$ Mev. (c) B is calculated from (46). (d) Furthermore we take $A \simeq A_{\text{expt.}} \simeq 1$ in evaluating

B and E, otherwise the values of B and E should be multiplied by a factor of A. (e) The entry of $x = 0$ corresponds to $E \to \infty$. The limit is effectively reached if $E \gtrsim 100$ Gev. And the $x = 0.1$ entry is corresponding to low energy results ($E \sim 10$ Gev) given for comparison. (f) The values of B and E strongly depend on the 4th and last terms of (45), which are neglected in Frautschi's method of approximation (19) and the corresponding values of B are given in parentheses.

From Table I, we make the following observations: (a) The value of A is consistent with $A_{expt.}$ in the order of magnitude, despite the rough estimation of V. Furthermore, since $\bar{n}$ includes neutral particles as well, if neutral particles and charged particles are equally popular in $\rho(m)$, then $\bar{n} \simeq 2\langle n_{ch.} \rangle$ and $A \simeq 2A_{expt.}$. The predicted value would be very accurate. (b) The value of B is strongly dependent on $m_0$, and decreases drastically in the lower energy region. Unfortunately, $m_0$ can not be precisely determined by $\rho(m)$ in the low mass region where the discrete spectrum has been approximated as a continuous function. For a more accurate test of the relation (46) between A and B, the contributions of the lower discrete portion of $\rho(m)$ should be calculated seperately. The predicted result will fit experimental values at $m_0 \simeq 300$ Mev. (c) The slight increasing of both A and B with energy is consistent with experiments. Note that in spite of inaccuracy, $B_{expt.}$ at high energy limit should be larger than its value at low energy, since the slope $A_{expt.}$ of the curve $\langle n_{ch.} \rangle$ is larger at high energy limit.

In conclusion, the results (43)-(46) of our model fit very well with experiments both in the form and numerical values.

## VI. TRANSVERSE MOMENTUM AND SINGLE PARTICLE INCLUSIVE SPECTRUM

Since the complete display of dependence on all momenta is impractical for high energy multiparticle reactions, the most important quantity usually quoted is the single particle inclusive spectrum. In the process

$$a + b \to c + \mathrm{X} \tag{47}$$

with momenta

$$p_a + p_b \to p + \ldots \tag{48}$$

where X stands for whatever else produced, the unpolarized single particle inclusive spectrum is defined as

$$\mathrm{F}(p_\parallel, p_\perp, s) = \mathrm{E}_p[d^3\sigma(a + b \to c + \mathrm{X})/d^3p] \tag{49}$$

Organization of the data on single particle inclusive spectra has been greatly facilitated by the scaling and limiting fragmentation hypotheses. The limiting fragmentation hypothesis[18] assumes that $\mathrm{F}(p_\parallel, p_\perp, s)$ approaches an asymptotic limit for large $s$, i.e.,

$$\mathrm{F}(p_\parallel, p_\perp, s) \simeq \mathrm{F}(p_\parallel, p_\perp) \tag{50}$$

as $s$ becomes large if $p_\parallel$ is held fixed. This is partially confirmed by experiments. While the scaling hypothesis[14] says that as $s \to \infty$,

$$\mathrm{F}(p_\parallel, p_\perp, s) \simeq \tilde{\mathrm{F}}(x, p_\perp) \tag{51}$$

where $x = 2p_\parallel^*/s^{1/2}$, and $p_\parallel^*$ is the longitudinal momentum in the CM system.

According to our model, the probability for producing a particle of energy $\varepsilon$ in the fireball decay is equal to

$$f(\varepsilon) = \text{const.}\frac{\mathrm{V}}{e^{\beta\varepsilon} \pm 1} \tag{52}$$

($-$ for fermion, $+$ for boson), where the constant $\beta$ can be determined from (39) and written in terms of the incident energy E. From (40), as $\mathrm{E} \to \infty$, $x \to 0$, i.e., $\beta \to b$. In other words, $\beta \geq b \simeq 1/160$ Mev. For hadrons, $m \gtrsim \beta^{-1}$; since $\varepsilon^2 = p^2 + m^2$, thus $\beta\varepsilon \gg 1$ and so

$$f(\varepsilon) \simeq \text{const.}\,\mathrm{V}\, e^{-\beta\varepsilon} \tag{53}$$

In the CM system, the kinetic energy of a produced particle is about the order of $\beta^{-1}$ according to statistical mechanics. Or

$$\left\langle \frac{p^2}{2m} \right\rangle \simeq \frac{3}{2}\beta^{-1} \lesssim \frac{3}{2}b^{-1}.$$

The transverse momentum $p_\perp$, which is invariant under longitudinal Lorentz transformation, is equal to

$$\langle p_\perp^2 \rangle = \frac{1}{3} \langle p^2 \rangle \lesssim m\, b^{-1} \tag{54}$$

or

$$\langle p_\perp \rangle \lesssim \sqrt{\frac{m}{b}} \lesssim 0.4\ \text{Gev/c} \tag{55}$$

if $m$ taken to be 1 Gev. This is in good agreement with experiments as quoted in section I. The smallness of $p_\perp$ is due to the exponentially divergent mass degeneracy (14), which implies that $\beta \geq b \simeq 1/160$ Mev.

From (52) and the basic assumption (2), the single-particle inclusive spectrum can be written as

$$F(p_\parallel, p_\perp, s) = \text{const.}\, \varepsilon\, I_i \frac{V}{e^{\beta\varepsilon} \pm 1} \tag{56}$$

$$\simeq \text{const.}\, I_i\, \varepsilon\, V\, e^{-\beta(p_\parallel^2 + p_\perp^2 + m^2)^{1/2}} \tag{57}$$

where $\langle p_\parallel^2 \rangle$ and $\langle p_\perp^2 \rangle$ are of the order $\beta^{-2} \lesssim (160\ \text{Mev})^2$ in the CM system. When transformed to the laboratory system $p_\perp$ stays unchanged, while $p_\parallel$ becomes the order of $\varepsilon$. As $s = E^2 \to \infty$, $I_i \to$ const. and $\beta \to b$. Since V is $s$-independent, the single particle inclusive spectrum (57) satisfies the scaling and limiting fragmentation properties (50)-(51).

Recent measurements[3-7] of large transverse momentum ($p_\perp > 1$ Gev/c) phenomena in wide angle scattering seem inconsistent with the exponential law (53), if V is $s$-dependent as in Fermi's model. Meng[19] had found that these large $p_\perp$ phenomena can fit (53), if V is assumed to be $s$-independent as in our model, and $\beta$ is proportional to $s^{-1/8}$ as obtained from Stefan's law. In other words, above mentioned data can fit the formula for $\theta = 90°$ obtained from (53)

$$\ln \frac{d^3\sigma}{dp^3}(\theta = 90°, p_\perp, s) \simeq \text{const.}\, p_\perp\, s^{-1/8} \tag{58}$$

for energies in the interval (23.2 Gev~62.4 Gev).

In our model, this must be calculated from (40). For large E, we keep only the first term of (40), and obtain

$$\beta \simeq b + \frac{cV}{(2\pi\beta)^{3/2}} \frac{1}{E} \qquad (59)$$

By (44), $cV/(2\pi\beta)^{3/2} = 2A$. In terms of Gev units for energy, taking $A = A_{expt.} \simeq 1$, and $b^{-1} \simeq 0.16$, one obtains

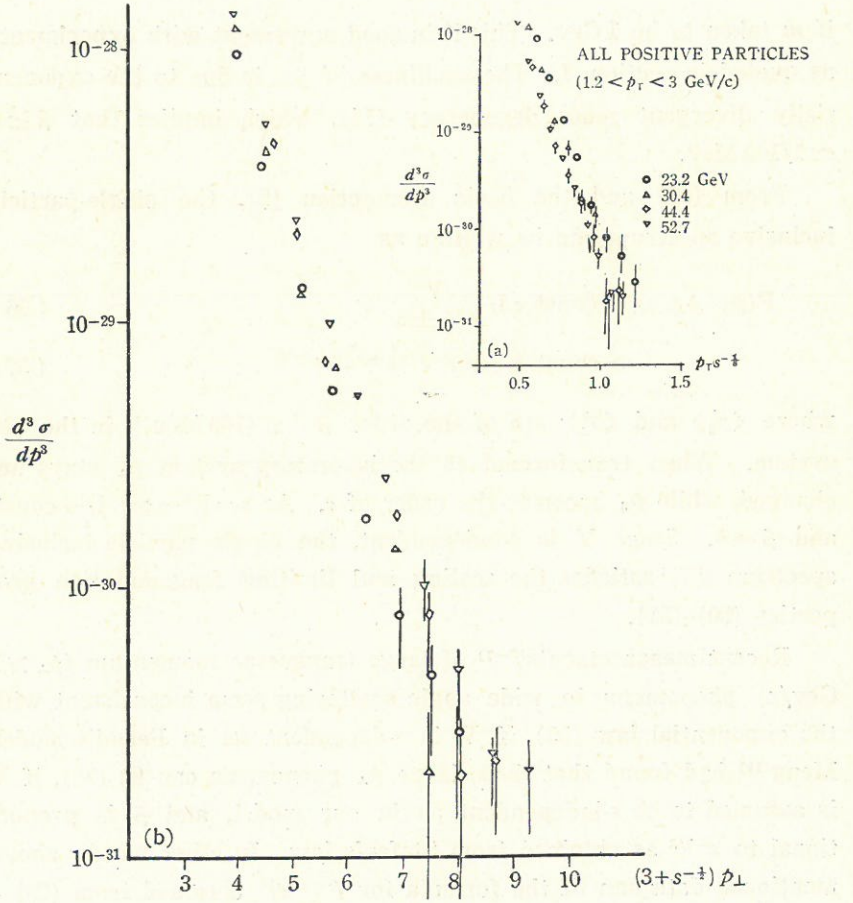


Fig. 1. Single particle inclusive cross section for all positive charged particles at $\theta = 90°$ in the CM system plotted according to (a) modified Fermi's model and (b) our model respectively, with $\sqrt{s}$ in Gev and $d^3\sigma/dp^3$ in $cm^2\,c^3/sr\,Gev^3$.

$$\beta \simeq 6 + 2s^{-1/2} \simeq 2(3 + s^{-1/2}) \qquad (60)$$

Note that the first term dominates. From (53) and (58), the resulting formula for $\theta = 90^\circ$ becomes (in the CM system)

$$\ln \frac{d^3\sigma}{dp^3}(\theta = 90^\circ, p_\perp, s) = \text{const.}\,(3 + s^{-1/2})\, p_\perp \qquad (61)$$

Studying the data and figures presented by Meng, we find that our result (61) fits the data better than that of the modified Fermi model (58). For comparison, a typical example is shown in Fig. 1, where the single charged particle inclusive cross-section for all positive particles at $\theta = 90^\circ$ are plotted according to (58) and (61) respectively. Other data show similar features and will be published in a separate paper. The essential ingredients that lead to the correct result (61) are a constant decay volume and a nearly constant decay temperature at high energy.

## VII. ANGULAR DISTRIBUTION

The angular distribution of produced particles in the CM system is not neccessarily isotropic, which is true only for central collision. In general, the distribution is expected to be somehow anisotropic in order to conserve total angular momentum. During collision, initial energy and angular momentum are dumped into a fireball of volume V, which is assumed to be independent of invariant energy $s$ in the high energy limit. Then the fireball decays into various channels.

Consider a side-tracked collision of two nucleons in the CM system as shown in Fig. 2. A reference system is introduced at

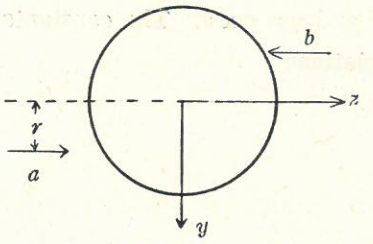


Fig. 2. The Decay of a Fireball.

the center of the fireball and with its $z$-axis along the direction of collision. Initially two nucleons $a$ and $b$ collide in $yz$-plane with an impact parameter $2r$. In high energy collision, each carries a momentum of about E/2, and so the initial total angular momentum is equal to

$$L_x \simeq \frac{E}{2} \cdot 2r = Er \tag{62}$$

where E is initial energy.

In the decay of the fireball, conservations of energy and angular momentum imply that the average number of produced particles in a state of energy $\varepsilon$ and angular momentum $l_x$ is proportional to

$$\frac{1}{e^{\beta\varepsilon - \lambda l_x} - 1}, \qquad \varepsilon^2 = p^2 + m^2 \tag{63}$$

The constants $\beta$ and $\lambda$ are fixed by energy and angular momentum conservation relations. For a particle emitted from the point $(x, y, z)$ in the fireball,

$$l_x = yp\cos\theta - zp\sin\theta\cos\varphi \tag{64}$$

where $(p, \theta, \varphi)$ indicates its momentum in spherical coordinates. Taking the mass degeneracy of (13) into account, the average number of particles produced can be calculated from

$$d\bar{n} = \frac{dV\, d^3p}{(2\pi)^3} \frac{\rho(m)\, dm}{e^{\beta\varepsilon - \lambda l_x} - 1}$$

$$= \frac{c}{(2\pi)^2} \frac{m^{-5/2} e^{bm} p^2\, dp\, d\eta\, dm\, dV}{e^{\beta\varepsilon - \lambda l_x} - 1} \tag{65}$$

where $\varepsilon^2 = p^2 + m^2$ and $\eta = \cos\theta$. The constants $\beta$ and $\lambda$ are fixed by the following relations

$$E = \int \varepsilon\, d\bar{n} \tag{66}$$

and

$$L_x = \int l_x\, d\bar{n} \tag{67}$$

The angular distribution is given by

$$\frac{d\bar{n}}{d\eta} = \frac{c}{(2\pi)^2}\int \frac{m^{-5/2}e^{b\,m}p^2\,dp\,dm\,dV}{e^{\beta\varepsilon-\lambda l_x}-1} \tag{68}$$

which in general will depend on $\varphi$ through $l_x$. In actual experiments, it is not just two particles in collision, instead, a continuous beam of particles collides with the target in axial symmetry. In that case, one should take the average over $\varphi$.

Unfortunately the integrals (65)-(68) can only be solved by a tedious computor work. Here we would like to extract some results by making approximations. For simplicity, we assume the fireball to be a flattened sphere, although the volume is $s$-independent, such that $z \simeq 0$ everywhere. Then $l_x \simeq py\eta$ and

$$\begin{aligned}\frac{d\bar{n}}{d\eta} &= \frac{c}{4\pi}\int_{m_0}^{\infty}dm\int_0^{\infty}dp\int_{-R}^{R}dy\,\frac{m^{-5/2}e^{b\,m}p^2(R^2-y^2)}{e^{\beta\varepsilon-\lambda p y\eta}-1}\\ &= \frac{3cV}{(4\pi)^2}\int_{m_0}^{\infty}dm\int_0^{\infty}dp\int_{-1}^{1}du\,\frac{m^{-5/2}e^{b\,m}p^2(1-u^2)}{e^{\beta\varepsilon-\alpha p u}-1}\end{aligned} \tag{69}$$

with $u = y/R$ and $\alpha = \lambda R\eta$. The integration can be done by series expansion of the exponential factor,

$$\begin{aligned}\frac{d\bar{n}}{d\eta} &= \frac{3cV}{(4\pi)^2}\int dm\,dp\,du\,m^{-5/2}e^{b\,m}p^2(1-u^2)\sum_{k=1}^{\infty}e^{-k(\beta\varepsilon-\alpha p u)}\\ &= \frac{cV}{(4\pi)^2}\int dm\,dp\,m^{-5/2}e^{b\,m}p^2e^{-\beta\varepsilon}\sum_{n=1}^{\infty}\frac{6n(\alpha p)^{2(n-1)}}{(2n+1)!}\\ &\quad+\sum_{k=2}^{\infty}\end{aligned} \tag{70}$$

where $\sum_k$ sums over terms obtained from the first part of (70) by the substitution $(\alpha \to k\alpha,\ \beta \to k\beta)$. The integration over $p$ can be done by setting $\varepsilon = m + Q$, and so $p^2 = 2mQ + Q^2$, $dp \simeq d(2mQ)^{1/2} \simeq m dQ/\sqrt{2mQ}$, then

$$\begin{aligned}\int_0^{\infty}dp\,e^{-\beta\varepsilon}p^{2n} &= e^{-\beta m}m\int_0^{\infty}\frac{dQ}{\sqrt{2mQ}}(2mQ+Q^2)^n e^{-\beta Q}\\ &= m\,e^{-\beta m}\sum_{l=0}^{n}\frac{n!}{(n-l)!\,l!}(2m)^{n-l-1/2}\frac{\Gamma(n+l+1/2)}{\beta^{n+l+1/2}}\end{aligned} \tag{71}$$

Substituting into (70), we obtain

$$\frac{d\bar{n}}{d\eta} = \frac{cV}{(2\pi)^2} \sum_{n=1}^{\infty} \sum_{l=0}^{n} \frac{\alpha^{2(n-1)}}{\beta^{n+l+1/2}} \cdot \frac{6n \cdot n!\, 2^{n-l-1/2}\, \Gamma(n+l+1/2)}{(2n+1)!\,(n-l)!\,l!} \mathrm{I}_{nl} + \sum_{k=2}^{\infty} \tag{72}$$

where

$$\mathrm{I}_{nl} = \int_{m_0}^{\infty} dm\, m^{n-l-2} e^{-(\beta-b)m} \tag{73}$$

$$= \begin{cases} \dfrac{1}{m_0}\left(e^{-x} - x\,\mathrm{E}_i(x)\right) & l = n \\ \mathrm{E}_i(x) & l = n-1 \\ e^{-x}\left(\dfrac{m_0}{x}\right)^{n-l-1} \displaystyle\sum_{m=0}^{n-l-2} \dfrac{(n-l-2)!}{(n-l-2-m)!}\, x^{n-l-2-m} & \\ \qquad \xrightarrow[x \ll 1]{} e^{-x}\left(\dfrac{m_0}{x}\right)^{n-l-1} (n-l-2)! & l \leq n-2 \end{cases} \tag{74}$$

where $x = (\beta - b)\, m_0$ and $x \to 0$ as $\mathrm{E} \to \infty$. After some rearrangement of terms,

$$\frac{d\bar{n}}{d\eta} = \frac{cV}{(2\pi\beta)^{3/2}} (\mathrm{T}_1 + \mathrm{T}_2 + \mathrm{T}_3) + \sum_{k=2}^{\infty} \tag{75}$$

where

$$\mathrm{T}_1 = \frac{1}{\beta m_0}\left(e^{-x} - x\,\mathrm{E}_i(x)\right) \sum_{n=0}^{\infty} \frac{6(n+1)\,\Gamma(2n+5/2)}{(2n+3)!\,\sqrt{\pi}}\, \rho^n, \qquad \rho = \left(\frac{\alpha}{\beta}\right)^2 \tag{76}$$

$$\mathrm{T}_2 = \mathrm{E}_i(x) \sum_{n=0}^{\infty} \frac{12(n+1)^2\,\Gamma(2n+3/2)}{(2n+3)!\,\sqrt{\pi}} \tag{77}$$

$$\mathrm{T}_3 = e^{-x} \sum_{n=2}^{\infty} \sum_{l=0}^{n-2} \sum_{m=0}^{n-l-2} \frac{6n \cdot n!\,(n-l-2)!\, 2^{n-l}\,\Gamma(n+l+1/2)}{(2n+1)!\,(n-l)!\,l!\,(n-l-2-m)!\,\sqrt{\pi}} \cdot \left(\frac{m_0}{x}\right)^{n-l-1} x^{n-l-2-m}\, \frac{\alpha^{2(n-1)}}{\beta^{n+l-1}} \tag{78}$$

$$\simeq e^{-x} \sum_{l=0}^{\infty} \frac{\rho^l}{l!}\, t_l \tag{79}$$

$$t_l = \sum_{n=0}^{\infty} \gamma^{n+1}\, \frac{6(n+l+2)(n+l+2)!\, 2^{2n+3}\,\Gamma(n+2l+5/2)}{(n+1)(n+2)(2n+2l+5)!\,\sqrt{\pi}}, \qquad \gamma = \left(\frac{\alpha^2 m_0}{2\beta x}\right) \tag{80}$$

The conditions for convergence of the above series are

$$\left(\frac{\alpha}{\beta}\right)^2 < 1 \quad \text{and} \quad r < 1 \tag{81}$$

For numerical evaluation, one should further estimate the values of these series (76)-(80). $T_1$ and $T_2$ can be written as

$$T_1 \simeq \frac{1}{\beta m_0}\left(e^{-x} - x\,E_i(x)\right)\left(\frac{3}{4} + \frac{21}{32}\rho + \frac{3\cdot 9\cdot 11}{4\cdot 8\cdot 16}\rho^2 + \cdots + S_{n_0}\right) \tag{82}$$

$$T_2 \simeq E_i(x)\left(1 + \frac{3}{4}\rho + \frac{81}{8\cdot 16}\rho^2 + \cdots + S_{n_0}\right) \tag{83}$$

where $S_{n_0}$ is the partial sum starting from $n = n_0$ and can be estimated by

$$S_{n_0} \simeq \begin{cases} \dfrac{6}{\sqrt{\pi}}\left(\dfrac{e}{2}\right)^{3/2}\dfrac{(n_0+2)^{1/2}}{\delta}\rho^{n_0}\left(1 - \dfrac{1}{2\delta} + \dfrac{3}{4\delta^2} - \cdots\right), \\ \qquad\qquad \delta > 1 \\ 6\left(\dfrac{e}{2}\right)^{3/2}(-\ln\rho)^{-1/2}\rho^{n_0}\left(1 - 2\sqrt{\dfrac{\delta}{\pi}}\right), \\ \qquad\qquad \delta \equiv -(n_0+2)\ln\rho \ll 1 \end{cases} \tag{84}$$

while $t_l$ can be approximated as a corresponding integral and then solved by the steepest descent method and Stirling's formula for factorials. The result shows that

$$t_l \simeq 6\sqrt{2}\, r \int_0^\infty e^{f(n)}\,dn,$$

$$\simeq 12\sqrt{2}\,\frac{r}{(-\ln r)}\,(-4r\ln r)^{-l}\,l! \tag{85}$$

$$f(n) = \ln\left[r^n\,\frac{6(n+l+2)(n+l+2)!\,2^{2n+3}\,\Gamma(n+2l+5/2)}{(n+1)(n+2)(2n+2l+5)!\,\sqrt{2\pi}}\right]$$

for $l \geq 3$ and $r \geq e^{-(1-2/l)}$. For low $l$, the series are calculated exactly,

$$t_0 = \frac{2}{3} + \frac{2}{r} - \ln(1-r) + \frac{2}{r^{3/2}}\tanh^{-1} r^{1/2} \tag{86}$$

$$t_1 = \frac{3}{8}\left[1 + \left(\frac{1}{r} - 2\right)\ln(1-r)\right] \tag{87}$$

$$t_2 = \frac{3}{64}\left[(14r^{-1} - 27)\ln(1-r) + 14 + \frac{2r}{1-r}\right] \tag{88}$$

Thus for $x \ll 1$,

$$T_3 \simeq e^{-x} \sum_{l=0}^{\infty} \frac{1}{l!} t_l \rho^l$$

$$\simeq e^{-x} \left( t_0 + t_1 \rho + \frac{1}{2} t_2 \rho^2 + \ldots + 12\sqrt{2} \frac{\gamma}{-\ln \gamma} I_{l_0} \right) \quad (89)$$

where $I_{l_0}$ is the partial sum starting from $l = l_0$ and

$$I_{l_0} = \sum_{l=l_0}^{\infty} z^l = \frac{z^{l_0}}{1-z} \quad (90)$$

with $z = -\rho/4\gamma \ln \gamma$. This series converges only for $z < 1$, i.e.,

$$\rho = \left( \frac{\alpha}{\beta} \right)^2 < -4\gamma \ln \gamma \quad (91)$$

From (66) and (67), the total energy and total angular momentum of the emitted particles can be written as

$$E = \frac{3cV}{(4\pi)^2} \int_{m_0}^{\infty} dm \int_0^{\infty} dp \int_{-1}^{1} d\eta \int_{-1}^{1} du \frac{m^{-5/2} e^{bm} p^2 \varepsilon (1-u^2)}{e^{\beta\varepsilon - \alpha p u} - 1} \quad (92)$$

$$L_x = \frac{3cV}{(4\pi)^2} \int_{m_0}^{\infty} dm \int_0^{\infty} dp \int_{-1}^{1} d\eta \int_{-1}^{1} du \frac{m^{-5/2} e^{bm} p^3 R u \eta (1-u^2)}{e^{\beta\varepsilon - \alpha p u} - 1} \quad (93)$$

Similar calculations and approximations lead to the result that

$$E = \frac{3cV}{(2\pi\beta)^{3/2}} (E_1 + E_2 + E_3) + \sum_{k=2}^{8} \quad (94)$$

with

$$E_1 = \frac{1}{\beta^2 m_0} (e^{-x} - x E_i(x)) \sum_{n=0}^{\infty} \frac{6(n+1)\Gamma(2n+7/2)}{(2n+3)!\,(2n+1)\sqrt{\pi}} \rho^n \quad (95)$$

$$\simeq \frac{1}{\beta^2 m_0} (e^{-x} - x E_i(x)) \left( \frac{15}{8} + \frac{63}{64} \rho + \ldots + S_{n_0} \right) \quad (96)$$

$$E_2 = E_i(x) \beta^{-1} \sum_{n=0}^{\infty} \frac{3\Gamma(2n+5/2)}{(2n+1)(2n+3)!\sqrt{\pi}} \quad (97)$$

$$\simeq E_i(x) \beta^{-1} \left( \frac{9}{4} + \frac{35}{32} \rho + \ldots + S_{n_0} \right) \quad (98)$$

$$E_3 = e^{-x} \sum_{n=1}^{\infty} \sum_{l=0}^{n-1} \frac{\alpha_0^{2(n-1)}}{\beta^{n+l-1}} \frac{6n(n+l+1)\, n!\, 2^{n-l}\, \Gamma(n+l+1/2)}{(2n-1)(n-l+1)(2n+1)!\,(n-l)!\, l!\sqrt{\pi}}$$

$$\cdot \left( \frac{m_0}{x} \right)^{n-l} \sum_{m=0}^{n-l-1} \frac{(n-l-1)!}{(n-l-1-m)!} x^{n-l-1-m} \quad (99)$$

$$\underset{x \ll 1}{\simeq} \frac{m_0 e^{-x}}{x} \left( e_0 + e_1 \rho + \frac{1}{2} e_2 \rho^2 + \ldots + 6\sqrt{2} \frac{1}{-\ln \gamma} I_{l_0} \right) \quad (100)$$

$$e_0 = \frac{3}{2}\left[\frac{1}{r} + (r-1)\, r^{-3/2} \tanh^{-1} r^{1/2}\right] \tag{101}$$

$$e_1 = \frac{3}{8}\left[5r^{-1} - 3r^{-1} \ln (1-r) - 5r^{-3/2} \tanh^{-1} r^{1/2}\right] \tag{102}$$

$$e_2 = \frac{3}{32}\left[\frac{10}{r} + \frac{1}{2(1-r)} + \left(\frac{10}{r^2} - \frac{54}{5}\right) \ln (1-r) - \frac{14}{3r}\left(\frac{1}{3} + \frac{1}{r} - \frac{1}{r^{3/2}} \tanh^{-1} r^{1/2}\right)\right] \tag{103}$$

where $\alpha_0 = \lambda R$, $\rho = (\alpha_0/\beta)^2$, and $r = \rho\beta/2(\beta - b)$. The total angular momentum,

$$L_x = \frac{cVR}{(2\pi\beta)^{3/2}}\left(\frac{2r}{\alpha_0}\right)(L_1 + L_2 + L_3) + \sum_{k=2}^{\infty} \tag{104}$$

with

$$L_1 = \frac{x}{(\beta m_0)^2}(e^{-x} - xE_i(x)) \sum_{n=0}^{\infty} \frac{3\Gamma(2n+9/2)}{(2n+5)(2n+3)^2(2n+1)!\sqrt{\pi}} \rho^n \tag{105}$$

$$\simeq \frac{x}{(\beta m_0)^2}(e^{-x} - xE_i(x))\left(\frac{7}{16} + \frac{9 \cdot 11}{10 \cdot 16}\rho + \ldots + S_{n_0}\right) \tag{106}$$

$$L_2 = \frac{x}{\beta m_0} E_i(x) \sum_{n=0}^{\infty} \frac{6(n+2)\,\Gamma(2n+7/2)}{(2n+5)\,(2n+3)^2\,(2n+1)!\,\sqrt{\pi}} \rho^n \tag{107}$$

$$\simeq \frac{x}{(\beta m_0)} E_i(x)\left(\frac{1}{2} + \frac{9 \cdot 9}{10 \cdot 16}\rho + \ldots + S_{n_0}\right) \tag{108}$$

$$L_3 = \frac{e^{-x}}{2r} \sum_{n=0}^{\infty} \sum_{l=0}^{n} \frac{6(n+2)!\, 2^{n-l+1}\Gamma(n+l+5/2)}{(2n+5)(2n+3)^2(2n+1)!\,(n+2-l)!\,l!\sqrt{\pi}} \cdot \frac{\alpha_0^{2(n+1)}}{\beta^{n+l+1}} \sum_{m=0}^{n-l} \frac{(n-l)!}{(n-l-m)!} x^{n-l-m} \tag{109}$$

$$\underset{x \ll 1}{\simeq} e^{-x}\left(M_0 + M_1\rho + \frac{1}{2}M_2\rho^2 + \ldots + 6\sqrt{2}\,\frac{1}{-\ln r} I_{l_0}\right) \tag{110}$$

$$M_0 = \frac{3}{2}\left[\frac{1}{r^2} + (r-1)\, r^{-5/2} \tanh^{-1} r^{1/2}\right] - \frac{1}{r} \tag{111}$$

$$M_1 = \frac{1}{8}\left[\frac{1}{3r} + \frac{1}{r^2} - \frac{2}{r} \ln (1-r) - \frac{1}{r^{5/2}} \tanh^{-1} r^{1/2}\right] \tag{112}$$

$$M_2 = \frac{3}{64r}\left[\frac{118}{25} + \left(\frac{14}{3r} - \frac{54}{5}\right) \ln (1-r) + \frac{r}{1-r} + \frac{4}{15}\left(\frac{1}{3r} + \frac{1}{r^2} - \frac{1}{r^{5/2}} \tanh^{-1} r^{1/2}\right)\right] \tag{113}$$

From (62) and (94)-(113), the impact parameter $r$ is given by

$$\frac{r}{R} = \frac{L_x}{RE} = \left(\frac{2r}{\alpha_0}\right) \frac{L_1 + L_2 + L_3}{E_1 + E_2 + E_3} \tag{114}$$

$$\underset{x \ll 1}{\simeq} \frac{\alpha_0}{\beta} \frac{(M_0 + M_1\rho + (1/2)M_2\rho^2 + \ldots + 6\sqrt{2}(1/-\ln r)I_{l_0}) + e^x(L_1+L_2)}{(e_0 + e_1\rho + (1/2)e_2\rho^2 + \ldots + 6\sqrt{2}(1/-\ln r)I_{l_0}) + (xe^x/m_0)(E_1+E_2)} \tag{115}$$

where all high order terms $\Sigma_{k=2}$ have been neglected, which at most brings a few percent uncertainty. For ordinary experiments, $r$ is not fixed, one should average over $r$ in order to obtain the correct answer. This is too complicated to be done for such a complicated function of $\alpha_0$ and $\beta$ as shown in (115). Instead of taking the average over $r$, we take a medium value $r = R/\sqrt{2}$ as Fermi did, and study the angular distribution at fixed energy. From (44), $cV/(2\pi\beta)^{3/2} = 2A$ and take $A \simeq A_{\text{expt.}} \simeq 1$, the total energy is given by

$$E \simeq 2(E_1 + E_2 + E_3) \tag{116}$$

The conditions for convergence of E and $L_x$ are the same as those of $d\bar{n}/d\eta$, (81) and (91), if only $\alpha$ is replaced by $\alpha_0$. Recall that $\alpha = \alpha_0\eta$ and $|\eta| \leq 1$, the over-all conditions for convergence are

$$\left(\frac{\alpha_0}{\beta}\right)^2 < 1, \quad r < 1 \quad \text{and} \quad \rho < -4r\ln r \tag{117}$$

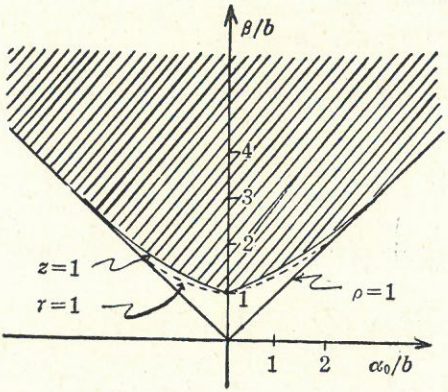


Fig. 3. The allowed region of $\alpha_0$ and $\beta$.

The allowed values of $\alpha_0$ and $\beta$ lie in the shaded region of Fig. 3 shown. On the boundary, E becomes infinite.

Take $bm_0 = 1$ and $l_0 = 4$, at $E = 32\,Gev$ and $r = R/\sqrt{2}$, we obtain from (115)-(116) and (90)

$$z = -\rho/4r \ln r = 0.727$$
$$r = 0.809 \qquad (118)$$

or $\beta \simeq 1.406b$, $\alpha_0 \simeq 0.99b$ and $\rho \simeq 0.5$. Substituting these into (75),

| $\eta$ | 0 | 0.2 | 0.4 | 0.6 | 0.8 | 0.9 | 0.94 | 0.98 | 1.0 |
|---|---|---|---|---|---|---|---|---|---|
| Theo. | 2.18 | 2.23 | 2.47 | 2.88 | 4.29 | 8.77 | 15.91 | 55.69 | 153.08 |
| Expt. | 2.18 | 2.20 | 2.37 | 2.89 | 4.75 | 8.60 | 13.00 | 30.00 | 157.05 |

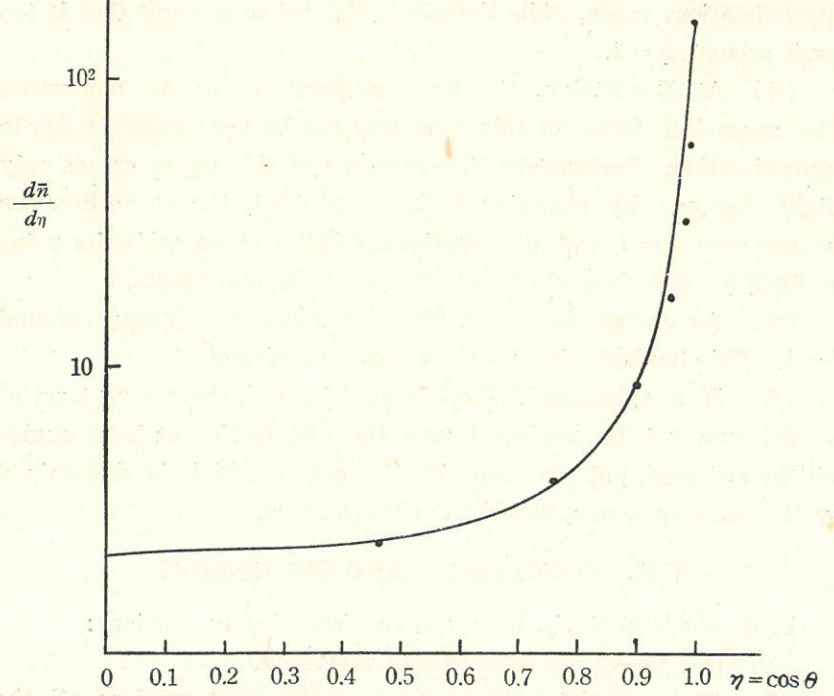


Fig. 4. The Angular Distribution at $E = 32\,Gev$. (The solid line represents the theoretical result, while dots indicate experimental data.)

the angular distribution is calculated. The result is shown in Fig. 4 in comparison with experiments. Note $d\bar{n}/d\eta$ is the over-all angular distribution at fixed energy and proportional to $d\sigma_n/\sigma_n d\eta$ at $n = \bar{n}$. Since experimental data[19] on $d\sigma_n/\sigma_n d\eta$ are not given in absolute values, the ordinate normalization of Fig. 4 is arbitrary, and so the theoretical result is normalized such that it coincides with experimental value at $\eta = 0$.

The above calculations, therefore, prove the following points:

(1) The angular distribution (75) is symmetric with respect to the $z = 0$ plane as expected, since both $\rho$ and $\tau$ are proportional to $\eta^2$.

(2) By (115), as $E \to \infty$, $r/R \simeq \alpha_0/\beta$; and for small $\beta$, $E \to \infty$ even though $\rho < 1$ as seen from Fig. 3.

(3) The angular distribution predicted by our model is in good consistency with experiments as shown in Fig. 4, in spite of rough approximations made, while Fermi's model led to a result that is too small around $\eta = 1$.

(4) At $E = 32$ Gev, the term proportional to $I_{l_0}$ dominates. The numerical factor of this term may not be very accurate due to approximation. Fortunately, the variation of this factor causes only slight change. By changing a factor of $10^{-1}$, the curve becomes steeper near $\eta = 1$ and fits experiments better there, while its value in $0.8 \lesssim \eta \lesssim 0.94$ is slightly less than experimental values.

(5) As energy increases, the curve becomes steeper around $\eta = 1$. This tendency is consistent with experiment.

(6) If a spherical fireball is used instead, the second term of $l_x$ (64) can not be neglected, and the distribution at large angles will be enforced, but the shape of the curve, which is determined by the mass spectrum, would not change much.

## VIII. CONCLUSION AND DISCUSSION

From above analysis, we reach the following conclusions:

(1) Our model fits experiments very well.

(2) The essential features of our model, that produce all the successful results, are that both the decay volume and the tem-

perature $\beta^{-1}$ approach constant values in the high energy limit. The temperature approaches a constant because of the exponential increasing nature of mass spectrum (13), which in turn may be related to constancy of the decay volume by statistics bootstrap method[15]. Furthermore, if we assume all hadronic matter to approach a constant minimum volume in the high energy limit, then the square well potential assumption (5) which states that the interaction factor $I_i$ is proportional to the overlapping space-time volume, will produce correct asymptotic behavior for total cross section.

(3) All these strongly suggest that all hadronic matter approaches a constant volume in the high energy limit, of a dimension corresponding to the exchange of one pion. This seems contradictory to relativistic contraction of length. Does this imply that relativity fails within such a short distance? No. The reason is that we are trying a semi-classical description to a pure quantum mechanics domain. Within such a distance $R \simeq \hbar m_\pi^{-1}$, particles may exchange energy of order $m_\pi$ via strong interaction. This will cause an uncertainty in the momentum of particles of the same order. The uncertainty relation then implies that there must be an uncertainty in position of order $\Delta x \geq \hbar m_\pi^{-1} \geq R$. Therefore it has no meaning to make a statement about the relativistic contraction within such a short distance as R.

(4) Note that Frautschi's model[15] and Veneziano model[20] allow also other possible values of $a$ of the mass spectrum (4), i.e., $a = -5/2, -3, -7/2, \ldots$. If $a < -5/2$ is taken instead, basically all above results except the multiplicity will not change. In this case, the average multiplicity would be $\bar{n} \simeq 2.4$, which is obviously contradictory to the experiments.

## ACKNOWLEDGEMENT

The auther would like to thank Mr. M. T. Lam, Mr. S. K. Pang and Mr. S. Y. Lee for checking some calculations of Sec. VII and typing the final part.

## REFERENCES

(1) J.W. Elbert *et al.*, *Phys. Rev. Lett.* **20**, 124 (1968).
(2) D.B. Smith *et al.*, *Phys. Rev. Lett.* **23**, 1064 (1969).
(3) B. Alper *et al.*, *Phys. Lett.* **44B**, 521 (1973).
(4) M. Banner *et al.*, *Phys. Lett.* **44B**, 537 (1973).
(5) F.W. Büsser *et al.*, *Phys. Lett.* **46B**, 471 (1973).
(6) J.W. Cronin *et al.*, *Phys. Rev. Lett.* **31**, 1426 (1973).
(7) D.C. Carey *et al.*, *Phys. Rev. Lett.* **32**, 24 (1974).
(8) L.W. Jones *et al.*, *Phys. Rev. Lett.* **25**, 1679 (1970).
(9) E. Fermi, *Prog. Theor. Phys.* **5**, 570 (1950).
(10) E. Fermi, *Phys. Rev.* **81**, 683 (1951).
(11) R. Hagedorn, *Nucl. Phys.* **B24**, 93 (1970).
(12) R. Hagedorn, Invited paper at the colloquium on "*High Multiplicity Hadronic Interactions*" held at Ecole Polytechnique, Paris, May (1970).
(13) J. Ranft, *Phys. Lett.* **31B**, 529 (1970).
(14) R.P. Feynman, *Phys. Rev. Lett.* **23**, 1415 (1969).
(15) S. Frautschi, *Phys. Rev.* **3D**, 2821 (1971).
(16) R. Hagedorn, *Nuovo Cimento* **52A**, 1336 (1967).
(17) W.R. Frazer *et al.*, *Rev. Mod. Phys.* **44**, 284 (1972).
(18) J. Benecke *et al.*, *Phys. Rev.* **188**, 2159 (1969).
(19) T. Meng, *Phys. Rev.* **9**, 3063 (1974).
(20) K. Huang and S. Weinberg, *Phys. Rev. Lett.* **25**, 895 (1970).

# TWO-CURRENT MODEL IN NICKEL-RICH NICKEL-CHROMIUM ALLOYS

YEONG-DER YAO


## ABSTRACT

It is demonstrated that the two-current model in nickel-rich nickel-chromium alloys is definitely limited. For Ni-Cr alloys with Cr concentration smaller than 5.5 at.%, the deviations from Matthiessen's rule of the resistivity can be explained by a two-current model. However, it is not valid for Ni-Cr alloys with Cr concentration larger than 11.3 at.%.


## INTRODUCTION

The concept of two current conduction was first suggested by Mott[1]. It was used to explain the deviations from Matthiessen's rule[2] of the resistivity measurements of dilute iron based alloys by I. A. Campbell *et al.*[3] Later, Schwerer and Conroy[4] reported that their experimental data of dilute Ni–Cr alloys with Cr concentration smaller than 5 at.% can be analyzed under the two current model. In this paper, we shall combine the experimental data of Ni–Cr alloys reported by Yao *et al.*[5] and Schwerer *et al.*[4] to analyze the limitation of the two-current conduction in nickel-rich nickel-chromium alloys.

Under the assumption that there is only one type of current carrier and that the scattering processes which cause resistance are independent, the Matthiessen's rule can be expressed as:

$$\rho_a(C, T) = \rho_p(T) + \rho_0(C) \qquad (1)$$

where $\rho_0(C)$ is the resistivity produced by the impurity at 0°K, $\rho_p(T)$ is the resistivity of an ideal pure metal, and $\rho_a(C, T)$ is the resistivity of a dilute alloy containing a concentration C of impurity.

In fact, there are always deviations from Matthiessen's rule. However, in many cases, these deviations are very small, and Matthiessen's rule represents quite a good approximation to the experimental data. We can always write $\rho_a(C, T)$ exactly as

$$\rho_a(C, T) = \rho_p(T) + \rho_0(C) + \Delta(C, T) \qquad (2)$$

Presuming that $\rho_b(T)$, $\rho_a(C, T)$ and $\rho_0(C)$ can be determined experimentally, Equation (2) provides a definition for the quantity $\Delta(C, T)$. We call this experimental value of $\Delta(C, T)$ the "Deviation from Matthiessen's Rule" associated with the concentration C of the given solute in the given solvent. The existence of a non-zero $\Delta(C, T)$ has been known for over 100 years, ever since the original study by Matthiessen and Vogt. However, with the exception of a flurry of interest in the early 1930's, quantitative investigation of the form and magnitude of $\Delta(C, T)$ proceeded rather slowly until quite recently. From the previous work devoted to this topic,[6-11] the existence of the deviation from Matthiessen's rule in systems involving defects other than substitutional impurities is demonstrated.

According to the two-current model in which spin up and spin down electrons conduct in parallel, the resistivity, $\rho_a(C, T)$, can be represented as follows:[3]

$$\rho_a(C, T) = \Big\{[\rho_\uparrow(0) + \rho_{a\downarrow}(T)][\rho_\downarrow(0) + \rho_{a\downarrow}(T)] + \frac{1}{2}\rho_{\uparrow\downarrow}(T)[\rho_\uparrow(0) + \rho_\downarrow(0) + \rho_{a\uparrow}(T) + \rho_{a\downarrow}(T)]\Big\} \Big/ \{\rho_\uparrow(0) + \rho_\downarrow(0) + \rho_{a\uparrow}(T) + \rho_{a\downarrow}(T) + 2\rho_{\uparrow\downarrow}(T)\} \quad (3)$$

where $\rho_\uparrow(0)$ and $\rho_\downarrow(0)$ are the impurity residual resistivities for the two spin directions, $\rho_{\uparrow\downarrow}(T)$ is the resistivity due to the spin-mixing which is characterized by a relaxation time $\tau_{\uparrow\downarrow}$. $\rho_{a\uparrow}(T)$ and $\rho_{a\downarrow}(T)$ are the thermal resistances of the alloy for each spin direction; in general, $\rho_{a\uparrow}(T) \neq \rho_{a\downarrow}(T)$. Let $\rho_{b\uparrow}(T)$ be the thermal resistances of the pure host metal for each spin direction, and $\rho_b(T)$ be the resistivity of the pure host metal at temperature T. At low temperatures, both the $\rho_a(T)$ and the $\rho_{\uparrow\downarrow}$ are small. For the simplest case,

$$\rho_{a\uparrow}(T) = \rho_{a\downarrow}(T) = \rho_{b\uparrow}(T) = \rho_{b\downarrow}(T) \equiv \rho(T),$$

and letting

$$\rho(0) = \frac{\rho_\uparrow(0)\,\rho_\downarrow(0)}{\rho_\uparrow(0) + \rho_\downarrow(0)} \quad (4)$$

we get for low temperatures:

$$\rho_a(C, T) = \rho(0) + \rho_h(T) + \frac{1}{2}\frac{[\rho_\uparrow(0)-\rho_\downarrow(0)]^2[\rho(T)+\rho_{\uparrow\downarrow}(T)]}{[\rho_\uparrow(0)+\rho_\downarrow(0)][\rho_\uparrow(0)+\rho_\downarrow(0)+2\rho(T)+2\rho_{\uparrow\downarrow}(T)]}$$
$$\approx \rho(0) + \rho_h(0) + \frac{1}{2}\left[\frac{\rho_\uparrow(0)-\rho_\downarrow(0)}{\rho_\uparrow(0)+\rho_\downarrow(0)}\right]^2[\rho(T)+\rho_{\uparrow\downarrow}(T)] \quad (5)$$

The third term is the deviation from Matthiessen's rule. For the general case, the deviation does not separate out quite as simply; however, it is always positive. The physical picture is that the electrons in the low resistance spin direction, which carry most of the current at low temperature, are "braked" as the temperature rises, and they are brought into contact with slower electrons. At high temperatures, the deviation should saturate. We shall then have:

$$\rho_a(C, T) = \frac{1}{2}[\rho_\uparrow(0) + \rho_\downarrow(0) + \rho_{a\uparrow}(T) + \rho_{a\downarrow}(T)] \quad (6)$$

## ANALYSIS AND DISCUSSIONS

A detailed list of proposed sources for the deviation from Matthiessen's rule is given in the review article by Bass.[11] In this paper, we only want to show the deviation from Matthiessen's rule of Yao *et al.*'s experimental data.[5] Due to the experimental difficulty, the value of $\rho_0(C)$ is replaced by the resistivity at 4.2°K. Also, we define a deviation parameter $\Delta(C, T)$ by

$$\Delta(C, T) = [\rho_m(T) - \rho_m(4.2)]_{alloy} - [\rho_m(T) - \rho_m(4.2)]_{pure}$$
$$\equiv \Delta\rho(C, T) - \rho_c \quad (7)$$

where

$$\Delta\rho(C, T) \equiv [\rho_{alloy}(T) - \rho_{pure}(T)]_{measured}$$
$$\equiv [\rho_m(T)]_{alloy} - [\rho_m(T)]_{pure} \quad (8)$$

$$\rho_c \equiv [\rho_m(4.2)]_{alloy} - [\rho_m(4.2)]_{pure} \quad (9)$$

and $\rho_m(T)$ is the measured resistivity at temperature T.

Figure 1 shows the temperature-dependent behavior of $\Delta\rho(C, T)$, which is the difference between the Ni-alloy resistivity and the

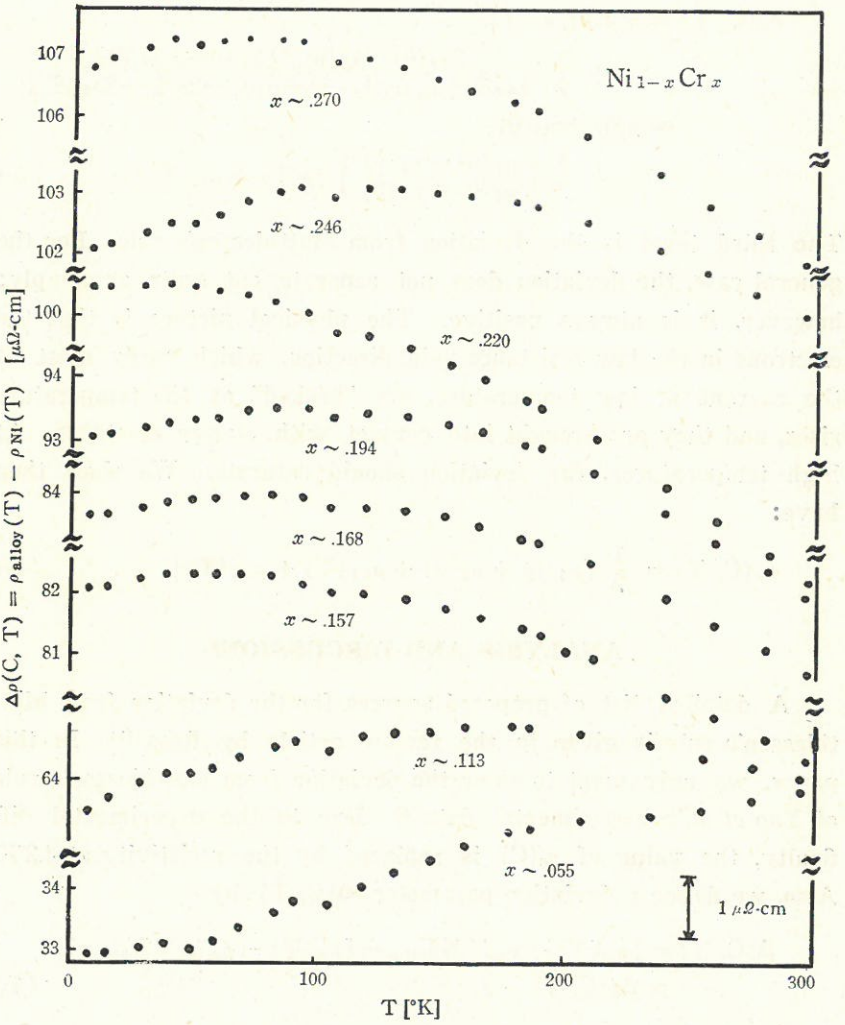


Fig. 1. The difference $\Delta\rho(C, T)$ between the alloy resistivity and the pure Ni sample resistivity for $Ni_{1-x}Cr_x$

"pure" Ni sample resistivity. According to this figure, the temperature-dependent behavior of $\Delta\rho(C, T)$ does not agree with the two-current model for Ni–Cr alloys containing Cr in amounts greater than 11.3 at.%. In other words, the two-current model is based on the spin polarization of the conduction electrons due to the ferromagnetic state of the host metal. For high concentration Ni–Cr

alloys (say, larger than 11.3 at.% Cr), the alloys do not show strong ferromagnetic ordering in the experimental temperature range; and we can probably say that it is in the weak ferromagnetic state for samples up to around 22 at.% Cr. We suggest that the critical composition for weak ferromagnetism is about 22 at.% Cr. We can further suggest that the maximum of the $\Delta\rho(C, T)$ vs. T curve could be a functional change of the Curie temperature of the alloys. Since pure Ni is in the ferromagnetic state below 631°K, the decrease of $\Delta\rho(C, T)$ with increasing temperature could mean that the resistivity of the alloy due to ferromagnetism disappears above a special temperature which is changed according to a special function of the maximum in the $\Delta\rho(C, T)$ curve.

Analyzing the experimental data of the Ni–Cr alloy containing 5.5 at.% Cr, together with the data reported by Schwerer and Conroy[4] for Ni–Cr alloys with Cr concentration smaller than 5 at.%, we conclude that these deviations of Ni–Cr alloys with Cr concentration smaller than 5.5 at.% can be explained by a two-current model in which spin-up and spin-down electrons conduct in parallel.

However, Figure 1 shows evidently that the two-current model is not valid for Ni–Cr alloys with Cr concentration larger than 11.3 at.%. A further detailed analysis of the proposed sources for the deviation from Matthiessen's rule for the Ni–Cr alloys with Cr concentration larger than 11.3 at.% will be published elsewhere.

## ACKNOWLEDGMENTS

I would like to thank Professor S. Arajs and Professor E.E. Anderson[5] who gave the opportunity of performing the experiments in their laboratory, and also to the National Science Council of Republic of China for the financial support of this analysis work.

## REFERENCES

(1) N.F. Mott, *Proc. R. Soc.* **153**, 699 (1936).
(2) A. Matthiessen, *Ann. Phys.* **7**, 761, 892 (1864).
(3) I.A. Campbell, A. Fert and A.R. Pomeroy, *Phil. Mag.* **15**, 977 (1967).

(4) F.C. Schwerer and J.W. Conroy, *J. Phys. F.* **1**, 877 (1971).
(5) Y.D. Yao, S. Arajs and E.E. Anderson, *J. Low Temp. Phys.* **21**, 369 (1975).
(6) G. Borelius, *Handbuch Metall. Physik* **1**, 1 (1935).
(7) H. Jones, *Handbuch der Physik* **19**, 227 (1956).
(8) D.K.C. MacDonald, *Handbuch der Physik* **14**, 137 (1956).
(9) A.N. Gerritsen, *Handbuch der Physik* **19**, 137 (1956).
(10) F.R. Fickett, *Cryogenics* **11**, 349 (1971).
(11) J. Bass, *Adv. Phys.* **21**, 431 (1972).

# DETERMINATION OF SULFOXIDE CONFIGURATION WITH SHIFT REAGENT

PETER JIH-YUNG CHAO

## INTRODUCTION

The addition of a little $Eu(dpm)_3$ [trisdipivalomethanatoeuropium III] to a solution of any of a great many lone pair-bearing organic compounds gives striking spectral simplifications by virtue of reversible complexation leading to pseudocontact shifts.[1-3] Functional groups give characteristic shift magnitudes in the order $-NH_2 > OH > > C=O > > 0 > -CO_2R > -CN$.[4] Fraser[5] and Wigfield, among others, have applied this shift reagent to sulfoxides and have found the induced shifts useful for assignment of configuration. In general, the chemical shift increases linearly with increasing $Eu(dpm)_3$ concentration for a given substrate concentration.[1-4] The magnitude of induced chemical shift ($\delta$) has been observed to depend also on the position of hydrogen relative to the lanthanide metal in the substrate. Hinckley[6] initially observed that the changes in chemical shifts of hydrogens in the spectrum of cholesterol induced by addition $Eu(dpm)_3$ $(pyridine)_2$ decreased as the cube of the distance of the proton from the coordination site. This observation, and similar results in other steroids[1] were considered to indicate that a pseudocontact (through space) interaction rather than a contact (through bonds) interaction was the major contributor to the observed paramagnetic shifts. Observed shifts using $Eu(dpm)_3$ have been found to correlate with $1/R^3$ in many cases.[7,8] In certain instances, a correction of $\delta$ with $R^{-n}$ $(n = 2-3)$[1,9] was observed, but values of $n$ not equal to 3 are unexpected since a $1/R^3$ dependency for pseudocontact shifts is well established. In solution, the pseudocontact shift (p.s.) may be expressed as follows:

$$\text{p.s.} \cong K(3\cos^2\theta_i - 1)/R_i^3$$

(K is a constant, $\theta_i$ is the angle between the complex axis of the crystal field and the radius vector from the metal to hydrogen $i$, and $R_i$ is the distance between the metal and hydrogen $i$).

Consequently, in addition to the distance relationship, an angular dependency should be found. In compound **4**[10] and **5**[5], upfield shifts were observed using $Eu(dpm)_3$ for the hydrogens with asterisks, while normal shifts to lower field were found for all other hydrogens. The abnormal shift of resonances to high field by $Eu(dpm)_3$ has been rationalized in terms of the angular dependence of the pseudo-contact shift arising from the $(3\cos^2\theta - 1)$ term. Usually, however, assuming the organic donor to be free to rotate about the substrate —Eu bond (whose length is 3 Å or more), the time-averaged value for $\cos^2\theta$ will not differ significantly from proton to proton in the donor. Thus the distance factor will often be the dominant influence on p.s. values, which should then provide valuable stereochemical information.

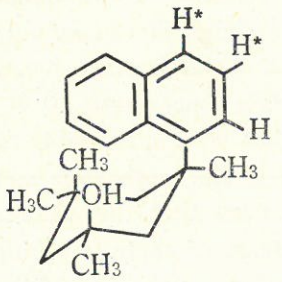


**4**

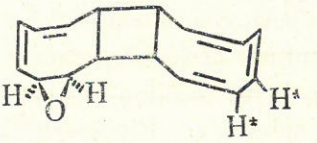


**5**

## RESULTS AND DISCUSSION

7, 8-Dichloro-9-thiabicyclo (4.2.1)-nonane **1** has been prepared in good yield by the addition of sulfur dichloride to *cis, cis*-1, 3-cyclooctadiene. The two chlorine atoms in **1** have been assigned by NMR as cis endo because of the symmetrical NMR spectrum and $J_{8,1} = 7$ ($J_{endo}$, bridgehead $\cong 0$). Treatment of **1** with sodium meta-periodate in ethanol solution gave in 80% yield the sulfoxide **2**, $\nu_{max}^{KBr}$ 1082 $cm^{-1}$ ($>S=O$). With 30% $H_2O_2$ in glacial acetic acid, **2** gave sulfone **3** in 73% yield; $\nu_{max}^{KBr}$ 1300 $cm^{-1}$ ($>SO_2$, $\nu_{as}$), 1110 $cm^{-1}$ ($>SO_2$, $\nu_s$). The configuration of the sulfoxide group in **2** was assigned on the basis of its NMR spectra with a "shift reagent" as described below.

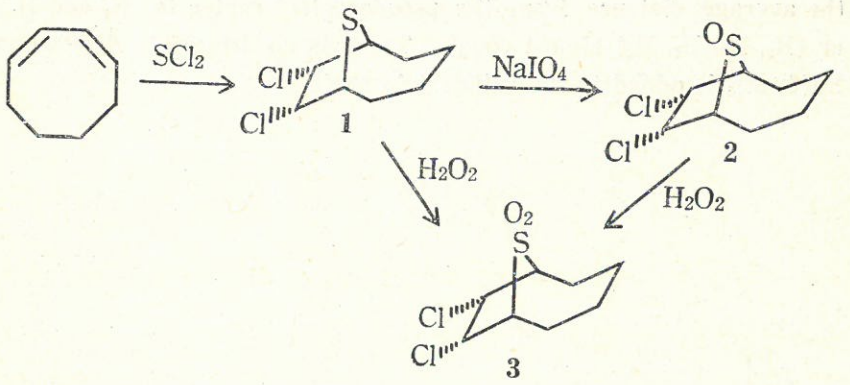


The effect on the resonance positions of the different protons in the sulfoxide **2** upon addition of increasing amounts of $Eu(dpm)_3$ is shown in Figure 1. Since a precipitate forms after the shift reagent is added, it is necessary to filter the solution before every run. All the spectra of **2** show four different shifts. It is difficult to find the exact concentration of $Eu(dpm)_3$ in the solution, but an alternative method can be applied. The change in chemical shift of the bridge protons upon addition of the shift reagent was assumed to be linear with concentration. Fig. 1 reveals that the chemical shift changes for the other protons vary linearly with $Eu(dpm)_3$ concentration defined in this way.

Because $H_7$ and $H_8$ in sulfoxide **2** have much larger concentration dependency than $H_2$, $H_3$, $H_4$ and $H_5$ as shown in Figure 1, the configuration of the sulfoxide group was assigned as syn to the two-carbon bridge.

Sulfone **3** in $CDCl_3$ also shows induced shifts when $Eu(dpm)_3$ is added (Fig. 2), but the magnitude of these pseudocontact shifts is smaller than that for sulfoxide **2**. Figure 2 demonstrates also an essentially linear dependence of the paramagnetic shifts on added $Eu(dpm)_3$ at the lower concentrations. The small curvature at higher concentration might be due to saturation and/or change in coordination geometry. It is worth noting that the slopes of ($H_7$ and $H_8$) and ($H_2$, $H_3$, $H_4$, $H_5$) are not so different as in sulfoxide **2**. The atom presumably complexed (successively) with both oxygens, making

the average distance from the pseudocontact center to ($H_7$ and $H_8$) or ($H_2$, $H_3$, $H_4$, $H_5$) almost equal. There is no detectable shift when $Eu(dpm)_3$ is added to the sulfide **1** in $CDCl_3$.

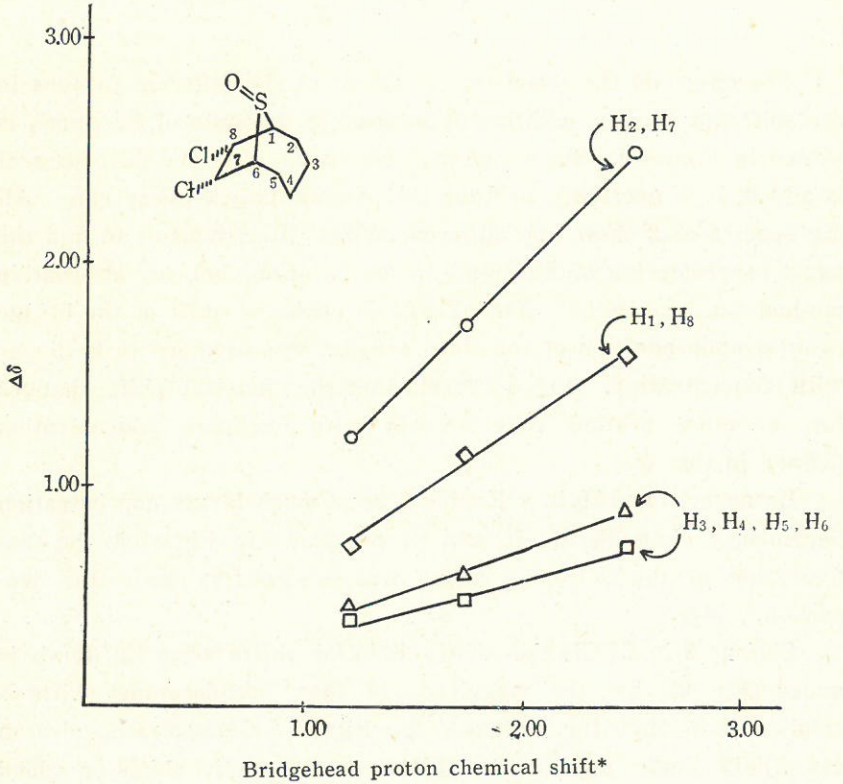


Fig. 1. Plot of changes in chemical shifts vs. concentration of $Eu(dpm)_3$ for protons of sulfoxide **2**

*The chemical shift change of bridgehead protons is assumed to be linear with the conc. of $Eu(dpm)_3$ which was difficult to measure directly due to some precipitation accompanying addition of the reagent.

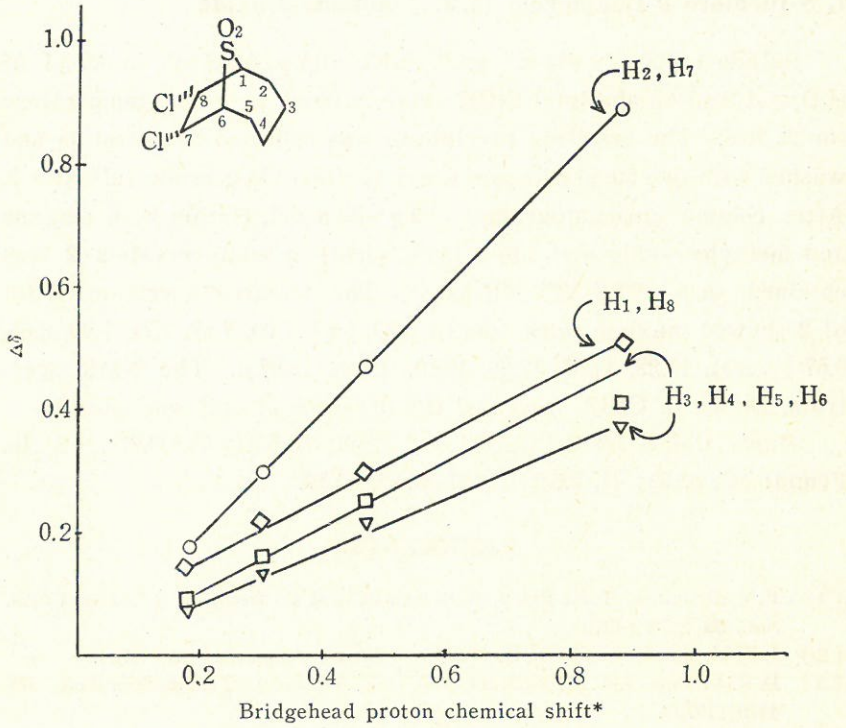


Fig. 2. Plot of changes in chemical shifts vs. concentration of $Eu(dpm)_3$ for protons of sulfone **3**

*The chemical shift change of bridgehead protons is assumed to be linear with the conc. of $Eu(dpm)_3$ which was difficult to measure directly due to some precipitation accompanying addition of the reagent.

## EXPERIMENT

### 7, 8-Dichloro-9-thiabicyclo (4. 2. 1) nonane

From separate funnels 58 g (0.56 m) of freshly-distilled sulfur dichloride in 700 ml of $CH_2Cl_2$ and a solution of 60.8 g (0.56 m) of 1, 3-cyclooctadiene were added with stirring to 1 liter of $CH_2Cl_2$ in a 5 liter 3-necked flask at room temperature (waterbath cooling) over 7 hr. The yellow solution was allowed to stir for an additional 12 hr. Solvent was removed by distillation, leaving 100 ml of brown syrup which was subjected to vacuum sublimination at 80°C twice to give 69.8 g (59.3%) of waxy crystals, m. p. 186–187° (lit. 185.5–186.5°).

**7, 8-Dichloro-9-thiabicyclo (4. 2. 1)-nonane-9-oxide**

Sulfide **1** (3.0 g, 0.014 m) and $NaIO_4$ (3.2 g, 0.015 m) in 25 ml of $H_2O$ and 3 ml of absolute EtOH were stirred at room temperature for 22 hrs. The resulting precipitate was collected by filtration and washed with two 50 ml of warm water to give 3.14 g crude sulfoxide **2**. After column chromatography (20 g silica gel, elution with pentane and methylene chloride) 1.87 g (81% yield) of white crystals **2** was obtained, m. p. 228.2-229° (oil bath). The infrared spectrum (KBr) of **2** showed maxima *inter alia* at 3.39, 6.89, 7.00, 7.57, 7.71, 7.90, 8.65, 9.67 (>SO), 10.22, 11.67, 12.20, 13.10, 13.45, 13.97 $\mu$. The NMR spectrum, shown in $CDCl_3$, revealed the presence of only one isomer.

*Anal.* Calcd. for $C_8H_{12}SOCl$: C, 42.48; H, 5.31; Cl, 30.97; S, 14.16. Found: C, 42.51; H, 5.33; Cl, 31.09; S, 14.19.

## REFERENCES

(1) P. V. Demarco, T. K. Elzey, R. B. Lewis, and E. Wenkert, *J. Amer. Chem. Soc.*, **92**, 5374 (1970).
(2) J. K. M. Sanders, and D. H. Williams, *Chem. Commun.*, 422 (1970).
(3) D. R. Crump, J. K. M. Sanders, and D. H. Williams, *Tetrahedron Lett.*, **50**, 4419 (1970).
(4) J. K. M. Sanders, and D. H. Williams, *J. Amer. Chem. Soc.*, **93**, 641 (1971).
(5) R. R. Fraser, and Y. Y. Wigfield, *Chem. Commun.*, 1471 (1970).
(6) C. C. Hinkley, *J. Amer. Chem. Soc.*, **91**, 5160 (1969).
(7) L. H. Keith, *Tetrahedron Lett.*, 3 (1971).
(8) W. Walter, R. F. Becker and J. Thiem, *ibid.*, 1971 (1971).
(9) B. L. Shapiro, J. R. Hlubucek, G. R. Sullivan ann L. F. Johnson, *J. Amer. Chem. Soc.*, **93**, 3281 (1971).
(10) M. R. Willcott and J. F. M. Oth, J. Thio, G. Plinke, and G. Schroeder, *Tetrahedron Lett.*, 1579 (1971).
(11) E. D. Weil, E. J. Smith and R. J. Gruber, *J. Org. Chem.*, **31**, 1669 (1966).

# A POSSIBLE MECHANISM FOR THE ACTION OF UNIFORM MAGNETIC FIELDS ON THE BIOELECTRIC RESPONSE OF *NITELLA*

LING-CHIA YEH


## ABSTRACT

The bioelectric signals from single internodal cells of the alga *Nitella clavata* have been studied in uniform magnetic fields up to 17 KOe. This study has been carried out by the author in collaboration with Professor Sigurds Arajs and T. E. Farrington, Jr. at the Clarkson College of Technology. The spike amplitude, excitation threshold and propagation velocity are all affected by exposure to magnetic fields either parallel or perpendicular to the streaming protoplasm of the cells. Wei's quantum model of nerve excitation is drawn upon, and a composite model is formulated to account for most of the observed phenomena. It is also shown that Wei's model seems to be capable of resolving the puzzle associated with the production of magnetic field accompanying bioelectric activity.


## INTRODUCTION

It is well known that large individual plant cells respond to electrical, chemical, or even mechanical stimulation in just the same way as a mammalian nerve cell does: with an electric impulse that sweeps along the cell. This instances in the green algae *Nitella* whose cells may be up to 10 cm long, 1 mm or more thick, and nearly cylindrical in shape. The detailed distribution of ions in and around the living cell accounts for its bioelectric properties.

There has been considerable interest in finding the effects of magnetic fields on biological systems[1]. In particular, contrary results have been obtained for studies of bioelectric signals in the presence of applied magnetic fields. For example, the observation made separately by McKendrick[2] and Erdman[3] that constant magnetic fields change the irritability of the isolated frog nerve was completely denied by Liberman *et al*[4]. Using intracellular measurement, Sachava and Samokhvalova[5] found that the membrane

resting potential decreased when *Nitella flexilis* internodes were subjected to constant magnetic field lines intersecting the streaming protoplasm of the *Nitella* cell orthogonally. Arajs, Yeh Lin and Farrington[6] found that, in general, the effect of the magnetic field on the bioelectric response was to reduce the spike amplitude, the propagation speed, as well as the excitability. On the other hand, Blatt[7] studied the effect of homogeneous magnetic fields on the action potentials of *N. flexilis* and *N. translucens* and did not observe any effect on the magnitude or the time course of the action potential.

The author believes that failure to obtain an appreciable effect of the magnetic field is due to unjustified underestimate of the importance of the residual fields of the electromagnets used. In fact, she found that magnetic forces came into play as soon as the experimental sample was introduced into the region between the pole pieces of the magnet. When the sample was allowed to stay long enough in the residual field ($\sim$30–60 min), the effect of the magnetic field gradually became saturated so that no further change would be noticed upon increase of the applied magnetic field strength. Thus the existence of modification in the action potential of *Nitella* due to applied uniform magnetic fields cannot be denied. Furthermore, these observations can be accounted for by using a relatively simple model.

While some investigators have focused their attention on the action of external magnetic fields on plants and animals, others have turned their minds on the magnetic dipole fields produced by plant and animal tissues. The magnetic fields apparently related to electrical impulses traveling along stimulated frog nerves have been recorded. Two important teams of investigators, Seipel *et al*[8] and Gengerelli *et al*[9] arrived at the same conclusion that neuron activity produced signals in coils that were designed to detect the existence of magnetic fields around a propagated nerve impulse. The detected signal was diphasic, and preceded by 0.5 msec the nerve impulse detected by conventional electrodes located at the same region of the nerve. Its direction of deflection was not affected by the direc-

tion of travel of the nerve impulse. No signal could be obtained when the axis of a series-wound coil was oriented at right angles to the long axis of the nerve, while a signal was detected when the axis of the coil was oriented parallel to the long axis of the nerve. This signal progressively dropped to zero when the nerve was gradually dying.

## MODELS OF NERVE EXCITATION

Various concepts have been derived to account for the many intriguing aspects of the electrical activity of the neuron. Qualitatively, these same concepts apply in discussing the electrical activity of the *Nitella*. Specifically, the basic idea of the Hodgkin-Huxley equivalent circuit model[10] is that the ionic characteristics of the membrane are uniquely determined by the potential difference across it. The assertion by Hodgkin and Huxley that sodium ions are all important in the generation of an action potential is, however, not true. A molecular model which includes this model as a special case is the "two-stable-states" theory formulated by Singer and Tasaki[11]. Here, the process of excitation is considered as involving a rapid, reversible cation exchange process, based on transitions between two stable conformational states of the membrane macromolecules. Although the two-stable-states theory accounts for many intriguing phenomena, it is only a qualitative mechanism for excitation and impulse propagation. Wei[12] was able to formulate a more quantitative molecular model. His viewpoint was that nerve impulses could be a macroscopic expression of quantum transitions of electric dipoles at the membrane surface upon stimulation. The quantum theory of nerve excitation started out with the Danielli-Davson model which includes an electric dipole layer at the membrane-external solution interface, with the negative end facing the aqueous phase, an excess of mobile negative ions within the membrane and, in the aqueous phase, an excess layer of mobile positive ions whose concentration is greater than that in the bulk solution. The barrier potential was found to be $E_0 = \sigma s/\varepsilon$, where $\sigma$ is the net charge per unit area on either plane of the dipole layer, $\varepsilon$ the permittivity and $s$ the barrier

width. Thus the barrier potential may be changed by changing the physical state of the dipoles. The latter may be simply achieved by reorienting the dipoles. There are two obvious stable orientations, one parallel and the other anti-parallel with the majority of dipoles in the unexcited membrane. When a negative potential is applied, the negative poles of the dipoles will, by Coulomb repulsion, turn away from the applied negative potential. If the kinetic energy (field strength × dipole moment) gained from the applied field is nearly equal to the energy difference between the two stable orientations, the dipoles will switch to the reverse orientation. If $N_1$ and $N_2$ are the populations per unit area of the parallel and antiparallel dipoles and Q is the charge of the dipole, the surface charge density is

$$\sigma = Q(N_1 - N_2) .$$

Thus, a cathodic potential can depopulate the parallel state and hyperpopulate the antiparallel state and therefore lower the barrier potential. When the barrier potential becomes sufficiently low, a nerve impulse results.

Assuming a value of 20 mV for the outer barrier potential $E_0$ and taking $s = 10$ Å, $\varepsilon = 8.85 \times 10^{-12}$ Farad/m one obtains

$$\sigma = \frac{E_0 \varepsilon}{s} = -1.77 \times 10^{-8} \text{ Coul/cm}^2 .$$

This is in order of magnitude agreement with the measured values by Segal[13] of $-1.9 \times 10^{-8}$ Coul/cm$^2$ and $-4.2 \times 10^{-8}$ Coul/cm$^2$ for squid and lobster respectively. Moreover, the infrared emission from stimulated nerve of crab's leg[14] and the birefringence change coinciding with the action potential observed in several species[15] lent some support to this model.

The identity of the dipoles at the membrane interface was related by Wei[16] to trimethylamine ions $-N^+ \equiv (CH_3)_3$ contained in in a phospholipid. From its structure, this ion species must possess a permanent dipole moment. The $N(CH_3)_3$ may be assumed to have a tetrahedral configuration with the $N^+$ ion sitting at the apex and vibrating relative to the base plane of the three $CH_3$ molecules.

Every time the $N^+$ inverses from "in" to "out", the dipole moment is reversed corresponding to a 180° rotation. Since the $N^+$ is linked to the lipid, it is restrained to spend more time inside than outside. Hence, at equilibrium, there are a greater number of dipoles with positive ends inside, which is compatible with the polarity of the potential difference across the resting membrane. Since nitrogen is a rather active chemical agent, the vibrational state of the trimethylamine ion could be largely affected by the environment.

While examining the dipole flip-flop model of nerve excitation, we discovered that this model can also be used to settle arguments regarding the magnetic field accompanying a nerve impulse. The fact that the direction of travel of the nerve impulse has no effect on the direction of deflection of the magnetic pulse rules out the possibility that such a magnetic pulse is produced by longitudinal currents in the nerve fiber. If one associates the magnetic pulse with transverse membrane currents alone — the inward surge of sodium ions and the subsequent outward surge of potassium ions[17] — then it is difficult to see why the detected magnetic signal preceded by 0.5 msec the nerve impulse detected by conventional electrodes located at the same region of the nerve[9]. A look at the time course of a typical action potential of the squid axon reveals that the duration of the rising phase lies around 0.5–1 msec[10]. It seems therefore more reasonable to assume that the first phase of the magnetic pulse originates from an event that precedes the maximum surge of transverse membrane currents. It is very likely that this event results from the dipole flips. The following arguments provide the basis for this assumption. First, since, the influx of membrane currents starts only after the upper dipole state is sufficiently populated so that the barrier potential is reduced to threshold value, the magnetic pulse due to the dipole flip is expected to precede the impulse detected by electrodes located at the same region of the nerve. Second, the dipoles always flip from the lower state to the upper state no matter from which side they are approached by the local circuit currents, and such a transition can be achieved through motion of charged particles (eg., $N^+$ in the trimethylamine ions) rather than

actual rotation of the dipoles. Thus, the sense of the magnetic pulse should not be affected by the direction of travel of the nerve impulse. An upward transition can be regarded as being equivalent to the $N^+$ ion moving outward along the radial direction. This constitutes a segment of outward directed current. Thus the deflection as indicated by the detection coil should have the same sense as that of the stimulus artifact, since ordinary stimulating currents are cathodic (outward) currents. That this is actually the case is apparent from the composite tracing of the electromagnetic action pulse obtained by Seipel and Morrow[8]. Third, the diphasic nature of the magnetic pulse can also be accounted for if we regard the magnetic pulse as originating from a superposition of two events — the dipole upward transition and the following action current which is also expected to give rise to a variation in the magnetic field. Fourth, as the electrical currents responsible for producing the magnetic pulse are transverse and not longitudinal currents, it is to be expected that a series-wound coil would not detect a signal when it is oriented perpendicular to the axis of the nerve[17]. Thus, the quantum theory of nerve excitation is a sound theory in itself.

## PROPOSED MODEL FOR THE ACTION OF UNIFORM MAGNETIC FIELDS ON THE BIOELECTRIC RESPONSE OF *NITELLA CLAVATA*

The experimental results of the effect of uniform magnetic fields on the action potential of *Nitella clavata* indicate that the applied magnetic fields act on magnetically anisotropic lipid molecules to which the dipoles belong. That such magnetcally anisotropic lipid molecules exist is supported by the observation of reorientation of lipid molecules in magnetic fields[18] and the fact that biological membranes consist mostly of a phospholipid which contains trimethylamine ions near the surface[19]. This model is capable of explaining most of the observed effects of uniform magnetic fields on the action potential of the *N. clavata* internode.

When a magnetic field acts on the polar and magnetically anisotropic molecules, some of them become more or less fixed by the

field, while others get reoriented, depending on the relative orientation of the field lines with respect to the magnetic anisotopy of the molecules. Considering the cylindrical symmetry of the cell, there are always some molecules whose axes of magnetic anisotropy lie at an angle to the magnetic lines of force. (We assume here that these axes are perpendicular to the membrane surface if thermal motion is neglected.) Reorientation necessarily brings some polar groups askew. According to Wei's theory, this causes a drop in the membrane potential. The observed decrease in the action potential of *N. clavata* in the presence of a magnetic field is thus quite understandable. That the membrane potential decreases in magnetic fields has indeed been observed in *N. flexilis*[5].

As a consequence of the fixation of the molecules by the magnetic field, one would expect the membrane to become more stable. At temperatures above absolute zero, the molecules as well as their constituent polar groups are constantly in motion. It is therefore difficult to obtain completely identical action potentials over a long period of time. This fluctuation of action potential amplitude is reduced greatly in the presence of a magnetic field in the case of *N. clavata*. In addition, spontaneous outbursts, which were frequently observed when the *Nitella* cells were newly introduced into the moist chamber, were nearly absent after the magnetic field was applied. This is in agreement with the inhibitory effect of static magnetic fields (1 KOe) on the spontaneous electrical activity of individual neurons in the rabbit head[20].

The observed reduction of the *Nitella* action potential in magnetic fields is gradual and there exists a shallow dip in the curve showing its time dependence (Fig. 1). These observations indicate that there is competition between the external magnetic forces and the internal intra- and intermolecular cohesive forces. The applied field seems to have the upper hand at first. The tug-of-war becomes keener as time goes on, and then repairing forces set in. Finally, a state of equilibrium is reached. At this moment, there is little variation in the action potential amplitudes recorded. The energy source of the repairing or restorative forces must come from metabolism. Thus,

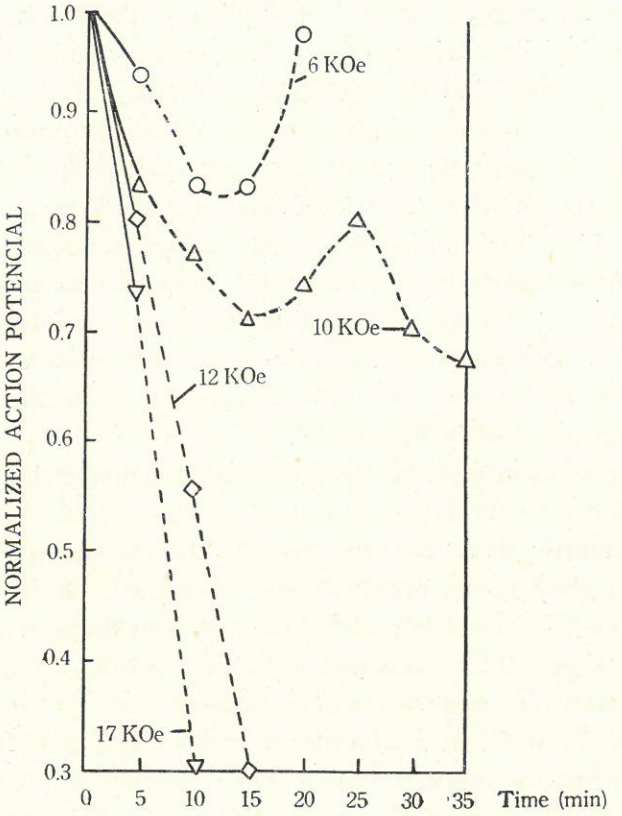


Fig. 1. Normalized Action Potential as a function of time at 25°C.

internodes in different "states of health" ought to give different equilibrium action potential amplitudes as a result of interaction with the same magnetic field. This explains the difficulty of establishing a quantitative proportionality relation between the amplitude of the applied field and the corresponding reduction percentage in the *Nitella* action potential spike amplitude. It also becomes understandable why in a few *Nitella* internodes, no effect on the action potential amplitude could be observed. When an internode had been in the residual field of the electromagnet for some time, no apparent effect of the magnetic field could be observed. This can be attributed to the internodes being already brought to a poor

state of health before the applied field strength was increased from "zero".

We shall now see how the magnetic field affects the excitation threshold of the *Nitella*. Assume that the polar groups responsible for the modulation of ionic flow in the quantum theory of nerve excitation are actually the trimethylamine ions with the $N^+$ vibrating relative to the base plane of the three $CH_3$ molecules. The force of a magnetic field $\vec{B}$ on a particle with charge $q$ and moving at velocity $\vec{v}$ is given by

$$\vec{F} = q\vec{v} \times \vec{B}.$$

Except when the field lines are parallel to $\vec{v}$, the charged particle will experience a sidewise push. Considering the cylindrical symmetry of the *Nitella* internode (and nerve axons in general), it is obvious that there will always be some polar molecules whose dipole axes intercept the magnetic lines of force whatever the relative orientation is between the field and symmetry axis of the cell. Hence, the magnetic field reduces the probability of inversion in either sense. The ratio of the probability of inversion in the presence of a magnetic field to that without the magnetic field is given by the ratio of the two-dimensional mean square displacement in the presence of the field to that without the field. The latter ratio has been found to be[21]

$$\frac{\langle r^2 \rangle_{EB}}{\langle r^2 \rangle_E} = \left[1 + \left(\frac{\Omega}{\nu}\right)^2\right] \exp\left[-w_p^2 \Omega^2 t / \nu(\nu^2 + \Omega^2)\right],$$

where $\Omega$ is the Larmor frequency, $\nu$ is the collision frequency and $w_p$ is the plasma frequency. This result has been derived for the Brownian motion of a charged particle in a viscous medium of constant charge density permeated by a steady magnetic field oriented parallel to the axis of cylindrical symmetry. Nevertheless, it is also applicable to the motion of the $N^+$ particle. The only difference lies in an additional restorative force term for the $N^+$ particle which averages out to zero in the evaluation of $\langle r^2 \rangle$. One should therefore expect the relaxation time of the dipoles in the upper state to

increase when the field is applied. Hence, the chronaxie, being dependent on the relaxation time[16], increases in the presence of the magnetic field. This is in accord with the experimental results on *N. clavata* which indicate that in most cases the threshold for excitation becomes larger in the presence of a magnetic field.

The effect of the magnetic field on the propagation velocity can also be understood from the proposed molecular mechanism. Increase in the relaxation time entails an increase in the latency of response at each point on the path of the action potential. Thus the time required for transmission from one point to another is increased, which decreases the propagation velocity. The slowing down in the action potential wave observed in the magnetic field, as evidenced by a broadening of the trace of the action potential (especially the after-potential), can also be accounted for by this increase in the relaxation time.

The experiments on *N. clavata* indicate that a statististically significant recovery occurs when the cells are exposed for short periods of time in weak fields. However, higher fields affect the cells irreversibly. An explanation may be that at very high fields, the lipid molecules get out of reach of the restorative forces. On removal of the field, the molecules turn loose and get into a state of random vibration and rotation. In this case, the rigidity of the potential barrier is destroyed and the cell fails to respond to further stimulation.

In conclusion, the repressive effect of a constant magnetic field on the action potential of *N. clavata* can be qualitatively described in terms of reorientation of membrane lipid molecules containing polar groups.

## REFERENCES

(1) Barnothy, M. F., *Biological Effects of Magnetic Fields*, Vols. I & II (Plenum Press, New York, 1969).
(2) McKendrick, J. C., *J. Anat. and Physiol.*, **13**, 219 (1879).
(3) Erdman, G. M., Tr. *In-ta biol. fiz.* **1**, 35 (1955).
(4) Liberman, E. A., Vaintsvaig, M. N. and Tsofina, L. M., *Biofizika*, **4**, 152 (1959).

(5) Sachava, T.S. and Samokhvalova, L.I., *Biofizika*, **15**, 89 (1970).
(6) Arajs, S., Yeh Lin L.C. and Farrington, T.E., Jr., *AIP Conf. Proceedings*, 1974 (Magnetism Conference, San Francisco, California).
(7) Blatt, F.J. and Kuo, Y., "*Absence of Biomagnetic Effects in Nitella*", 1975 (to be published in *Biophysical Journal*).
(8) Seipel, J.H. and Morrow, R.D., *Wash. Aca. Sc. Journal*, **50**, 6 (1960).
(9) Gengerelli, J.A., Holter, N.J. and Glasscock, W.R., *J. Psych.*, **52**, 317 (1961).
(10) Hodgkin, A.L. and Huxley, A.F., *J. Physiol.*, **117**, 500 (1952).
(11) Singer, I. and Tasaki, I., in *Biological Membranes, Physical Fact and Function*, edited by Chapman, D. (Academic Press, New York, 1968).
(12) Wei, L.Y., *Biophys. J.*, **18**, 396 (1968).
(13) Segal, J.R., *Biophys. J.*, **8**, 470 (1968).
(14) Fraser, A. and Frey, A.H., *Biophys. J.*, **8**, 731 (1968).
(15) Cohen, L.B., Keynes, R.D. and Hille, B., *Nature*, **218**, 438 (1968).
(16) Wei, L.Y., *Bull. Math. Biophysics*, **33**, 187 (1971).
(17) Gengerelli, J.A., Holter, N.J. and Glasscock, W.R., *J. Psych.*, **57**, 201 (1964).
(18) Gaffney, B.J. and McConnell, H.M., *Chem. Phys. Letters*, **24**, 310 (1974).
(19) Liener, T.E., *Organic and Biological Chemistry* (The Ronald Press, New York, 1966), p. 165.
(20) Kholodov, Yu.A., Alexandrovskaya, M.M., Luk'yanova, S.N. and Udarova, N.S., in *Biological Effects of Magnetic Fields*, Vol. II, edited by Barnothy, M.F. (Plenum Press, New York, 1969), p. 219.
(21) Liboff, R.L., *Phys. Rev.*, **141**, 222 (1966)

"Intensive agriculture is a research-intensive enterprise, and each developing nation must be enabled to manage its agricultural research for itself. The burden is upon scientists in developed nations to assist nations learning the rudiments of this function."

Philip Handler in *Biology and the Future of Man.*

# *DNA* SYNTHESIS IN THE APEX MERISTEM OF WATERMELON SEEDLINGS

PETER B. W. LIU

## INTRODUCTION

It has been reported[9] that gibberellic acid (GA) markedly reduces the length of cell cycles in the genetic dwarf of watermelon primarily by shortening the S phase from 11.3 to 7.2 hours. The shortening of the S phase by GA does not necessarily reflect faster rates of DNA synthesis. Since Mitchison[11] indicated that there were numerous DNA replicating sites which were activated at different times during the S phase in eukaryotes, the decrease of duration of the S phase might result from an increase of the numbers of DNA replicating sites. Kusanagi[6] found that the replication of DNA in barley chromosomes only occurred at the early and late stages during DNA synthetic period but scarcely took place in the middle of the S period. These results suggested that the replication of chromosomal DNA in barley during the S period did not proceed in a continuous temporal sequence. Thus, a continuous or discontinuous DNA synthesis may also affect the length of the S phase. In this experiment, we compare the rate of DNA synthesis at different sequences of time during the S phase between dwarf and GA-treated dwarf watermelon seedlings in order to elucidate the effect of GA on nuclear DNA synthesis in apex meristem.

Brain and Heming[1] first demonstrated that a genetically dwarf variety of pea could be converted to normal phenocopy by GA treatment. Subsequently, a number of similar results of the reversal of genetic dwarfism by GA has been reported in pea[3], corn[13], tomato[14], and cucurbits[10]. It was thus suggested that lower levels of endogeneous GA in genetic dwarfs is the limiting factor in causing the retardation of growth. The attempt to reveal the action of the *dw*-2 dwarf gene in watermelon through DNA synthesis comparison in seedlings of normal and GA-treated dwarf watermelon is conducted.

DNA in Mitochondria and Chloroplast[12,16] which carries essential information necessary for the function and replication of mitochondria may be well correlated with the process of cell division. Degani and Atsmon[2] indicated that GA-enhanced DNA synthesis took place outside the cell nucleus, probably in mitochondria and chloroplast. The effect of hormone on cytoplasmic DNA synthesis is also included in the subsequent studies.

## MATERIALS AND METHODS

Two strains of watermelon seedlings were used for the experiments; a *dw*-2 dwarf inbred line designated WB-2[8] and a normal cultivar, Sugar Baby (SB) (Joseph Harris Seeds Inc., Rochester, N. Y.). Seeds were germinated on two layers of filter paper in petri dishes filled with 15 ml. of distilled water. After 72 hours of germination, the uniform radicles were transferred to the $10^{-4}$ M FURD (5-Fluro-deoxyuridine) solution for 18 hours which was found to be the optimum condition to synchronize the apex meristematic cells in watermelon seedlings by arresting the cells in the G1 stage of cell cycle (unpublished personal data). Following this, all seedlings were transferred to the treatment solutions. The beginning of transference was called initial stage. Four treatments were included in this study; SB control, WB-2 control, WB-2 treated with $3.2 \times 10^{-4}$ M FUDR, containing eight groups of seedlings with 10 in each treatment.

In the meantime, a half hour pulse of 20 ml $^{3}$H-thymidine (10/$\mu$ci/ml) was given at every 2 hours interval to each group of seedlings in the respective treatment for 8 consecutive intervals. At the end of each interval, cotyledons in each seedling were removed and 2 cm of hypocotyl from the tip was cut and rinsed thoroughly. Tips of hypocotyl were defatted in several changes of acetone and ether. The defatted tips were ground in a Tris-45 homogenizer at 4°C adjusted to operate with the continuous additions of approximately 400 ml of grinding medium. During the grinding, the PH of the medium was maintained at 7.2 with 6N NaOH. The grinding medium consisted of 0.3 M mannitol, 0.1% bovine serium albumin, 1 mM

EDTA, 0.05% cysteine and 0.05 M Tri-HCL buffer at PH 7.2. The homogenate was filtered through a layer of membrane filters and the filtrate was centrifuged at 1000×g for 15 minutes. The precipitation was assumed to be the nuclear fraction whereas the supernatant included chloroplast and mitochondria[16]. Both fractions were determined by passing them from absolute ethanol to toluene scintillation fluid (4 g PPO, 0.05 g POPOP in 1 liter of toluene) and counted in a Liquid Scintillation Counter.

## RESULTS AND DISCUSSION

Rates of DNA synthesis in nuclei fraction of shoot apex of SB, SB + FUDR, WB-2, and WB-2 + GA over 8 consecutive intervals are shown in Table 1. About 90% of cumulative DNA synthesis in SB was inhibited by FUDR. It has been reported[7] that 90% of growth in SB was inhibited by $10^{-4}$ M of FUDR. Thus, nuclear DNA synthesis is positively correlated with the seedling growth in watermelon. Only a low level of DNA synthesis was observed in the first 4 hours after the release of FUDR inhibition among all treatments. Comparative patterns of nuclear DNA synthesis between SB and WB-2+GA are observed in Table 1 except at 4 hours interval where SB shows a substantially higher rate of DNA synthesis than

*Table 1.* The rate of $^3$H-thymidine incorporation in nuclei of shoot apex of SB, SB + FUDR, WB-2 and WB-2 + GA over 8 consecutive intervals. Each value (C. P. M.) represents a mean of 10 shoot apex

| Treatments | Hours after initial stages | | | | | | | | Total[b] |
|---|---|---|---|---|---|---|---|---|---|
| | 0 | 2 | 4 | 6 | 8 | 10 | 12 | 14 | |
| SB | 16 | 79 | 974 | 1,767 | —[a] | 2,282 | 1,180 | 651 | 8,974 |
| SB+FUDR | 42 | 128 | 107 | 183 | 37 | 96 | 121 | 141 | 855 |
| WB-2 | 36 | —[a] | 108 | 760 | 658 | 1,798 | 1,712 | 1,807 | 6,951 |
| WB-2+GA | 32 | 84 | 371 | 1,948 | 2,811 | 1,982 | 937 | 405 | 8,570 |

*a*: The data were missing.

*b*: The missed data to be summed in total was filled with the average of preceding and following values.

WB-2 + GA. It could be explained that the lag period of exogeneous GA to reach to the regulating sites of DNA synthesis in WB-2 nuclei caused the lightening of the initial rate of DNA synthesis in WB-2 + GA seedlings. The initiation of DNA synthesis began 6 hours after the initial stage in WB-2 whereas 4 hours after initial stage in WB-2 + GA. It was therefore indicated that GA could enhance the initiation of DNA synthesis in WB-2 dwarf to a parallel stage of that in SB. Thus, Jacqmard's hypothesis[5] stated that the effect of GA on cell division was to control the progression of cell from the G1 to S phase of the cell cycle could be proved by the present study. Moreover, the drastic increment of DNA synthesis in WB-2 + GA occurred at the second interval from the initiation of DNA synthesis where as the similar increase in WB-2 was detected at third interval from the initiation of DNA synthesis. The results implied that in those stages, an expansion of numbers of DNA replicating sites were occurred rather than the increase of absolute rate of DNA synthesis since the increments were magnified by almost 3 folds within 2 hours period as compared to the preceding stage. In this manner, GA would not only accelerate the initiation of DNA synthesis but also increase the number of replicating sites by 2 hours sooner in WB-2 dwarf as compared to their respectively untreated stages. A constant rate of DNA synthesis was observed in WB-2 seedlings after the peak in S phase had been reached. On the other hand, the rate of DNA synthesis in WB-2 + GA varied in different intervals during the S phase. Housman and Huberman[4] also indicated that the rate of DNA replication might change at different times during S phase in mammalian cells. In this experiment, GA intensified the rate of DNA synthesis to rise to a peak at 6 hours after the initial DNA synthesis. The significantly less total counts in WB-2 than WB-2+GA or SB implicated that the full DNA synthesic period in WB-2 was not completed since all of them should possess the same amount of DNA synthesis in each complete S phase. It was identified by the results from cell cycle study[9] where the S period of WB-2 was 11.3 hours. However, only 10 hours of S period was included in the present experiment. Thus, the present

study did not include a complete S phase of WB-2. GA restored the mode of DNA synthesis during the sequence of S phase in WB-2 to that of SB. The evidence indicated that dwarf gene *dw*-2 exerted its effect on cell division through the retardation of DNA synthesis by the low level of endogneous GA. The lower level of endogeneous GA in genetic dwarf than normal strain was indeed found in beans[15], corn[13], and peas[3].

Rates of $^3$H-thymidine incorporation into cytoplasmic DNA among 4 treatments are shown in Table 2. Similar types of cytoplasmic DNA synthesis during a 14 hours period were found among SB, WB-2, and WB-2 + GA. Thus, it was suggested that the shortening of S phase in WB-2 seedlings by GA was mainly caused by an enhancement of DNA synthesis in the nucleus but not outside the nucleus. In addition, the inhibition of FUDR on cytoplasmic DNA synthesis was not as significant as on nuclear DNA synthesis in watermelon.

*Table 2.* The rate of $^3$H-thymidine incorporation in cytoplasm of shoot apex

| Treatments | Hours after initial stages | | | | | | | | Total[b] |
|---|---|---|---|---|---|---|---|---|---|
| | 0 | 2 | 4 | 6 | 8 | 10 | 12 | 14 | |
| SB | 74 | 32 | 166 | 148 | 216 | 117 | 182 | 188 | 1,123 |
| SB+FUDR | 47 | 93 | 109 | —[a] | 85 | 76 | —[a] | 91 | 682 |
| WB-2 | 41 | 88 | 146 | 79 | 116 | 192 | 182 | 237 | 1,081 |
| WB-2+GA | 39 | 68 | 175 | 249 | —[a] | 150 | 196 | 145 | 1,222 |

Same footnotes as in Table 1.

## REFERENCES


(1) Brain, P. W., G. W. Elson, H. E. Hemming, and M. Radley. 1954. The Plant-growth promoting properties of gibberellic acid, a metabolic product of the fungus *Gibberella fujikuroi*. *J. Sci. Food Agr.* **5**, 602-612.

(2) Degani, Y. and D. Atsmon. 1970. Enhancement of non-nuclear DNA synthesis associated with hormone—induced elongation in the cucumber. *Exytl. Cell Res.* **37**, 516-539.

(3) Gorter, G. J. 1961. Dwarfism of Peas and the action of gibberellins on internodal tissue of *Phasedus Vulgaris* L. *Amer. J. Bot.* **45**, 520-522.

(4) Housman, D. and J. A. Huberman. 1975. Changes in the rate of DNA

folk movement during S phase in mammalian cells. *J. Mol. Biol.* **74**, 173-181.

(5) Jacqmard, A. 1968. Early effects of gibberellic acid on mitotic activity and DNA synthesis in the apical bud of *Rudbeckia bicolor*. *Physiol. Veg.* **6**, 409-416.

(6) Kusanagi, A. 1966. Rate of DNA replication in the DNA synthetic period of the barley chromosomes. *Chromosoma* **20**, 125-132.

(7) Liu, P. B. W. 1974. *Cell proliferation and elongation in normal, dwarf, and gibberellin—treated dwarf watermelon seedlings.* Ph. D. Dissertation University of New Hampshire, Durham.

(8) Liu, P. B. W. and J. B. Loy. 1972. Inheritance and morphology of two dwarf mutants in watermelon. *J. Amer. Soc. Hort. Sci.* **97**, 745-748; 1976. Action of gibberellic acid on cell proliferation in the subapical Meristem of Watermelon Seedlings. *Amer. J. Bot* **63**(5), 700-704.

(9) Loy, J, B. and P. B. W. Liu. 1974. Response of seedlings of a normal strain of watermelon to gibberellins. *Plant Physiol.* **53**, 325-330.

(10) Nass, M. M. K., S. Nass, and B. A. Afzelius. 1965. The general occurrence of mitochondrial DNA. *Exptl. Cell Res.* **37**, 516-539.

(11) Mitchson, J. M. 1971. *The Biology of Cell Cycle.* pp. 58-90, pp. 158-180, and pp. 244-249. Cambridge University (London) Press.

(12) Phinney, B. O. 1956. Growth response of single dwarf mutants in maize to gibberellic acid. *Proc. Nat. Acad. Sci.* **42**, 185-189.

(13) Plummer, T. H. and M. L. Tomes. 1957. Effects of indoleacetic acid and gibberellic acid on normal and dwarf tomatoes. *Bot. Gaz.* **119**, 613-618.

(14) Proano, V. A. and G. L. Greene. 1968. Endogeneous gibberellins of radiation induced single gene dwarf mutant of bean. *Plant Physiol.* **43**, 613-618.

(15) Ris, H. and W. Plaut. 1962. Ultrastructure of DNA-containing areas in the Chloroplast of Chlamydomonas. *J. Cell Biol.* **13**, 383-391.

(16) Wells, R. and J. Ingle. 1970. The constancy of the Buoyant Density of Chloroplast and Mitochondrial DNA in a range of higher plants. *Plant Physiol.* **46**, 178-179.

# A STUDY ON THE MANUFACTURING OF BLACK QUEEN GRAPE JUICE

J. M. TSIANG, J. C. HSIEH & J. J. DONG

## INTRODUCTION

The rapid rise in the consumption of canned and bottled fruit juices all over the world has been one of the most significant developments of the food industry in the recent years. Commercial manufacturing of grape juice started in 1869 in the United States, and the majority of grape juice is made from Concord grapes which grow mostly in cooler climates.[8]

In the past few years, natural fruit juice consumption in Taiwan has increased rapidly. Grape juice along with other non-tropical juices was imported from other countries. Under the government Accelerated Rural Development Program (ARDP), the growing and processing of grapes is one of the important items. To develope a new method of processing grapes besides wine making is urgent at the present time. Due to this fact, the study of "grape juice manufacturing" raised great interest among many food scientists.

The climate in Taiwan is not ideal for growing grapes. Black Queen variety from Japan is one of the best grape varieties suitable to be grown locally, so we are interested in its processing quality.[6]

This paper includes the storage condition of the raw materials, the processing methods of the juice, and the effects of containers, so as to complete the whole manufacturing procedure.

## MATERIALS AND METHODS

### A. Materials.

Black Queen grapes were obtained from the vineyard of Ho Le Village, Taichung County, Taiwan.

Black Queen variety (vitis vinifera × vitis labrusca cv. Black Queen), cross variety of Baily × Golden Queen, was harvested

around the end of June. The size of the fruit is large with reddish-purple color.

**B. Methods.**

1. *Storage test of raw materials.* Grapes were placed separately in plastic buckets (depth 23 cm, length 60 cm, width 41 cm) with a content of 10 Kg each, and covered loosely with polyethylene sheets. The grapes were then stored under different temperature and humidity conditions for testing and observation.

For the experiment, 500 g of grapes were picked at random, were washed, destemmed and blended, then cold pressed and filtered through two layers of cheese cloths to obtain juice samples for testing. Total sugar was measured with an Atago refractometer and was reported as °Brix. pH was measured with a pH meter photovolt, and total acidity was titrated with 0.25N NaOH and reported as tartaric acid.

2. *Depectinizing study.* Grapes were washed, destemmed, heated to approximately 60°C, and this temperature was held for 10 minutes before pressing. The heated grape mass run into press cloth bags for pressing with a hydraulic press. A depectinizing enzyme, wallerstein pectinase, was added into the extracted juice with different concentrations. The extracted juice was then held in a steam jacketed stainless steel kettle at 60°C with different lengths of time for the degradation of pectin.

Pectin residue was determined by using dehydrated isopropyl alcohol. 2 ml of the enzyme treated juice was centrifuged at 3000 rpm for 10 min to remove the suspended solids. 1 ml of this juice was pipetted into a 10 ml centrifuged tube and was diluted to 2 ml with distilled water. To this, 4 ml of dehydrated isopropyl alcohol was added. The tube was shaken gently for a few seconds, then centrifuged at 3000 rpm for 10 min. The determination of the pectin residue was based on the observation of the insoluble white colloid pectin precipitate in the tube after centrifuging.

3. *Detartration study.* Sodium caseinate and calcium lactate were used for the study of rapid settling and elimination of argol (crude

tartrates) from Black Queen grape juice.[7]

To the depectinized grape juice, 2% sodium caseinate solution was added, followed by a 20 min settling period before centrifugal separation. 2% dialite was used as a filter aid.

The centrifugal juice was flesh pasteurized through a tabular heat exchanger for 10 sec at 85–90°C, and poured into the filler. The pasteurized juice was then filled into sterilized hot 1.6 liter bottles for storage. The bottles were placed horizontally for 10 min before cooling. Different storage conditions were used for the settling of argols. Samples to be stored in a sharp freezer at −20°C were prepared by cooling the pasteurized juice before filling into 20 liter plastic containers.

Another method of removing argols involved the addition of 2% calcium lactate instead of sodium caseinate, and the prepared sample was stored at low temperature 0–4°C for the detartration of the juice.[7]

After settling out the argols through storage, the juice was filtered by centrifuging with 2% dicalite as a filter aid to obtain a clarified juice.

4. *Flavor evaluation.* Juice from which argols had been removed was conveyed to a holding tank. Sugar and artificial flavors were then added. Different sugar contents and variations of flavors at different levels were evaluated by several groups of people.

A rank sum at the 5% significant level was used for flavor evaluation of the juice.[8]

5. *Testing of containers.* The juice was pumped from the tank through the tubular heat exchanger for 10 sec at 90–95°C, and was poured into the filler. The hot juice was then filled into different sterilized containers. After filling, the containers were sealed and inverted for 5–10 min, then cooled with cold water.

The juice packed in different can containers was stored at different temperatures for testing and evaluation. The vacuum of the canned grape juice was measured with a vacuum gauge and was reported as cmHg. The evaluation of color and aroma was based on hedonic preference 40 as full scale. Tin in the canned juice was

determined by the iodometric method.[4]

## RESULTS AND DISCUSSION

1. **Storage test of raw materials.** Storage of raw materials is necessary during the harvest season when the food factory is not able to process all the fruits at once. Proper storage of the fruits for a few days to more than a few weeks will not only prolong the period of processing, but in some cases may also allow the fruit to mellow.

Fig. 1 shows that during storage there is a gradual decrease in total sugar of the samples stored at 0–4°C, while a more rapid loss in total sugar was observed in the samples stored at room temperature (26–30°C).

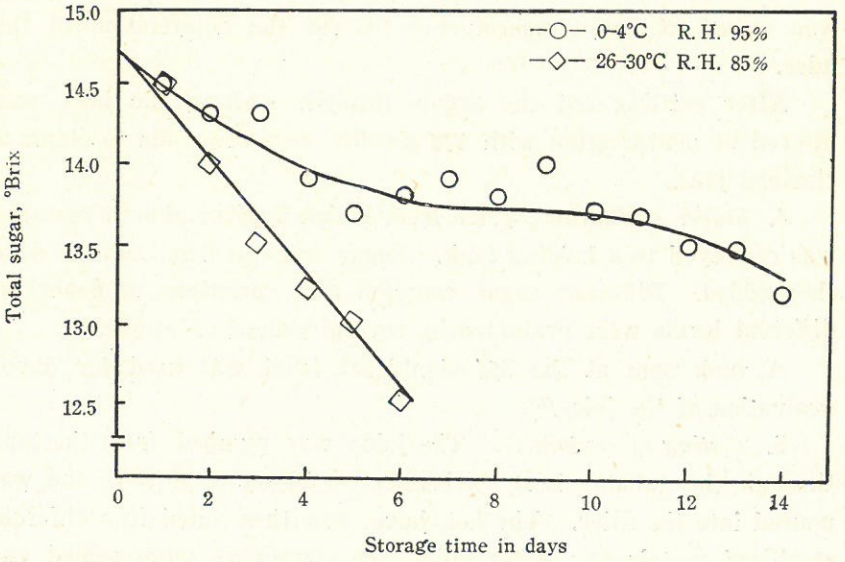


Fig. 1. Effect of storage temperature and humidity on total sugar of Black Queen grapes

The changes of pH and titratable acidity of grape as influenced by storage temperature are shown in Fig. 2 and Fig. 3. A slight increase in total acidity was observed in both conditions, due to the loss of water during storage. So the slight increase in total acidity

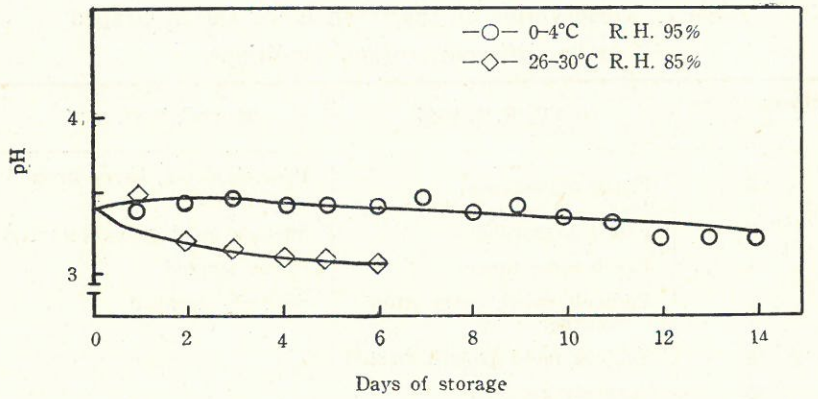


Fig. 2. Change of pH during storage

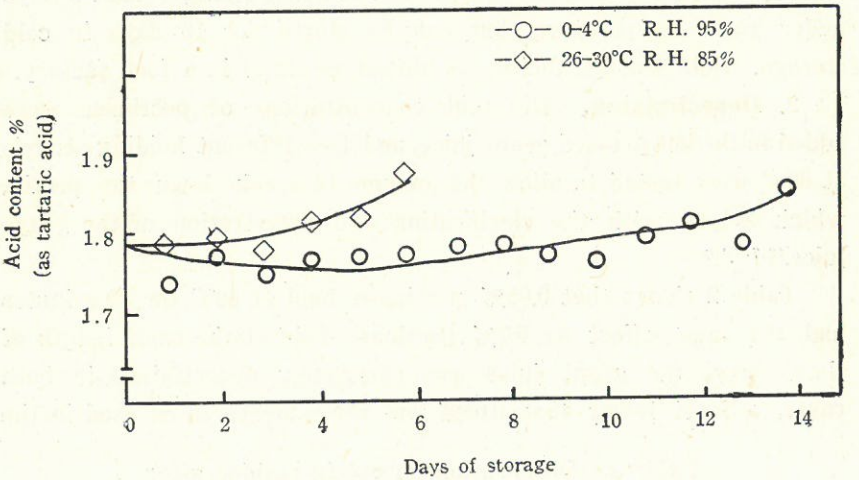


Fig. 3. Change of acid content during storage

is insignificant in this case. A slight decrease in pH was observed after 3 days at room temperature, and after 10 days at 0–4°C which is correlated to the overall quality changes recorded in Table 1.[5]

Table 1 indicates that the grapes started to decay after 3 to 4 days at room temperature, while those stored at 0–4°C did not change their appearance until the 10th day.

It is quite obvious that relatively low storing temperature will prolong the life of fresh grapes. Under summer condition in this

*Table 1.* Observation on the fresh Black Queen Grapes under different storage conditions.

| Storage time, days | 0-4°C, R. H. 95% | 26-30°C, R. H. 85% |
|---|---|---|
| 2 | Fresh appearance | Pedicels dried, berry drop occurred |
| 3 | Fresh appearance | Surface mold growth started |
| 4 | Fresh appearance | Decay started |
| 6 | Pedicels dried, berry drop occurred | Severely decayed |
| 10 | Surface mold growth started | |
| 12 | Severely decayed | |

country, fresh Black Queen grapes can be held no longer than 3 days under room temperature, but can be stored for 10 days in cold storage. Cold storage facility is almost essential in a food factory.

2. **Depectinizing.** Different concentrations of pectinase were added to the hot pressed grape juice, and two different holding periods at 60°C were tested to allow the enzyme to break down the pectin, which helped with the clarification and detartration of the grape juice.[2,7,9,10]

Table 2 shows that 0.05% pectinase held at 60°C for 30 minutes had the same effect as 0.1% pectinase held at the same length of time. Since the grape juice was completely depectinized in both cases, a level lower than 0.05% was recommeded to be used in the

*Table 2.* Observation on pectin residue after depectinizing of Black Queen grape juice.

| Pectinase % | Holding time at 60°C, min. | |
|---|---|---|
| | 20 | 30 |
| 0.025 | ++ | ++ |
| 0.05 | + | − |
| 0.1 | + | − |

++ Heavy precipitate
\+ Slight precipitate
− No precipitate

manufacturing of grape juice.

3. **Detartration.** To prevent sediments in bottled juice after storage, detartration (removal of crude tartrate-argols) of grape juice is necessary. Different detartration methods were studied and the results are shown in Table 3.

*Table 3.* Observation on reprocessed bottled Black Queen grape juice treated with different detartration methods and storage temperatures.

| Detartration treatments | | | Observation on the bottled juice product | |
|---|---|---|---|---|
| Sample | Storage temp. | Storage time | Precipitate in volume | Forms of precipitate |
| 1. Depectinized juice | 26-30°C | 4 mon. | — | Suspended particles (no precipitation) |
| 2. Depectinized juice 2% Na±Caseinate | 26-30°C | 4 mon. | 0.5%* | Fine particles |
| 3. Depectinized juice 2% Na±Caseinate | −2°C | 3 mon. | 0.1% | Crystals with fine particles |
| 4. Depectinized juice 2% Na±Caseinate | −20°C | 1 or 2 wk. | 0.2% | Crystals |
| 5. Depectinized juice 2% Ca±lactate | −2°C | 4 mon. | 0.1%* | Fine particles |

* The precipitation was still going on.

According to the results, depectinized grape juice (sample 1) without further detartrated treatment showed a suspended cloudiness in the bottled grape juice, while the use of sodium caseinate or calcium lactate proved to be a much better method for removing argols.

The form of the precipitate has great influence on the clarification of the juice. Fine particles observed in samples 2 and 5 could be a sign of incomplete crystallization of the crude tartrates, and could be a form of very fine crystals which make the seperation quite difficult.

By comparing samples 3 and 5, it is evident that the use of sodium caseinate is better than calcium lactate in the juice clarification. By comparing samples 2, 3 & 4, it is shown that the lower temperature treatment, especially the freezing action, in addition to

the sodium caseinate treatment will not only improve the precipitation, but will also shorten the length of storage time necessary for detartration. So it is clear from this experiment that the use of sodium caseinate and low temperature treatment after the juice has been depectinized proved to be a very effective method in detartrating the Black Queeen grape juice.[8]

4. **Flavor evaluation.** The purpose of this study is to determine consumer preferences for a most acceptable grape juice. The overall quality of a grape juice is determined by its color and flavor. Since the original flavor of Black Queen grape juice not only has a taste of astringency and tartness, but also lack of a pronounced, characteristic flavor of grapes, the adding of sugar and artificial flavor will be most important in improving this type of grape juice.

Different sugar to acid ratios were tested and evaluated repeatedly. The studies showed that a sugar to acid ratio of 20 was most acceptable.

Artificial flavors from Taiwan, Japan, and Holland etc. at different levels have been tested and evaluated. The final evaluation on the two best artificial flavors is shown in Table 4. The result in this table shows that sample 17 with flavor A at 25 ppm is significantly better than sample 29.

Food industry experts were asked to evaluated Black Queen grape juice which was manufactured according to the best processing methods as a result of this study. Table 5 shows that this survey on the overall quality of Black Queen grape juice was favorable.

5. **Testing of containers.** The selection of proper types of containers is important for the final overall quality of grape juice, especially its flavor and color. Single and double coated tin containers from West Germany, Japan, and the United States were used in this experiment, plain tin cans without coating made locally were used for comparison.

The Mobil type tin can, with single or double coating, has the best effect in maintaing high vacuum in the can as shown in Table 6.

*Table 4.* Rank sum of Black Queen grape juice samples (S/A=20) with different flavors evaluated by 13 panelists.

| Panelists | Rank | |
|---|---|---|
| | Sample 17* | Sample 29* |
| 1 | 1 | 2 |
| 2 | 2 | 1 |
| 3 | 1 | 2 |
| 4 | 1 | 2 |
| 5 | 1 | 2 |
| 6 | 1 | 2 |
| 7 | 1 | 2 |
| 8 | 1 | 2 |
| 9 | 1 | 2 |
| 10 | 1 | 2 |
| 11 | 1 | 2 |
| 12 | 2 | 1 |
| 13 | 1 | 2 |
| Rank Sum | 15 | 24 |

Significant range 16-23
*Sample 17—Holland grape juice flavor 25 ppm
*Sample 29—Holland grape flavor Wonf. 50 ppm

*Table 5.* A survey on the overall quality of Black Queen grape juice by 31 panelists.

| Panelists / Opinion | Color | Grape Juice Qualities | | | |
|---|---|---|---|---|---|
| | | Aroma | Sweetness | Tartness | Astringency |
| Too weak (light) | 3 | 12 | 2 | 1 | 1 |
| Just right | 25 | 19 | 22 | 21 | 22 |
| Too strong | 3 | 0 | 7 | 9 | 8 |
| | Poor | Fair | Good | Excellent | |
| Black Queen grape juice | — | 4 | 17 | 9 | |

Location: Conference room of the Federation of Fruit Marketing Cooperatives, Taipei.
Date: October 18, 1875

*Table 6.* Changes of vacuum of Black Queen grape juice packed in different tin containers stored at different temperatures.

| Sample | Code* | Storage condition, °C | Vac., cmHg | | |
|---|---|---|---|---|---|
| | | | Storage time, months | | |
| | | | 0 | 1 | 3 |
| 1 | WS | 21 | 31 | 32 | 39 |
| 2 | WS | 29 | 31 | 34 | 31 |
| 3 | WS | 37 | 31 | 26 | 29 |
| 4 | WD | 21 | 31 | 26 | 31 |
| 5 | WD | 29 | 31 | 25 | 23 |
| 6 | WD | 37 | 31 | 24 | 12 |
| 7 | JS | 21 | 31 | 29 | 32 |
| 8 | JS | 29 | 31 | 29 | 22 |
| 9 | JS | 37 | 31 | 23 | 25 |
| 10 | JD | 21 | 31 | 25 | 29 |
| 11 | JD | 29 | 31 | 24 | 17 |
| 12 | JD | 37 | 31 | 22 | 11 |
| 13 | MS | 21 | 31 | 30 | 35 |
| 14 | MS | 29 | 31 | 31 | 29 |
| 15 | MS | 37 | 31 | 32 | 27 |
| 16 | MD | 21 | 31 | 27 | 36 |
| 17 | MD | 29 | 31 | 29 | 35 |
| 18 | MD | 37 | 31 | 27 | 27 |
| 19 | TP | 21 | 31 | 29 | 26 |
| 20 | TP | 29 | 31 | — | 19 |
| 21 | TP | 37 | 31 | 20 | 20 |

*Tin can manufactured by different companies in different countries
W—Glasruit, West Germany
J—Tokyo, Japan
M—Mobil, United States
T—Taiwan
S—Single coating
D—Double coating
P—Plain tin can without coating

The degree of detinning of grape juice in different containers is shown in Table 7 and Fig. 4. The detinning was very severe in

*Table 7.* Changes of tin (Sn) content of Black Queen grape juice packed in different tin containers stored at different temperatures.

| Sample | Code* | Storage condition, °C | Sn Content, ppm | | |
|---|---|---|---|---|---|
| | | | Storage time, months | | |
| | | | 0 | 1 | 3 |
| 1 | WS | 21 | 7.4 | 10.4 | 36.1 |
| 2 | WS | 29 | 7.4 | 12.3 | 19.7 |
| 3 | WS | 37 | 7.4 | 16.8 | 19.3 |
| 4 | WD | 21 | 7.4 | 16.8 | 12.3 |
| 5 | WD | 29 | 7.4 | 15.3 | 13.3 |
| 6 | WD | 37 | 7.4 | 13.4 | 13.8 |
| 7 | JS | 21 | 7.4 | 34.1 | 44.4 |
| 8 | JS | 29 | 7.4 | 53.9 | 16.3 |
| 9 | JS | 37 | 7.4 | 52.4 | 55.4 |
| 10 | JD | 21 | 7.4 | 12.4 | 28.7 |
| 11 | JD | 29 | 7.4 | 12.8 | 49.4 |
| 12 | JD | 37 | 7.4 | 15.8 | 16.8 |
| 13 | MS | 21 | 7.4 | 7.9 | 32.1 |
| 14 | MS | 29 | 7.4 | 12.4 | 12.3 |
| 15 | MS | 37 | 7.4 | 11.4 | 17.8 |
| 16 | MD | 21 | 7.4 | 5.1 | 7.9 |
| 17 | MD | 29 | 7.4 | 5.9 | 8.9 |
| 18 | MD | 37 | 7.4 | 8.4 | 9.4 |
| 19 | TP | 21 | 7.4 | 121.0 | 118.5 |
| 20 | TP | 29 | 7.4 | 133.5 | 138.5 |
| 21 | TP | 37 | 7.4 | 151.3 | 238.5 |

* Same as in table 6

plain tin cans especially at higher storage temperature 37°C as shown in Fig. 5. Low storage temperature as well as the coating treatment of the tin can be proved to be important factors in controling detinning. The detinning in grape juice could be caused by the presence of anthocyanins which served as a depolarizer. Anthocyanins will either be reduced or form complex ions with Sn which will accelerate detinning.[1]

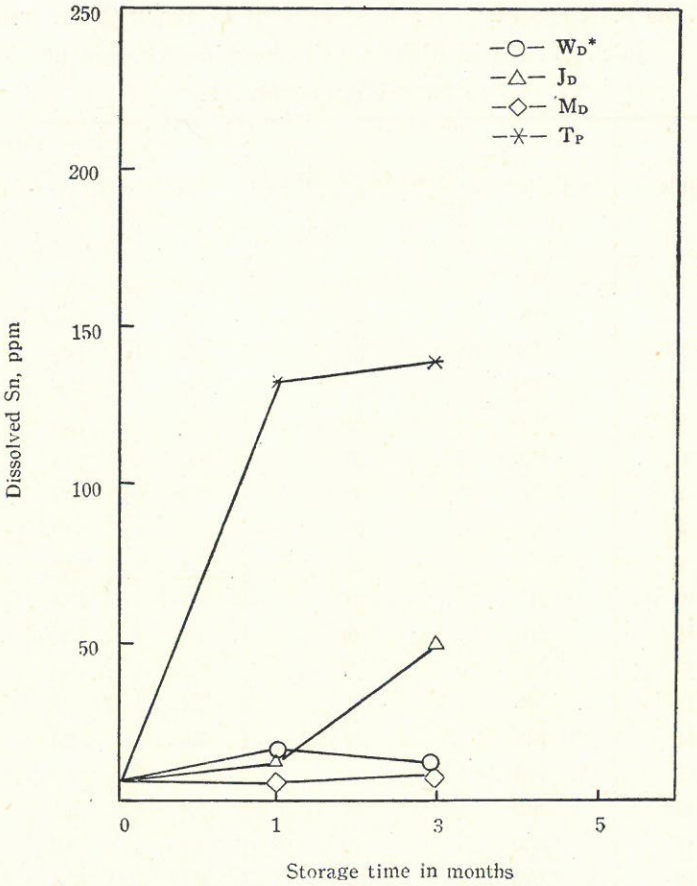


Fig. 4. Detinning of Black Queen grape juice in different containers stored at 29°C

*Refer to Table 6.

The overall quality, especially the color, of Black Queen grape juice in Mobil type double coated cans seems to be best after 3 months storage at different temperatures as shown in Table 8, while the juice in plain tin cans caused severe discoloration. The mechanism could be explained by the fact that the anthocyanin pigments which are responsible for the reddish-purple color in the grape juice were either reduced by electrons to form Leuco-type anthocyanins[1] or reacted with metalic ions released from the steel plate of the can after detinning occured.

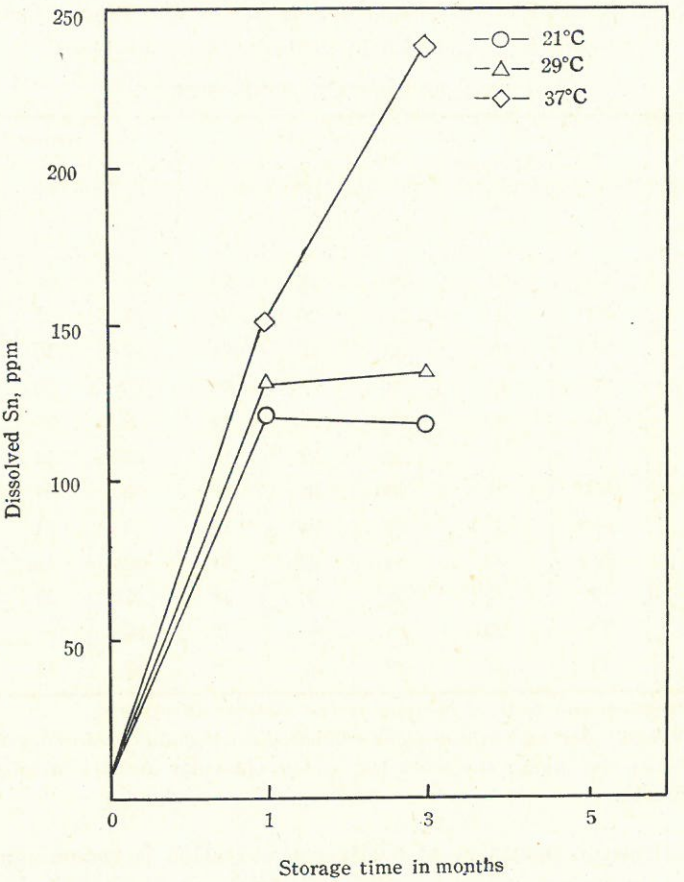


Fig. 5. Effect of storage temperature on the detinning of Black Queen grape juice in plain tin cans

## CONCLUSION

During the period of July 1975 till December 1975, storage and processing experiments were carried out on the manufacturing of Black Queen juice in order to find a most suitable manufacturing method for the production of Black Queen grape juice. The conclusion of this study is summarized as follows.

The life of raw Black Queen grape materials can be prolonged sufficiently by storing at low temperatures 0–4°C. Cold storage facility is almost essential in the grape juice manufacturing process.

*Table 8.* Color and aroma evaluation on the Black Queen grape juice packed in different tin containers stored at different temperatures.

| Sample[a] | Code[a] | Storage condition, °C | Color[b] | | | Aroma[b] | | |
|---|---|---|---|---|---|---|---|---|
| | | | Storage time, months | | | Storage time, months | | |
| | | | 0 | 1 | 3 | 0 | 1 | 3 |
| 4 | WD | 21 | 38 | 28 | 26 | 32 | 32 | 16 |
| 5 | WD | 29 | 38 | 26 | 24 | 32 | 28 | 15 |
| 6 | WD | 37 | 38 | 22 | 20 | 32 | 10 | 12 |
| 10 | JD | 21 | 38 | 28 | 26 | 32 | 29 | 15 |
| 11 | JD | 29 | 38 | 27 | 22 | 32 | 32 | 14 |
| 12 | JD | 37 | 38 | 22 | 20 | 32 | 14 | 13 |
| 16 | MD | 21 | 38 | 30 | 26 | 32 | 32 | 14 |
| 17 | MD | 29 | 38 | 28 | 24 | 32 | 31 | 16 |
| 18 | MD | 37 | 38 | 22 | 21 | 32 | 13 | 12 |
| 19 | TP | 21 | 38 | 30 | 18 | 32 | 32 | 12 |
| 20 | TP | 29 | 38 | — | 17 | 32 | — | 12 |
| 21 | TP | 37 | 38 | 22 | 16 | 32 | 14 | 10 |

[a]. Number and code of samples is the same as in table 6.

[b]. Visual color and aroma were evaluated on hedonic preference from 0 to 40, the higher the score the richer the color and the stronger the aroma.

Wallerstein pectinase at 0.05% concentration is recommended for the depectinized treatment of grape juice from heat extraction of the grape. For best result, the treated juice is to be held at 60°C for 30 minutes. The removal of the protective colloids accomplished by this treatment facilitates crystallization of the crude tartrates.

In order to get a clear and stable grape juice after reprocessing and bottling, detartration treatment of removing crude tartrate from the pressed grape juice is necessary. The most effective detartration method for Black Queen grape juice is the use of 2% sodium caseinate, in combination with low temperature treatment of the juice.

The tart and astringency taste of the juice can be improved by the adding of sugar, sugar to acid ratio at 20 is most acceptable.

The lack of distinguished grape flavor of the juice can also be enriched by a slight amount of artificial flavor. The overall palatable quality of the Black Queen grape juice has proved to be quite acceptable.

Detinning of grape juice in plain tin-plate cans causes discoloration. The most suitable way of solving this problem is the selection of proper containers. Besides glass bottles, double coated tin-plate cans seem to be ideal containers for grape juice. Low storage temperature also has great effect on keeping the quality of canned grape juice.

Mavidin of the anthocyanins, the major pigment which contributes to the reddish color of Black Queen grape juice, proved to be quite stable during storage of the canned grape juice. (Work done by Dr. T. R. Cheng, National Taiwan University.) Due to the relatively high stability in heat processing and storage of Black Queen grape juice, the Black Queen grape could be developed and cultured for the best grape juice manufactured in Taiwan.

## REFERENCES


(1) Chang, P. Y. 1971. *Internal Corrosion in Tin Plate Cans for Foods.* Food Industry Research and Development Institute, Hsinchu, Taiwan.

(2) Clore, W. J., A. M. Neubert, G. H. Carter, D. W. Ingalsbe, and V. P. Brummund. 1965. Composition of Washington-Produced Concord Grapes and Juices. Washington Agricultural Experiment Station. *Technical Bulletin* **48**.

(3) Kramer, A. 1963. Revised Tables for Determining Significance of Differences. *Food Technol.*, **17**(12), **124**.

(4) *Laboratory Manual for Food Canners and Processors. Vol. II.* 1968. National Canners Association Research Laboratories, Taiwan.

(5) Robinson, W. B., N. Shaulis, G. C. Smith and D. F. Tallman. 1959. Changes in the Malic and Tartaric Acid Contents of Concord Grapes. *Food Research* **24**.

(6) Shing K. C. Grape Prospects in Taiwan. *Journal of the Agricultural Association of China.* New Series XXXIII, March 1961.

(7) Tressler, D. K. and Joslyn M. A. 1971. *Fruit and Vegetable Juice Processing Technology, 2nd Edition.* AVI Publishing Co., Westport, Conn.

(8) Woodroof, J. G. and B. S. Luh. 1975. *Commercial Fruit Processing.* AVI Publishing Co., Westport, Conn.

(9) 葉正茂 1973. 果汁加工技術 (Fruit Juice Processing Technology). 長歌出版社.

(10) 葡萄果汁，葡萄果汁的製造 食品科學文摘 第三卷第四期。

"As population growth continues, inevitably there will be instances in which the food supply to one or another region will become, even if temporarily, grossly inadequate and on so large a scale that organized world food relief will woefully incommensurate. And the resultant political instability could have gigantic consequences for all mankind."

Philip Handler in *Biology and the Future of Man.*

## CONTRIBUTORS TO THIS NUMBER

Heinrich Hesselfeld SVD 郝思漢 Ph. D. is Dean of the College of Natural Sciences and professor and chairman of Physics at Fu Jen University

Yi-Ching Yen 顏一清 is professor of Mathematics at Fu Jen University

Jen-I Chen 陳振益 Ph. D. is professor of Physics at Fu Jen University

Yeong-Der Yao 姚永德 Ph. D. is Associate Research Fellow at the Institute of Physics, Academia Sinica, and associate professor of Physics at Fu Jen University

Peter Jih-Yung Chao 趙寄蓉 Ph. D. is associate professor of Chemistry at Fu Jen University

Ling-Chia Yeh 葉玲珈 Ph. D. is associate professor of Physics at Fu Jen University

Peter Bao-Wei Liu 劉寶瑋 Ph. D. is associate professor of Biology at Fu Jen University

Jean Mey Tsiang 蔣見美 M. S. is associate professor and head of Nutrition and Food Science at Fu Jen University

PRINTED BY

Ching Hua Press Co., LTD., Taipei